Interconnection and damping assignment passivity-based control of an unmanned helicopter

PJ Kruger

22336680

Dissertation submitted in fulfilment of the requirements for the degree *Magister* in Electrical and Electronic Engineering at the Potchefstroom Campus of the North-West University

Supervisor: Prof KR Uren

Co-supervisor: Prof G van Schoor

November 2015

Dedicated first to my wife, who had to listen to seemingly endless ramblings to only know what I was doing after the first year.

To my mother who taught me to work first and play later.

And to my dad, who encouraged me not to stop studying before my P.hD was completed. I hope that will be true.

Potchefstroom, November 2015

ABSTRACT

The field of passivity-based control is a relatively new study field. As such, literature on the application of this optimal non-linear control technique to complex control problems is limited. Only as recently as 2014 has Interconnection and Damping Assignment Passivity-based Control (IDA-PBC) been applied to quad-rotor models [29, 30]. The main motivation for selecting this specific form of PBC is its ability to shape the total energy of the system and control both the Cartesian and orientation states of the system [29]. Within this work, IDA-PBC is applied to helicopter dynamics for the same purpose.

This work serves to provide an introduction to the control design of such a helicopter system for the purposes of trajectory tracking. The trajectory tracking case is a special case of regular IDA-PBC design, which serves primarily to control the system at a specified operating point that does not change continuously. For some aircraft systems, this is acceptable [29]. However, when the aircraft needs to track a dynamic trajectory, an alternate set of equations is used [30]. This work presents the information necessary to design a control system for both purposes. However, the ultimate controller design and validation tests are presented for the trajectory tracking case.

The problem statement for the research is given as follows:

> *This study aims to apply Interconnection and Damping Assignment Passivity-based Control (IDA-PBC) to an unmanned helicopter platform with the aim to investigate if significant flight accuracy and energy efficiency benefits may be obtained, and to understand if there is merit in the further study of this optimal control technique for the field of RWUAVs.*

The flight accuracy and energy efficiency mentioned here are two questions that arose from previous studies. It is well understood that non-linear controller design is often more difficult to implement. Also, the robustness of the control system stability is often questioned. It is necessary to understand whether this non-linear technique has its benefits in application or only within academic purposes. Also worth understanding is whether the "energy-based" control technique will ultimately provide increased energy efficiency during control. This study aims to answer those questions and also guide further research topics at the North-West University.

Within this work, the reader will find a critical review of the literature on passivity-based control. The basic modelling of the helicopter is discussed, but with the addition of an explanation of how to set up the model for the port-Hamiltonian modelling framework that is used for IDA-PBC. The 6 degree-of-freedom (DOF) modelling of the helicopter is done with Newton's equations, but allows for the rotating Earth reference frame. The model accepts forces and torques as inputs to produce the Cartesian and orientation variables as outputs. These are sufficient to describe a helicopter's motion.

The work continues to show the design of the trajectory tracking IDA-PBC controller. With some preliminary understanding of IDA-PBC of other mechanical systems, it is possible to select the appropriate energy function with ease. This energy function also serves as the cost function for the optimal control strategy. The IDA-PBC controller is designed with the help of MAPLE™ 18. The controller accepts reference trajectories as inputs for each DOF within the body reference frame. The outputs of the controller

are signals describing the forces and torques necessary for the helicopter to fly such a reference trajectory. The controller makes use of the energy-based cost function to optimise tracking of reference trajectories. Such a controller is easily linked with the 6-DOF model to allow adequate simulation of the designed control strategy.

The energy-based cost function incorporates several free parameters that are left to the designer to choose. Unfortunately, there is not yet an analytical technique that allows one to calculate the value of those gains as is the case with Ackerman's formula for linear systems [6]. Instead, the values were determined empirically with the help of a simple optimisation strategy. The strategy was not the focus of this study and can be dramatically improved, but it served the purposes of this work. It may be mentioned here, that the free parameters may be optimised for more strict trajectory-tracking at the expense of the high gains that are associated with such conditions. Typically, increased gains may be associated with lowered energy efficiency, which is precisely what this study aimed to avoid with the optimal control technique. For this reason, the gains are selected as low as possible while maintaining excellent trajectory tracking.

For validation of the control system, measured data of a piloted helicopter system were used to evaluate the performance of the controller. The measured data inputs from the pilot were processed with a human pilot transfer function from [26] to estimate the flight path that the pilot attempted to fly. This estimated trajectory was then supplied to the controller to see how the controller would follow the path in conjunction with the derived helicopter model. Results showed excellent trajectory tracking. From this can be concluded that the system will provide control inputs as well as, if not better than, an experienced pilot, even for manoeuvres that test the non-linear abilities of the controller. This should make the designed control system suitable for routine surveillance flights as well as aggressive avoidance manoeuvres, if the reference trajectories for these manoeuvres can be adequately estimated.

AFRIKAANSE OPSOMMING

Die veld van passiwiteit-gebaseerde beheer (PBC) is 'n relatief nuwe studieveld. Verskeie bronne in die literatuur oor die onderwerp is slegs binne die afgelope twee dekades gepubliseer. Sodanig is literatuur oor die toepassing van hierdie optimale, nie-lineêre beheer tegniek vir komplekse beheer probleme relatief beperk. Eers so onlangs as 2014 is interkonneksie en demping toekening passiwiteit-gebaseerde beheer (IDA-PBC) toegepas op vier-rotor vliegtuig modelle [29, 30]. Die belangrikste motivering vir die keuse van hierdie spesifieke vorm van PBC is die vermoë om die volledige energie funksie van die stelsel te hervorm en te beheer in beide die Cartesiese en oriënteringsvlakke van die stelsel [29]. Binne hierdie verhandeling is IDA-PBC toegepas op helikopter dinamika om dieselfde doel.

Hierdie verhandeling dien om 'n inleiding te voorsien tot die beheer ontwerp van so 'n helikopter stelsel vir die doeleindes van trajekvolging. Die trajekvolging geval is 'n spesiale geval van gewone IDA-PBC ontwerp wat hoofsaaklik dien om die stelsel te beheer op 'n bepaalde bedryfspunt wat nie voortdurend verander nie. Vir sommige vliegtuig stelsels is dit aanvaarbaar [29]. Wanneer die vliegtuig egter 'n dinamiese trajek moet volg, word 'n alternatiewe stel vergelykings gebruik [30]. Hierdie werk bied die inligting wat nodig is om só 'n stelsel te ontwerp vir albei beheer doeleindes. Die uiteindelike beheerder ontwerp en valideringstoetse word egter selgs aangebied vir die trajekvolging geval.

Die probleemstelling vir die navorsing is soos volg gegee:

> *Hierdie studie het ten doel om interkonneksie en demping toekenning passiwiteit-gebaseerde beheer (IDA-PBC) toe te pas op 'n onbemande helikopter platform, met die doel om te ondersoek of beduidende vlugakkuraatheid en energie effektiwiteits-voordele verkry kan word en om te verstaan of daar meriete in die verdere studie van hierdie optimale beheer tegniek vir die gebied van helikopterbeheer is.*

Die vlugakkuraatheid en energie effektiwieteit wat hier genoem word, is twee vrae wat ontstaan het uit vorige studies. Dit is algemeen bekend dat nie-lineêre beheerder ontwerp dikwels moeiliker is om te implementeer. So ook word die robuustheid van die beheerstelsel stabiliteit dikwels bevraagteken. Dit is nodig om te verstaan of die nie-lineêre tegniek voordele in die toepassing daarvan of slegs binne akademiese doeleindes bied. Ook belangrik om te weet is óf die "energie-gebaseerde" beheer tegniek uiteindelik beter energie-effektiwietiet tydens beheer sal voorsien. Hierdie studie het ten doel om dié vrae te beantwoord en ook verdere navorsingsstudies by die Noordwes-Universiteit te lei.

Binne hierdie verhandeling sal die leser 'n kritiese oorsig van die literatuur oor passiwiteits-gebaseerde beheer vind. Die basiese model van die helikopter word bespreek. Daar word wel 'n verduideliking bygevoeg van hoe om die opstelling van die model te doen vir die poort-Hamiltoniese modelleringsraamwerk, wat gebruik word vir IDA-PBC. Die modellering van die ses grade-van-vryheid van die helikopter word gedoen met Newton se vergelykings, maar maak voorsiening vir die roterende verwysingsraamwerk van die aarde. Die model aanvaar kragte en draaimomente as insette om die Cartesiese en oriëntering veranderlikes as uitsette te gee wat dan die beweging van 'n helikopter voldoende kan beskryf.

Hierdie werk gaan voort om die ontwerp van die trajekvolging IDA-PBC beheerder ten toon te stel. Met ’n voorafgaande begrip van IDA-PBC van ander meganiese stelsels is dit moontlik om die toepaslike energie funksie met gemak te kies. Hierdie energie-funksie dien ook as die koste-funksie vir die optimale beheer strategie. Die IDA-PBC beheerder is ontwerp met die hulp van MAPLE™ 18. Die beheerder aanvaar verwysingstrajekte as insette vir elke vryheidsgraad binne die liggaam-verwysingsraamwerk. Die uitsette van die beheerder is seine wat die kragte en draaimomente beskryf wat nodig is vir die helikopter om so ’n verwysingstrajek te vlieg. Die beheerder maak gebruik van die energie-gebaseerde koste funksie om die volging van verwysingstrajekte te optimaliseer. So ’n beheerder kan dan maklik gehaak word aan die ses-vryheidsgrade model wat hierbo beskryf is. So kan voldoende simulasie van die beheerstrategie uitgevoer word.

Die energie-gebaseerde kostefunksie inkorporeer verskeie vrye parameters wat daar gelaat is vir die ontwerper om te kies. Ongelukkig is daar nog nie ’n analitiese tegniek wat mens toelaat om die waarde van die winste te bereken soos in die geval van Ackerman se formule vir lineêre stelsels [6]. In plaas daarvan, is die waardes empiries bepaal met behulp van ’n eenvoudige optimaliseringsstrategie. Die strategie was nie die fokus van hierdie studie nie en kan wesenlik verbeter word, maar dit dien die doel vir hierdie werk. Dit mag hier genoem word dat die vrye parameters geoptimaliseer kan word vir beter trajekvolging ten koste van die hoë winste wat geassosieer word met hierdie vereistes. Tipies kan verhoogde winste geassosieer word met verlaagde energie-doeltreffendheid. Dit is presies wat hierdie studie daarop gemik is om te verhoed met die optimale beheer tegniek. Om hierdie rede word die winste so laag as moontlik gekies terwyl baie goeie trajekvolging nog steeds gehandhaaf word.

Vir validasie van die beheerstelsel is gemete data van ’n helikopter stelsel wat deur ’n vlieënier beheer is, gebruik om die werking van die beheerder te evalueer. Die gemete insette van die vlieënier is verwerk met ’n "menslike vlieënier oordragsfunksie" vanuit [26] om die vlug pad wat die vlieënier probeer vlieg het, te skat. Hierdie beraamde trajek is toe aan die beheerder verskaf om te sien hoe die beheerder die trajek sou volg in samewerking met die afgeleide helikopter model. Resultate het uitstekende trajekvolging van die beraamde trajekte vertoon. Hieruit kan afgelei word dat die beheerstelsel insette sal lewer wat só goed is, indien nie beter nie, as wat ’n ervare vlieënier s’n sal wees. Dit geld selfs vir bewegings wat die nie-lineêre vermoëns van die beheerder op die proef stel. Dit behoort die beheerstelsel geskik te maak vir gewone observasie vlugte asook aggressiewe bewegings, solank die verwysing trajekte vir hierdie bewegings goed genoeg beraam kan word.

ACKNOWLEDGMENTS

Special thanks to my Lord,
Who gave me the talent and opportuntinty to pursue this study.

Thank you to my wife, her parents and mine,
who offered many prayers on my behalf.

Also thank you to my study leaders, Prof. Kenny Uren and Prof. George van Schoor, who taught me more than I had bargained for and different things than I had hoped.

Thank you to Mr. JC Botha from Denel Aviation for his technical assistance on numerous occasions.

Thank you to the THRIP Research Fund that helped me make a living from this research. [1]

And lastly, thank you to André Miede, Nicholas Mariette and Ivo Pletikosić who produced a template that I would be proud to my publish books with.

1 This work was supported by the National Research Foundation of South Africa under the following grant number: TP2011073100016. Note, however, that the grant holder acknowledges that the opinions, findings, conclusions and recommendations expressed in any publication generated by the NRF supported research project are that of the author. The NRF accepts no liability in this regard.

CONTENTS

I DISSERTATION 1

1 INTRODUCTION TO RESEARCH 3
- 1.1 Problem background 3
- 1.2 Problem statement 4
- 1.3 Issues to be addressed 4
- 1.4 Project scope 5
- 1.5 Methodology 5
- 1.6 Dissertation outline 7

2 CRITICAL REVIEW OF THE LITERATURE 9
- 2.1 Modelling of helicopters 9
  - 2.1.1 Rigid body equations 9
  - 2.1.2 Force and torque equations 10
  - 2.1.3 Input-to-thrust equations 10
  - 2.1.4 Transformation between reference frames 12
  - 2.1.5 Rotation between reference frames 12
- 2.2 Introduction to PBC and its applications 13
  - 2.2.1 Modelling benefits 14
  - 2.2.2 Controller design benefits 16
  - 2.2.3 Stability benefits 16
  - 2.2.4 Energy efficiency benefits 17
- 2.3 Critical evaluation of PBC techniques 17
  - 2.3.1 Lagrangian approaches 17
  - 2.3.2 Port-Hamiltonian approaches 18
- 2.4 Conclusions 19

3 DERIVATION OF HELICOPTER MODEL 21
- 3.1 Three levels of modelling 21
- 3.2 Gyroscopic forces and the Coriolis effect 23
- 3.3 Force-to-state equations 25
- 3.4 Actuator-to-force equations 25
- 3.5 Input-to-actuator equations 27
- 3.6 Restructuring of model 28
- 3.7 Conclusions to modelling approach 28
  - 3.7.1 Presence of Euler angles within the Hamiltonian function 28
  - 3.7.2 Position coordinates within the Earth Reference Frame 28
  - 3.7.3 Complexity of model 29

4 FOUNDATIONAL THEORY OF IDA-PBC 31
- 4.1 Regular IDA-PBC 31
  - 4.1.1 Basic design objectives 32
  - 4.1.2 Matching equations 32
  - 4.1.3 Formal proposition for stable controllers 33
  - 4.1.4 Definition of the control law 35
  - 4.1.5 Three methodologies for solving matching equations 36
- 4.2 Trajectory tracking IDA-PBC 36
- 4.3 Conclusions to the foundational theory 38

5 IDA-PBC DESIGN OF A HELICOPTER CONTROL SYSTEM 39
5.1 Introduction 39
5.2 Satisfying IDA-PBC requirements 40
5.3 Homogeneous and non-homogeneous equations 41
5.4 Solution of homogeneous equations 41
5.5 Potential energy terms 42
5.6 Solutions to matching equations 42
5.7 Damping assignment 43
5.8 Conclusions to controller design procedure 44
5.8.1 Pitfalls 44
5.8.2 Simulation of error dynamics 44
5.8.3 Testing the system 45
5.8.4 Compensation for the Coriolis effect in low-level control 45
5.8.5 Selecting control-law gains 46
6 VALIDATION OF THE CONTROL SYSTEM 49
6.1 Proposed validation procedure 49
6.2 Measured data as reference trajectories 50
6.3 Realistic reference trajectories 51
6.4 Estimation of reference trajectories 52
6.5 Validation results 55
6.6 Conclusions 57
6.6.1 Inaccuracies of gyroscope data 57
6.6.2 Deviations in estimated yaw angle trajectories 57
7 CONCLUSIONS 61
7.1 Difficulties within the work 61
7.1.1 Understanding IDA-PBC 61
7.1.2 Producing satisfactory validation results 62
7.2 Recommendations for future work 62
7.2.1 Evaluation of the control system on a physical platform 62
7.2.2 Aggressive testing 62
7.2.3 Improved gain optimisation 63
7.2.4 Redundancy of input signals 63
7.3 Evaluation of final results 64
7.3.1 Ease of design 64
7.3.2 Reference vs. actual trajectories 64
7.3.3 Accuracy of control system 65
7.3.4 Stability of control systems 65
7.3.5 Energy efficiency of control system 65

II APPENDIX I 69
A QUICK-STOP MANOEUVRE 71
B QUICK-STOP-TO-THE-RIGHT MANOEUVRE 73
C WIND-UP TURN MANOEUVRE 75

III APPENDIX II 77

BIBLIOGRAPHY 85

LIST OF FIGURES

Figure 1.1 Research methodology 6
Figure 2.1 Three levels of modelling 10
Figure 2.2 Illustration of the moment arm distances of ${}^{b}\tau$ [10] 11
Figure 2.3 Illustration of the longitudinal and vertical TPP angles [10] 11
Figure 2.4 Structure-preserving interconnection 14
Figure 2.5 Decomposition into subsystems 15
Figure 3.1 Three levels of modelling 21
Figure 3.2 Helicopter axis illustration 22
Figure 3.3 Illustration of the longitudinal and vertical TPP angles [10] 22
Figure 3.4 Illustration of the moment arm distances of ${}^{b}\tau$ [10] 23
Figure 3.5 The Coriolis effect 24
Figure 3.6 Prominence of the Coriolis effect 24
Figure 3.7 Flapping equation mixing within [10] 27
Figure 5.1 Effect of damping for incorrect initial conditions 44
Figure 6.1 Illustration of selected validation procedure 50
Figure 6.2 Illustration of a typical helicopter control loop 52
Figure 6.3 Illustration of trajectory generation procedure 52
Figure 6.4 Difference between measured and estimated pilot trajectories 55
Figure 6.5 Validation results for positions about the $x-$axis 56
Figure 6.6 Validation results for positions about the $y-$axis 56
Figure 6.7 Validation results for positions about the $z-$axis 57
Figure 6.8 Engine governor vs. torque for roll-reversal manoeuvre 58
Figure 6.9 Engine governor vs. torque for quick-stop manoeuvre 59
Figure 7.1 RLC system 66
Figure 7.2 Energy consumption of an RLC system 67
Figure A.1 Validation results for positions about the $x-$axis - QS 71
Figure A.2 Validation results for positions about the $y-$axis - QS 71
Figure A.3 Validation results for positions about the $z-$axis - QS 72
Figure A.4 Engine governor vs. torque - QS 72
Figure B.1 Validation results for positions about the $x-$axis - QSR 73
Figure B.2 Validation results for positions about the $y-$axis - QSR 73
Figure B.3 Validation results for positions about the $z-$axis - QSR 74
Figure B.4 Engine governor vs. torque - QSR 74
Figure C.1 Validation results for positions about the $x-$axis -WUT 75
Figure C.2 Validation results for positions about the $y-$axis - WUT 75
Figure C.3 Validation results for positions about the $z-$axis - WUT 76
Figure C.4 Engine governor vs. torque - WUT 76

LIST OF TABLES

Table 5.1 Controller parameters and gains 47
Table 6.1 Comparison of validation methods within literature 50

KEYWORDS

passivity-based control, interconnection and damping assignment passivity-based control, helicopter, non-linear control, trajectory tracking,

ACRONYMS

RWUAV Rotary-Wing Unmanned Aerial Vehicle

PBC Passivity-based Control

BIDA Basic Inteconnection and Damping Assignment

EB-PBC Energy-balancing Passivity-based Control

IDA-PBC Inteconnection and Damping Assignment Passivity-based Control

DOF Degree-of-Freedom

PDE Partial Differential Equation

TPP Tip-Path-Plane

BF Body Reference Frame

EF Earth Reference Frame

SF Spatial Reference Frame

MAGLEV Magnetic Levitation

RLC Resistor-Inductor-Capacitor

PID Proportional-Integral-Derivative

LIST OF SYMBOLS

x	position along x-axis, either in the body or earth reference frame
y	position along y-axis, either in the body or earth reference frame
z	position along z-axis, either in the body or earth reference frame
u	velocity along x-axis, either in the body or earth reference frame
v	velocity along y-axis, either in the body or earth reference frame
w	velocity along z-axis, either in the body or earth reference frame
${}^{b}p$	rotational velocity about x-axis, always in the body reference frame
${}^{b}q$	rotational velocity about$y$-axis, always in the body reference frame
${}^{b}r$	rotational velocity about$z$-axis, always in the body reference frame
${}^{b}\omega$	the angular velocity vector, always in the body reference frame
ϕ	roll angle, always about x-axis
θ	pitch angle, always about y-axis
ψ	yaw angle, always about z-axis
Θ	vector of Euler angles - $\Theta = \begin{bmatrix} \phi & \theta & \psi \end{bmatrix}^{\intercal}$
m	mass of the helicopter system, measure in kg
I_{jj}	inertia of the helicopter system along j-axis
f_i	sum of the forces along the $i-$axis, measured in N
τ_{jj}	sum of the torques about the j-axis, measured in $\mathrm{N} \cdot \mathrm{m}$
h_m	distance of COG to main rotor along z-axis. See figure 3.4.
l_m	distance of COG to main rotor along x-axis. See figure 3.4.
y_m	distance of COG to main rotor along y-axis. See figure 3.4.
h_t	distance of COG to tail rotor along z-axis. See figure 3.4.
l_t	distance of COG to tail rotor along x-axis. See figure 3.4.
g	gravitational acceleration - $g = 9.81\ {}^{m}/_{\mathrm{s}}$
T_{MR}	thrust of main rotor of the helicopter
T_{TR}	thrust of the tail rotor of the helicopter
β_{1s}	lateral Tip-Path-Plane, or flapping angle. See figure 3.3.
β_{1c}	longitudinal Tip-Path-Plane, or flapping angle. See figure 3.3.
L	torque about x-axis, same as τ_{xx}
M	torque about y-axis, same as τ_{yy}
N	torque about z-axis, same as τ_{zz}
u_{lat}	lateral pilot input on cyclic control of the helicopter
u_{lon}	longitudinal pilot input on cyclic control of the helicopter
u_{col}	pilot input on collective control of the helicopter
u_{ped}	pilot input on pedal controls of the helicopter

$\mathbf{x}$	vector of position and momentum variables
$\mathbf{e}$	vector of error signals - $\mathbf{e} = \mathbf{x} - \mathbf{x_d}$
$\mathbf{q}$	generalized coordinate vector
$\mathbf{p}$	generalized momentum vector
$\mathbf{v}$	the velocity vector - $\mathbf{v} = \begin{bmatrix} u & v & w \end{bmatrix}^\intercal$
$\boldsymbol{\text{ø}}$	torque vector - $\boldsymbol{\text{ø}} = \begin{bmatrix} \tau_{xx} & \tau_{yy} & \tau_{zz} \end{bmatrix}^\intercal$
$\mathbf{K_p}$	vector of pilot gain values
$\beta(\mathbf{x})$	control law input
R_{22}	damping constant value found in the $2,2$ position of a 4×4 matrix
$k_{p\ i}$	control law position gain in the direction of variable i
$k_{v\ i}$	control law velocity gain in the direction of variable i
$\mathbf{f}(\mathbf{x})$	general function dependent on $\mathbf{x}$
$\mathbf{J(x)}$	interconnection matrix of a port-Hamiltonian system
$\mathbf{R(x)}$	damping matrix of a port-Hamiltonian system
$\mathbf{Q}(\mathbf{x})$	interconnection and damping matrix - $\mathbf{Q}(\mathbf{x}) = \mathbf{J}(\mathbf{x}) - \mathbf{R}(\mathbf{x})$
$\mathbf{H(x)}$	Hamiltonian function of a system
$\mathbf{g}(\mathbf{x})$	input gain matrix
$\mathbf{g}(\mathbf{x})^\dagger$	left-annihilator of input gain matrix - $\mathbf{g}(\mathbf{x})^\dagger \mathbf{g}(\mathbf{x}) = 0$
$\mathcal{L}(\mathbf{q}, \dot{\mathbf{q}})$	Lagrangian function of a system
$T(\mathbf{q}, \dot{\mathbf{q}})$	kinetic energy of a system
$V(\mathbf{q})$	potential energy of a system
$\mathbf{D}(\mathbf{q})$	generalised mass matrix of a port-Hamiltonian system
$\mathbf{C}(\omega, \dot{\mathbf{x}})$	Coriolis matrix
$P_{BS}(\Theta)$	transformation matrix from Euler angles to rotational coordinates
$P_{SB}(\Theta)$	transformation matrix from rotational coordinates to Euler angles
$R_{BS}(\Theta)$	rotation matrix from body reference frame to spatial reference frame
$R_{SB}(\Theta)$	rotation matrix from spatial reference frame to body reference frame

Part I

DISSERTATION

1 INTRODUCTION TO RESEARCH

This chapter explains the the background, motivation and research goals for this project. Section 1.3 notes the issues that the research will address. Section 1.4 discusses the limits of the scope of the research. Section 1.5 illustrates the methodology followed. It notes the most important literature sources and software packages that are used to understand and perform the calculations and tests. A detailed outline of the dissertation concludes this chapter. Within this outline, the reader will find a discussion of the thought process behind the content of each of the following chapters of the dissertation.

1.1 PROBLEM BACKGROUND

This study focusses on a form of non-linear control of a helicopter system. It forms part of the Rotary-Wing Unmanned Aerial Vehicle (RWUAV) research project of the North-West University. One previous study within this project applied optimal linear control to a grey-box helicopter model. However, the primary focus of that study was the system identification procedure that was used to determine the parameter values of the grey-box model [32]. During the same time, another student worked on a neural network-based control strategy of a helicopter [9]. Both of these studies delivered valuable knowledge to the project. However, they also created room for another study, one that would address additional questions and issues that had been identified within these first studies.

The said questions and issues related primarily to the optimal non-linear control of the helicopter system. To that end, another project concept was developed to progress toward an analytical non-linear control strategy like Passivity-based Control (PBC). With the analytical approach, more confidence may be placed in the stability of the system, which was an important consideration for stakeholders of this project. Although Hager [9] provided a proof for stability of the neural network-based controller, there was the pending question whether a more transparent control algorithm could be implemented to obtain the non-linear control benefits.

In addition to the questions about robustness and stability, there was an interest in control of RWUAVs from an energy-based perspective. Because PBC has intimate connection with the energy of the system it control [22–24], it was used as a starting point for investigations into energy-based control. As such, the project was originally defined as an investigation PBC of unmanned helicopters. As the project developed, the scope of the project was narrowed to Inteconnection and Damping Assignment Passivity-based Control (IDA-PBC) of an unmanned helicopter. More about the scope of the project will be discussed in section 1.4.

An important aspect of the project proposal of this study was the questions that should be answered within the investigation. The first and second primary questions have been mentioned above. The third question is one that has received surprisingly little attention in the literature as it pertains to PBC.

The first question focusses on benefits of the energy-based non-linear control strategy. Would there be benefits like improved accuracy or faster response to inputs? Would there be benefits to the non-linear control of a helicopter? This is an important question, because many consider linear strategies as sufficient for aircraft control. The reasoning is that while it is true that many linear control techniques may provide sufficient control for a large variety of flight manoeuvres, aggressive manoeuvres are required during certain situations, such as collision avoidance. The use of a non-linear control technique may facilitate the use of a greater flight envelope.

The second question is related to the first. It addresses the stability benefits that one may expect from such techniques. The flight accuracy aspect mentioned above includes stability. Without stability, accuracy is lost, but stability is also specifically mentioned, because it is critical for aviation problems.

A final important question that formed part of this study was that of energy efficiency. One would hope that an energy-based control strategy would also offer superior use of the energy required to operate the system, but it was not clear whether this would indeed be so. The project placed the answer to this question as primary outcomes of this study.

1.2 PROBLEM STATEMENT

The above considerations led to the definition of the following problem statement:

> *This study aims to apply Interconnection and Damping Assignment Passivity-based Control (IDA-PBC) to an unmanned helicopter platform with the aim to investigate if significant flight accuracy and energy efficiency benefits may be obtained, and to understand if there is merit in the further study of this optimal control technique for the field of RWUAVs.*

1.3 ISSUES TO BE ADDRESSED

The problem statement of section 1.2 brings about certain issues that will require attention during the study. The first is that of obtaining the necessary knowledge of the relatively young field of PBC. The method makes use of complex mathematics which the student needs to study thoroughly. Also, it is important that the student makes himself familiar with examples from literature, even to the point of being able to repeat the designs of the proposed controllers and test them within a simulation environment.

Beyond gaining the necessary background knowledge, it was important that the student obtain a model for a helicopter system that is compatible with PBC design techniques. PBC is usually based on two different but related forms of modelling. One is Euler-Lagrange modelling [22]. Newer research focusses more on the second form, namely Port-Hamiltonian modelling [23, 24]. Thus, the student needs to adapt a model available from literature to the appropriate form to accommodate the chosen PBC technique.

These first two issues are foundational ones, intimately related to the literature on the subject. The design of the control system itself is newer work. While there are several examples of PBC being applied to quadrotor systems [5, 29, 30], the application of PBC to a helicopter system is a new adaptation to such work. The rigid body equa-

tions for both aircraft are very similar, but the way that the actuators interact with the environment is different.

Special attention should be given to validation of the control system. It was important that the sufficient proof for confidence in the stability of the system be presented. This study should show that the control system compares favourably with other control systems or at least with the accuracy that may be expected of the control system as compared to the accuracy of a competent pilot. Such comparison requires the development of an acceptable procedure for testing the controller. It is accepted that this may be done within a simulation environment. These tests need to satisfy external moderators that the control system would be likely to perform sufficiently well in real-world situations. Finally, the questions mentioned in the problem statement of section 1.2 need to be addressed.

1.4 PROJECT SCOPE

Given the nature of the study and the considerations mentioned above, the scope was specifically limited to the study of PBC. With continued study, it was further decided to limit the focus even further to the application of IDA-PBC. This decision will be properly motivated within the critical literature review of this dissertation. The reader will find this in section 2.4 of chapter 2.

At the beginning of this study, there existed the possibility of a concurrent study to develop an experimental helicopter platform for the university. If such a platform were available, it would be an ideal test bench for the control algorithm developed within this work. Sadly, the platform was not developed. However, it should be clearly stated that such work does not form part of the scope of this study.

The project scope expected the studentto develop at least a stable controller. It is possible that the controller would not hold significant accuracy and efficiency benefits. In this case, the student is expected to offer validated comments on these characteristics.

The previous studies mentioned in section 1.1 above made use of real world data of a full-scale helicopter to validate the control algorithms. This approach would also be available for this study if a more appropriate alternative could not be found. This would require scaling of the model to the full size of a commercially produced helicopter. Of course, there are restrictions to the data that may be made available to this project. An important part of the project scope is the decision that the work be limited to the available data.

One final aspect of the scope is worthy of mention. It is accepted that additional work may be required on a interface between the controller and the actual system. Since the controller is expected to work for helicopters in general, specific interfaces between the particular helicopter system and the controller would need to be developed if this system is to be implemented. This study is focussed on answering the questions about PBC for helicopters, not implementing it on a physical system. This was an important consideration because an aircraft is not necessarily available to deploy the control system on that aircraft.

1.5 METHODOLOGY

A broad view of the methodology of this project is illustrated in figure 1.1. This methodology directs the research from the research questions to the final validation

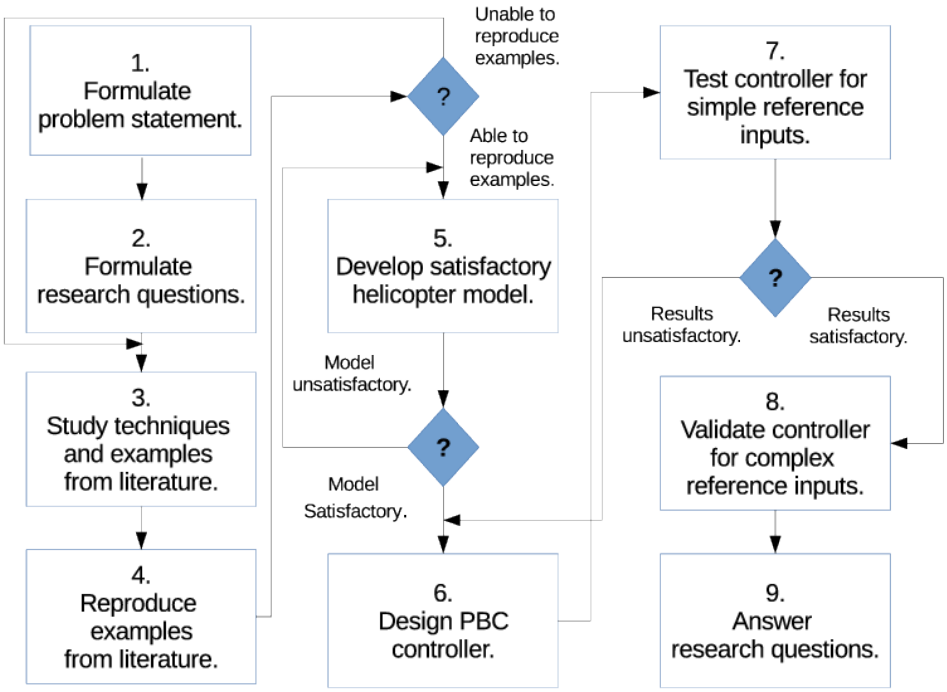

Figure 1.1: Research methodology

and answering of the said questions. Several review opportunities are included in the methodology. These are also indicated on the figure 1.1.

The reader's attention is specifically directed to step 3. This is the literature survey and study sections that is discussed in chapters 2 and 4 respectively. Attentive readers will notice that much of the literature about PBC is authored by Romeo Ortega [4, 21–24] and Arjan van der Shaft [23, 24]. However, the work by Dorfler et al. [6] is also highlighted for the readers attention. These works are foundational to this part of the methodology.

A very important part of the methodology is the process of reproducing examples from literature, as noted in step 4. This entails the detailed study of the model and the controller design until the control law could be reproduced and simulated. This process is repeated for a two-tank process from [6], the Magnetic Levitation (MAGLEV) example from [24] and the quadrotor example from [30]. This strategy affords considerable understanding about the controller design methodology.

The helicopter model of step 5 is discussed in chapter 3. The modelling procedure is wholly based on Newton's laws of motion for rigid bodies. Within the literature, this is a very common method for modelling aircraft.

Step 6 only entails the application of the knowledge gained from steps 3 and 4. During this process, extensive use is made of the Maple™ software package, because it is so considerably adept to handling symbolic calculations.

For the testing and validation of the control system, the MATLAB® SimuLink™ environment is used extensively. These procedures are represented by steps 7 and 8. MATLAB® is also used to evaluate the control benefits, stability and energy efficiency of the system.

1.6 DISSERTATION OUTLINE

Throughout this dissertation, the chapters focus on the *what*, *why* and *how* questions of the topic at hand. The reader may read the chapters with that in mind. Each chapter tries to explain *what* the concept entails and *what* option was selected among those available. Often, reasoning for that choice is inter-weaved into the discussion. As a result, one cannot clearly differentiate between the *what* and *why* part of the discussion. Only once the concept and reasoning behind it has been explained, will the discussion progress to *how* the concept is implemented. It is hoped that the reader will experience this as the most logical progression of thoughts. The discussion below offers a brief outline of each chapter within the context of these *what*, *why* and *how* headings.

This first chapter about the basic motivation and scope of the study is followed by a critical literature review. Chapter 2 delivers introductory information about PBC and its applications. The reasoning for why this is beneficial for control system design is offered within sections 2.2.1 to 2.2.4. Section 2.3 offers a critical evaluation of the Lagrangian and port-Hamiltonian approaches to PBC with the aim of providing the background to how one selects the most appropriate type for an application. Chapter 2 does not go into the finer details of IDA-PBC design, but does offer a motivation for the choice to limit the scope of the project to this form of control.

Chapter 3 gives an in-depth discussion of the modelling of a helicopter system using rigid body equations. The modelling procedure is first explained at a high-level. It also includes a discussion of the Coriolis effect and gyroscopic forces. It also notes why these are included or ignored. The chapter then continues to explain how the model is derived in a top-down approach. Finally, readers will find a discussion of how this model is restructured into a port-Hamiltonian format. A conclusion to the chapter discusses special observations regarding the model. Readers will find this chapter to be concise and foundational to the following chapter that focusses on the controller design.

Chapter 4 focusses on various levels of detail of the information about IDA-PBC and trajectory tracking IDA-PBC. In essence, this is a *how* chapter. However, the chapter begins with preliminary assumptions and design objectives of regular IDA-PBC. This serves to explain what the design procedure begins with and why the options are selected as presented. The discussion progresses to a detailed discussion of how regular IDA-PBC is implemented, from the use of matching equations through to the solving of the control law. The chapter extends the concepts of regular IDA-PBC to trajectory tracking IDA-PBC.

A concerted effort is made to accommodate readers with no knowledge of PBC. With focussed study, readers are expected to be able to understand all the methods discussed within this dissertation from the material contained within chapter 4. Proofs of the principles, where they are applicable, are only referenced within this text. This allows the material to serve as a layman's guide to the application of PBC theory to a control problem such as the trajectory tracking control and flight stabilization.

Chapter 5 applies the techniques from chapter 4 specifically to the helicopter control problem. The chapter begins with an introduction to the notation and the ways that this design procedure satisfies the requirements for IDA-PBC. A detailed discussion follows to explain how the potential and kinetic energy terms are obtained and how the matching equations are solved. It also explains how damping may be added to improve the stability of the response. The chapter is concluded with a discussion of pitfalls and testing procedures that proved valuable during phased of the project. The

design procedure is based on the model from chapter 3. It discusses the procedure in sufficient detail for the reader to reproduce the results. The chapter also shows the method for selecting the free parameters that are introduced into the controller design equations.

Chapter 6 begins with a discussion of validation procedures within the literature. It also explains why a specific procedure is selected for this system within the context of what data is available to the project. The chapter progresses toward a procedure for selecting reference trajectory as inputs to the control system. It also presents the validation test results for one manoeuvre of the control system.

By the nature of use of Newton's laws of motion for the modelling of the helicopter system, the model does not need to be specifically validated. To perform such validation, it would be necessary to measure the forces and the states of the system. Such data is not available to the project. Instead, practical measurements of a large-scale helicopter are used to input an estimated trajectory to the control system. The control system then performs the necessary calculations to follow that trajectory. The flight trajectory proposed by the model is then compared to the reference input to ensure that the control system would induce accurate flight comparable with the expected behaviour of a real-world system.

The dissertation is concluded with chapter 7. Comments on the observations of the study and recommendations for future research are offered here. Answers to the questions that were introduced in section 1.1 are also presented.

Two Appendixes follow this final chapter. These document the work done to gain a thorough understanding of the PBC technique. It also presents validation results for three additional flight manoeuvres.

2

CRITICAL REVIEW OF THE LITERATURE

Chapter 1 mentions very specifically that this study will focus on helicopters. To this end, a brief review of helicopter modelling is given within this review. The more complete model derivation is discussed in chapter 3.

Chapter 1 also states that the primary focus of this study is PBC and more particularly IDA-PBC. The main benefit of this technique is its application to non-linear systems and the fact that it is an optimal control technique. However, the reader may not be completely familiar with the motivation for the study of non-linear control in itself. This review discusses such a motivation from the literature. It then continues with a critical review of PBC, its applications, implementations and benefits. A motivation for the high quality of its stability is also included. The chapter is closed with a critical review of the various forms of PBC and explains why IDA-PBC was selected for this study.

2.1 MODELLING OF HELICOPTERS

Within a large variety of literature resources [9–11, 32], derivation of the 6-Degree-of-Freedom (DOF) model is begun with the rigid body equations for a aircraft. The same approach is taken in Chapter 3. The purpose of this section within the literature review is not to reproduces these equations, but to inform the reader of their existence. The complete derivation is rather included within its own chapter for ease of reading.

Both Hald et al. [10] and Hager [9], discuss a "top-down" approach to modelling a helicopter. Their approach is illustrated in figure 2.1. A similar approach is discussed by Koo et al. [11], but with the modelling effort divided into four levels. However, all these approaches work from the pilot inputs of u_{lat}, u_{lon}, u_{col} and u_{yaw} to ultimately describe the position and orientation variables that may be used as states of the helicopter system.

2.1.1 *Rigid body equations*

The rigid body dynamics are stated within the Force-to-state equations of figure 2.1. These are based on Newtonian mechanics, but take into account the fact that the Earth Reference Frame (EF) is not entirely an inertial reference frame. The assumption is made that the surface of the EF is uniformly flat and extends infinitely in all directions [32]. Though one would want the reference frame to be stationary, the fact is that it is not. The Coriolis effect does have an effect and should be taken into consideration. If one does, one can approach the EF as an inertial reference frame.

The rigid body equations are, however, considerably simpler to model from a Body Reference Frame (BF). This is also the approach of all the above sources. The position coordinates are an exception, however. Position must be described relative to an inertial reference frame like the EF. Velocity, acceleration, angular velocity and angular acceleration may all be described within the BF. The Euler angles and Euler rates are

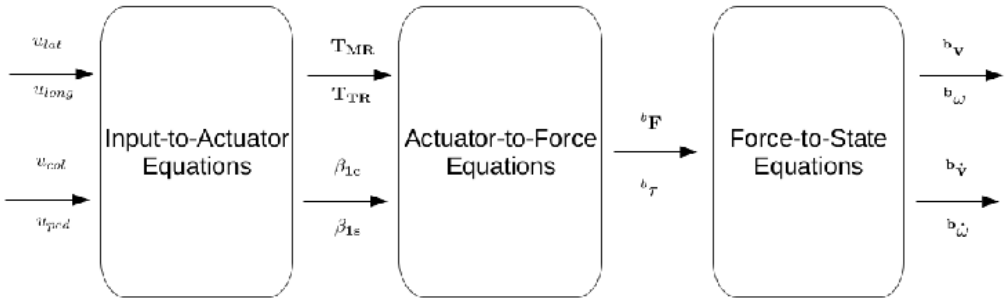

Figure 2.1: Three levels of modelling

described within the Spatial Reference Frame (SF), which shares its position with the BF, but its orientation with the EF.

2.1.2 *Force and torque equations*

The forces and torques acting on the rigid body are used as inputs to the first level of modelling. However, they are also the outputs of the second level. The forces on the rigid body are produced by the thrusts of the main and tail rotors. Because these forces do not act directly at the centre of mass, torques are also produced. The moment arms of these torques are shown in figure 2.2.

The main rotor primarily applies upward thrust, that is to say in the positive $z-$direction if your axis is defined to face upward through the rotor of the helicopter. To allow for forces from the main rotor to act in both the $x-$ and $y-$direction, an allowance is made for changing the Tip-Path-Plane (TPP) angles. The orientation of these TPP angles is illustrated in figure 2.3. A change in the TPP angles allows the thrust to produce a pitch or a roll motion. These TPP angles form part of the second level of modelling.

While the use of TPP angles is very popular in literature [9–11, 32], it is a conceptual angle that can be modelled. In practice, however, it is not so easy to measure. [10] describes equations for the TPP angles. Therefore, one can calculate their values as long as one has the correct system parameters. [32] also determined values for these angles by a system identification procedure, but measurement of the TPP angles is a complex issue, so complex that certain aerospace designers don't even make the effort to do so. The simplest way to measure the TPP angles is to make use of high-speed cameras, but one would need to extract the angle information from each image frame, which is again a complex procedure. For that reason, the TPP angles are noted within this work, but not necessarily used within the controller design.

2.1.3 *Input-to-thrust equations*

The first level of modelling as noted in figure 2.1 is the one that translates the inputs from the pilot on the helicopter controls to the thrusts and TPP angles. The equations that model these actuator dynamics are very complex and will usually require recursive solving [10]. This is brought about by the fact that two of those dynamic equations are dependent on each other. Fortunately, Hald [10] reports that only about five iterations are necessary to solve for these variables.

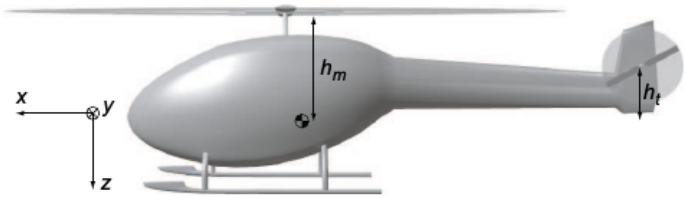

(a) Side view of the helicopter. h_m is the distance from COG to the main rotor, and h_t is the distance from COG to the tail rotor (both along the z axis).

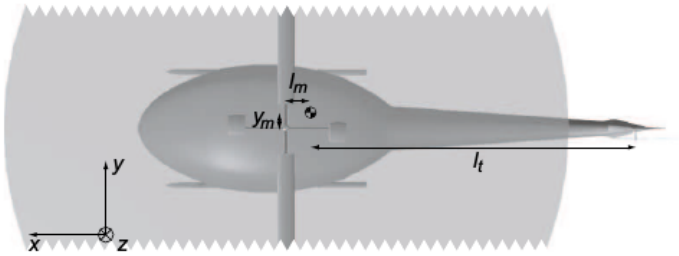

(b) Top view of the helicopter. l_m is the distance from COG to the main rotor, and l_t is the distance from COG to the tail rotor (both along the x axis). y_m is the distance from COG to the main rotor along the y axis.

Figure 2.2: Illustration of the moment arm distances of ${}^b\tau$ [10]

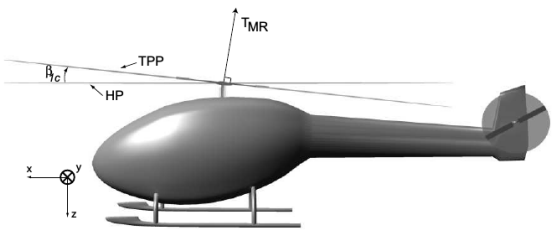

(a) A side view of the helicopter depicts β_{1c} used to denote the longitudinal flapping (angle between the HP and TPP).

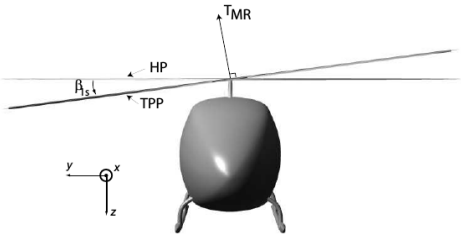

(b) A front view of the helicopter depicts β_{1s} used to denote the lateral flapping (angle between the HP and TPP).

Figure 2.3: Illustration of the longitudinal and vertical TPP angles [10]

The challenge with these equations is again the issue of obtaining the relevant parameters. It is not necessarily a given fact that the designers of a helicopter system are able to supply those parameters. This may simply be because the designers never found that parameter to be important. They may have linearised the dynamic behaviour or simply considered the parameter irrelevant to a functional design. That is certainly the case for the helicopter system that was considered for this project. For that reason, this level of modelling is also ignored for the model derivation and controller design.

2.1.4 *Transformation between reference frames*

Section 2.1.1 made brief mention of the three reference frames that are important for modelling helicopters. Many readers will be familiar with the concept that transformation of coordinates between these various reference frames is an important aspect of modelling. This is no different for helicopters. The objective of this section is not to explain the theory of how such transformations are derived. The interested reader is encouraged to read the explanation by Hald [10] for a brief overview of the transformation of angular velocities between the BF and the SF. This is important for determining Euler rates from the angular velocity vector and vica versa. Both forms are important for the rigid body modelling.

The rotational velocity vector $\omega = \begin{bmatrix} p & q & r \end{bmatrix}$ is given by

$$\underbrace{\begin{bmatrix} p \\ q \\ r \end{bmatrix}}_{\omega} = \underbrace{\begin{bmatrix} 1 & 0 & -\sin(\phi) \\ 0 & \cos(\phi) & \sin(\phi)\cdot\cos(\theta) \\ 0 & \sin(\phi) & \cos(\phi)\cdot\cos(\theta) \end{bmatrix}}_{P_{BS}(\Theta)} \cdot \underbrace{\begin{bmatrix} \dot{\phi} \\ \dot{\theta} \\ \dot{\psi} \end{bmatrix}}_{\dot{\Theta}}, \tag{2.1}$$

where where $\Theta = \begin{bmatrix} \phi & \theta & \psi \end{bmatrix}^{\mathsf{T}}$ are the Euler angles for the roll, pitch and yaw variables respectively.

The inverse relationship is also true and the transformation matrix $P_{BS}(\Theta)$ that transforms SF coordinates to BF coordinates is precisely the inverse of $P_{SB}(\Theta)$. The readers should note that the convention for the subscripts lists the frame symbols in a *to-from* order. The inverse of equation (2.1) is given by

$$\underbrace{\begin{bmatrix} \dot{\phi} \\ \dot{\theta} \\ \dot{\psi} \end{bmatrix}}_{\dot{\Theta}} = \underbrace{\begin{bmatrix} 1 & \sin(\phi)\cdot\tan(\theta) & \cos(\phi)\cdot\tan(\theta) \\ 0 & \cos(\phi) & -\sin(\phi) \\ 0 & \sin(\phi)/\cos(\theta) & \cos(\phi)/\cos(\theta) \end{bmatrix}}_{P_{SB}(\Theta)} \cdot \underbrace{\begin{bmatrix} p \\ q \\ r \end{bmatrix}}_{\omega}.$$

2.1.5 *Rotation between reference frames*

Just like the transformation matrices, there also exist rotation matrices. These transform positions from the BF to the SF or vice versa[10, 32]. In the case of rotation matrices, the rotation order is important. The standard rotational sequence from the SF to the BF requires the rotation first about the roll-axis, then the pitch-axis and finally the yaw-axis. These are respectively the $x-$, $y-$, and the $z-$axes. Unfortunately, the

transformation matrices are arduous to show. To make the illustration easier, cosine and sine arguments are indicated with the symbols s and c.

$$
{}^{\mathbf{B}}\mathbf{x} = \underbrace{\begin{bmatrix} c(\theta)c(\psi) & s(\phi)s(\theta)c(\psi) - c(\phi)s(\psi) & c(\phi)s(\theta)c(\psi) + s(\phi)s(\psi) \\ c(\theta) \cdot s(\psi) & s(\phi)s(\theta)s(\psi) + c(\phi)c(\psi) & c(\phi)s(\theta)s(\psi) - s(\phi)c(\psi) \\ -s(\theta) & s(\phi)c(\theta) & c(\phi)c(\theta) \end{bmatrix}}_{R_{BS}(\Theta)} \cdot {}^{\mathbf{S}}\mathbf{x}.
$$

A transformation from SF to BF positions is given by

$$
{}^{\mathbf{S}}\mathbf{x} = \underbrace{\begin{bmatrix} c(\theta)c(\psi) & c(\theta)s(\psi) & -s(\theta) \\ s(\phi)s(\theta)c(\psi) - c(\phi)s(\psi) & s(\phi)s(\theta)s(\psi) + c(\phi)c(\psi) & s(\phi)c(\theta) \\ c(\phi)s(\theta)c(\psi) + s(\phi)s(\psi) & c(\phi)s(\theta)s(\psi) - s(\phi)c(\psi) & c(\phi)c(\theta) \end{bmatrix}}_{R_{SB}(\Theta)} \cdot {}^{\mathbf{B}}\mathbf{x}.
$$

2.2 INTRODUCTION TO PBC AND ITS APPLICATIONS

To understand PBC, one first needs to understand what passive systems are. Passive systems are a class of dissipative systems for which the input $\mathbf{u} \in \mathbb{R}^m$ and the output $\mathbf{y} \in \mathbb{R}^n$ satisfy the requirement that the term $\mathbf{u}^\intercal\mathbf{y}$ has units of power. The term $\mathbf{u}^\intercal\mathbf{y}$ is called the supply-rate function [20, 22]. PBC is a controller design methodology that aims to render a closed-loop system passive [22, 24]. This simply means that the system obeys the law of conservation of energy [20], and thus obeys an energy-balancing equation.

The multidisciplinary application of PBC has greatly supported its development during the past two decades. Ortega *et al.* [22] mention a tremendous range of applications that they had applied PBC to. They focused primarily on the fields of power electronics, especially DC-to-DC and AC-to-DC converters as well as AC and induction motors. They have even investigated the problem of low frequency oscillation suppression in power systems. Furthermore, they note the application of PBC to robotics in several chapters of their book [22].

An application that may seem more surprising is the use of PBC in dynamic damping of vibrations in a civil structure [22]. The Norwegian University of Science and Technology has done much research intimately related to PBC by applying controlled Lagrangians to underwater vessels [14, 22]. PBC has also found its way into the control of chemical processes [6, 36, 37], spacecraft [2, 7], aerial dynamics of a quadrotor [5, 29, 30], and the transient stabilisation of power systems [15]. [24] also notes its use in MAGLEV and mass-balance systems. The range of passive systems that may be controlled by Lagrangians and Port-Hamiltonian formulations are indeed varied and offer application to a wide range of engineering disciplines.

Because PBC is a non-linear control technique, it's applications are most often focussed on non-linear control problems. The most recent developments in the area of control theory are almost exclusively in the area of non-linear control. This is largely because the field of linear control theory is so well developed [22]. For more than two decades, researchers have been motivating the benefits of non-linear control. Its ability to capture the true behaviour of the system so much more accurately is one supportive argument [22]. Murray [19] states that understanding about the geometric behaviour of mechanical systems is suppressed through linearisation. Geometric behaviour can

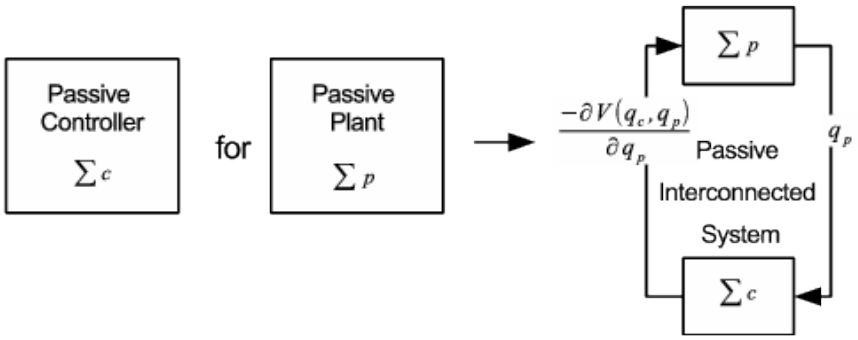

Figure 2.4: Structure-preserving interconnection

be used to improve the global behaviour of the system by means of better control laws, but that information is lost within linear models.

Murray [19] goes further to point out the importance of non-linear control for a certain class of control problems. This particular class is concerned with the planning and trajectory tracking of systems such as "unmanned or remotely piloted aeroplanes performing surveillance and inspection tasks." This is precisely the type of work relevant to RWUAVs. Other examples include as robots that performs medical inspections and operations within the human body. A final example is the use of mobile robots surveying the surface of Mars. As Murray[19] states, "All these systems are highly non-linear and demand accurate performance."

From these arguments, one can certainly see the value of studying PBC for applications such as RWUAVs. However, the field of non-linear control also includes backstepping control or model predictive control. Many of these have been explored for RWUAV applications [25, 30]. Das et al. [5] worked to blend backstepping control with the Lagrangian form of dynamics which is often, though not exclusively, associated with PBC. Roy et al. [27] blended backstepping and PID control. There are a large number of variations, each with its associated benefits. However, discussing these benefits within this work does not form part of the scope of this study. As noted in section 1, the scope was limited to the study of PBC.

Section 2.3 will discuss the Lagrangian and port-Hamiltonian forms of PBC in greater detail. Within this introduction, it is only necessary that the reader understand that there are two approaches. The Lagrangian method was developed first, but in latter literature, the port-Hamiltonian approach is favoured.

2.2.1 *Modelling benefits*

PBC makes the control methodology simpler because it does not require full state feedback [22]. The input-output properties linked to PBC allow the designer to interconnect two passive subsystems whilst preserving their passivity, provided that some preliminary conditions are met. Without discussing the technicalities and proofs, figure 2.4 illustrates more intuitively what is meant by this property. Similarly, systems may be decomposed [22, 24] as shown in figure 2.5. These properties were specifically noted for Lagrangian systems, but Wang [35] noted a similar property for Hamiltonian applications. It is useful to know that these properties are available before embarking on the use of the PBC. These properties add confidence in the applicability of the theories to RWUAV applications.

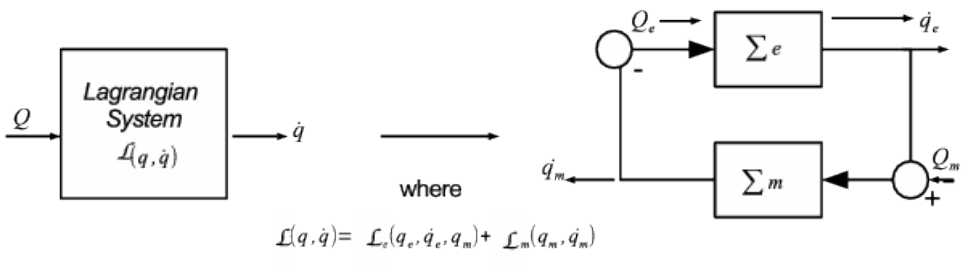

Figure 2.5: Decomposition into subsystems

Literature indicates that the modelling framework offers additional benefits specifically within the IDA-PBC approach. Though this technique will be discussed in greater detail within section 2.3.2 and chapter 4, these benefits are mentioned here for the sake of completeness.

The energy-based modelling methods may be applied to multi-domain systems, such as electromechanical systems, with greater ease [20, 22, 23]. Furthermore, the port-Controlled Hamiltonian framework groups the dynamic variables together for more intuitive understanding. It even allows one to define which states exchange energy among each other by shaping the interconnection-matrix $\mathbf{J(x)}$. Similarly, one may, to a degree, influence the rate of the response is by determining the values within the dissipation-matrix $\mathbf{R(x)}$. Lastly, the equilibrium points are influenced by the energy function $\mathbf{H(x)}$ [20]. Specifically referring to IDA-PBC, [6] summed this up by saying, "This Passivity-based approach to non-linear systems is superior over cancelling out nonlinearities and assigning high gain feedback because it can be interpreted physically."

The multi-domain quality of energy offers another benefit, not only to the modelling aspect, but also the control which is discussed further in section 2.2.2. The "energy" focus allows the designer to do the modelling and control from a single framework [20]. It is one that is commonly understood over various disciplines of engineering. In fact, [24] called energy concepts the *"lingua franca"* among various engineering disciplines.

The single modelling and control framework is opposed to a time domain modelling and a frequency domain controller design. Of course, time domain controller design, such as state-space design, is possible, but this is limited to linear systems. According to [20] and [24], the design of controllers becomes more intuitive when viewed from an energy-shaping perspective, which allows one to move away from approaching controllers as signal processors. In some cases, it can be beneficial to see how the controller effects the stability of the system when viewed as an energy-transforming system [18, 24]. The modelling framework may also help the designer to see what effect the different variables have on the dynamics of the system. The benefits of approaching the controller design from the energy system perspective over the energy processing perspective is even further elaborated upon in [24]. For general control applications, it is important that neither of the approaches be rejected quickly. Koon and Marsden [12] point out that the two approaches have contributed toward each other. For instance, the failure of the Poisson bracket to satisfy the Jacobi identity was noticed when working on the Hamiltonian formulation. On the other hand, the advantage of the momentum equations and the construction equations were first no-

ticed when working on the Lagrangian formulation. It is important is to be aware of the fact that working with one formulation may indeed bring insight into the other formulation. This may be particularly relevant when working on a complicated system such as the control of an autonomous helicopter.

2.2.2 *Controller design benefits*

Two benefits worthy of mention are the fact that that Euler-Lagrange and port-Hamiltonian systems define passive maps [22, 23] and that the storage function may be determined to be the total energy of the system. The benefit of this property is the ability of passive maps to point out the variable that may be controlled most easily. It also points the designer to the choice of a good storage function. PBC offers all of these benefits within a very performance-oriented control method. In fact, Ortega et al. wrote in [22], "After optimal control, this is the most performance-oriented technique in control theory."

From a non-linear control perspective, PBC simplifies the controller development strategy. Ortega et al. state that monolithic theory for the non-linear control is simply too difficult for such a vast array of different systems [22]. PBC has at least served for some form of unification for non-linear control theory, albeit that not all systems may be described as passive. It was shown in section 2.2 that PBC has been applied to a very large variety of fields. Thus, control of these varied systems may at least be approached with a similar set of effective tools.

Naudé [20] did a very interesting study on various energy-shaping control techniques and showed how phase portraits may ease the design and analysis of control systems within the energy framework. He also showed the value of phase portraits for understanding non-linear system dynamics. This understanding can be incorporated into more intuitive controller design. Though this approach is not applied within this paper, it supports the case to be made for the use of PBC techniques as a relatively simpler method of non-linear control.

2.2.3 *Stability benefits*

Although technically also part of the controller benefits, the stability benefits of PBC are discussed here under their own heading to highlight their importance. It is well known that PBC yields a robustly stable controller [8, 22]. In fact, Dorfler et al. [6] pointed out that for the general control problem, "PBC always guarantees certain robustness with regard to input uncertainties." This high quality of stability is partly facilitated by the stringent criteria used to evaluate the stability. The inverse optimality properties that apply to passive systems also contribute in this respect [22]. In the control of electrical machines, exponential stability has been proved. The more recent development of IDA-PBC solves for all possible asymptotically stable controllers of port-Hamiltonian systems. This property has been termed the "universal stabilising" property and was mathematically proven by Ortega et al. in 2002 [23].

This high quality of stability is indeed promising, but some of its benefit would be negated if the stability was difficult to evaluate. The "universal stabilising" property helps to ensure stability for all systems controlled by IDA-PBC design. However, successful controller design cannot be guaranteed [23]. Also, one may want to use a different form of PBC, such as the controlled Lagrangian technique, but the "universal stabilising property" does not apply to those systems. Thankfully, PBC lends itself to

Lyapunov stability criteria [3, 20, 23]. Often, the Hamiltonian mechanics of the system may be directly adapted to the Lyapunov storage function [22, 23]. In some cases, passive systems may be stabilised with as little control as a proportional gain [22]. As Naudé [20] stated, "Energy-shaping is at the heart of stability proof of non-linear systems." He pointed out that stability may be analysed by simply considering the sign of the first derivative of the energy, which is very useful when your controller is based on energy considerations.

2.2.4 *Energy efficiency benefits*

Chapter 1 very specifically mentioned the interest of this research project in energy efficiency and the benefits that PBC can bring to this aspect of the control of non-linear systems. The literature makes strong statements about stability and even performance. Within control theory, PBC is a very performance-oriented technique [22]. However, performance is often associated with "fast and smooth responses" and that is not necessarily guaranteed. None of the literature sources cited in this chapter specifically address the issue of efficiency. Ortega et al. [22] do mention the use of PBC for "optimal energy transfer." The impression from literature is also that most examples of applications of PBC are not necessarily tested beyond the realm of simulation. These factor makes a review of energy-efficiency more difficult.

2.3 CRITICAL EVALUATION OF PBC TECHNIQUES

Having considered these various benefits of PBC approaches, the focus now shifts to which technique is most suitable for the application of RWUAV control. As mentioned in section 2.2, the techniques may be broadly divided into port-Hamiltonian approaches and Lagrangian approaches. Both of these approaches are discussed below. Finally, the selection of IDA-PBC for this study is motivated.

2.3.1 *Lagrangian approaches*

Murray [19] notes that Lagrangian mechanics has largely been favoured for control until 1997. He proposes that at least one of the reasons for this is that several forces such as constraint and external forces are dealt with more effectively within the Lagrangian framework. Port-Hamiltonian approaches appear mostly after the turn of the century. Bloch and Leonard [2] admit that they have done work using Hamiltonian approaches, but the Lagrangian approach allowed them to develop a more systematic algorithm. What is important to note is that there are different approaches that make use of Lagrangian mechanics. One is the "standard" PBC described in [22, 24]. The other is Controlled Lagrangians as described in [1–3].

From the literature, readers may come under the impression that the Controlled Lagrangian and similar techniques are used exclusively for potential energy-shaping. This is possibly led on by references to kinetic energy shaping that proved inadequate for the application such as that discussed by Secchi *et al.* [29] and Ortega and García-Conseco [21]. Also, [23] state, "Unfortunately, for applications that required the modification of the kinetic energy, the closed-loop—although still defining a passive operator—is no longer an EL system, and the storage function of the passive map

(which is typically quadratic in the errors) does not have the interpretation of total energy."

It is important to note the kinetic energy may be modified even with Lagrangian approaches. It is indeed possible to shape the kinetic energy of the system exclusively [2, 3, 20]. Also, one can shape both the kinetic and potential energy with the Controlled Lagrangian technique [1]. However, this is not necessarily termed "Passivity-based" control.

2.3.2 *Port-Hamiltonian approaches*

The alternative way of approaching PBC is the port-Hamiltonian formulation of the energy equations. Castaños and Ortega [4] provide a classification system for different types of PBC. One of the classes is the Basic Inteconnection and Damping Assignment (BIDA) systems. These are control systems that only modify the energy function of a system described by the port-Hamiltonian formulation. These systems do not make any changes to the interconnection and damping matrices. Also described are Energy-balancing Passivity-based Control (EB-PBC) and IDA-PBC. Of these, IDA-PBC is the most popular [21].

To apply these said techniques, one needs to understand the basic ideas of modelling a system within the port-Hamiltonian framework. This may be begun with a note on the Lagrangian of a system. While the Lagrangian of a system is given by

$$\mathcal{L}(\mathbf{q}, \dot{\mathbf{q}}) \quad = \quad T(\mathbf{q}, \dot{\mathbf{q}}) - V(\mathbf{q}),$$

with $T(q, \dot{q})$ and $V(q)$ the kinetic and potential energy for a system with generalized coordinates q [22], the Hamiltonian is given by

$$H(\mathbf{q}, \dot{\mathbf{q}}) \quad = \quad T(\mathbf{q}, \dot{\mathbf{q}}) + V(\mathbf{q}).$$

It is a simple modification. Also, it is not difficult to determine the port-Hamiltonian equations for many systems, provided that you can describe the energy of the system. This is particularly easy for mechanical systems where the Hamiltonian generally takes the form

$$H(\mathbf{q}, \dot{\mathbf{q}}) \quad = \quad \frac{1}{2}\dot{\mathbf{q}}^{\intercal}\mathbf{D}(\mathbf{q})\dot{\mathbf{q}} + V(\mathbf{q}) \tag{2.2}$$

with $\mathbf{D}(\mathbf{q}) = \mathbf{D}^{\intercal}(\mathbf{q}) > 0$ being the generalized mass matrix [24]. Since helicopters are mechanical systems, this equation applies to the system investigated in Chapter 3.

Within port-Hamiltonian models of mechanical systems, it is common practice to use the momentum variables $\mathbf{p} = \mathbf{D}(\mathbf{q})\dot{\mathbf{q}}$ [30]. With this definition, (2.2) may also be given as:

$$H(\mathbf{q}, \dot{\mathbf{q}}) \quad = \quad \frac{1}{2}\mathbf{p}^{\intercal}\mathbf{D}(\mathbf{q})^{-1}\mathbf{p} + V(\mathbf{q}).$$

Once one is able to described the Hamiltonian of a system, one should be able rewrite a model derived with Newtonian mechanics or even Kirchoff's voltage and current laws in port-Hamiltonian format. Readers who are interested in this process may review [13] found within part III of this dissertation. This work discusses the modelling and control of both an Resistor-Inductor-Capacitor (RLC) model and a MAGLEV

model as discussed within [24]. It also points out a typing error within their [24] and shows system simulations for both examples. Readers who review this article should find much of the basic information about port-Hamiltonian modelling and IDA-PBC design. With careful study, reader should also be able to reproduce the results for the system parameters given within [13].

2.4 CONCLUSIONS

Section 2.2 specifically pointed out that the choice between Lagrangian and port-Hamiltonian approaches should not be made too quickly. However, having reviewed the literature further, the port-Hamiltonian IDA-PBC approach seems to be the most viable choice. Much of the motivation for this choice is done by Secchi et al. [29]. They point out that their objective was to control the entire behaviour of the quadrotor instead of just the potential energy of the system. Their motivation is primarily the accuracy of this approach. Souza et al. [30] chose the same technique without the accuracy motivation. Their focus was simply to make use of a different technique to that of model predictive or backstepping control.

These two articles motivated the choice of IDA-PBC, because it offered a firm level of comparison for RWUAV applications. While Das et al. [5] did derive a Lagrangian model for a quadrotor, their approach was primarily the application of backstepping control. [29] and [30] offered a more secure reference in this regard. From the literature it was seen that significant benefits such as accuracy are offered by IDA-PBC without sacrificing controllability or stability. The definitive introduction to IDA-PBC as prosed Ortega et al. [24] also motivates the benefits of IDA-PBC over the Lagrangian approach. The port-Hamiltonian approach was ultimately more intuitive, and the study naturally progressed toward the IDA-PBC approach. This choice allows the use of all the benefits mentioned in section 2.2 and the model mentioned in section 2.1 can be adapted to the Port-Hamiltonian form as noted within section 2.3.2.

3

DERIVATION OF HELICOPTER MODEL

This chapter offers an overview of the non-linear modelling of a helicopter system. The information is primarily based on the work by a research group of Aalborg University [10] and is supported by [11]. Section 3.1 discusses the modelling approach. Section 3.2 discusses two apparent forces that may be added to the standard Newtonian equations to make these equations applicable to helicopters despite the fact that helicopters no longer move in an inertial reference frame. These two sections serve as an introduction as to what process will be followed and why.

Section 3.3 and 3.4 discusses the modelling equations, which are rewritten in port-Hamiltonian form in Section 3.6. Section 3.5 is included for reference, but the modelling equations are not given. These sections should inform the reader how the modelling approach was implemented. The chapter is concluded with a summary of the important modelling assumptions and decisions discussed throughout the chapter.

3.1 THREE LEVELS OF MODELLING

For the purposes of this study, it is most helpful to compartmentalize the modelling of a helicopter into three levels. This particular compartmentalization was first noted within [10] and also discussed within [9] under different headings. A similar four-level compartmentalization is applied within [11]. Figure 3.1 illustrates the levels that are discussed within this chapter.

The first level obtains actuator dynamics as outputs from the inputs on instruments of the helicopter. The variables u_{lat} and u_{long} describe the lateral and longitudinal inputs on the cyclic stick of the helicopter, respectively. These control roll and pitch angles of the helicopter. They also introduced lateral and longitudinal motion to the helicopter frame [10]. u_{col} describes the collective input that controls the thrust on the main rotor. [10] calls this a heave translatory motion and may be interpreted primarily as movement in the $z-$direction. However, depending on the u_{lat} and u_{long} inputs, thrust will also act in the $y-$ or $x-$directions. The axis-directions are illustrated in figure 3.2.

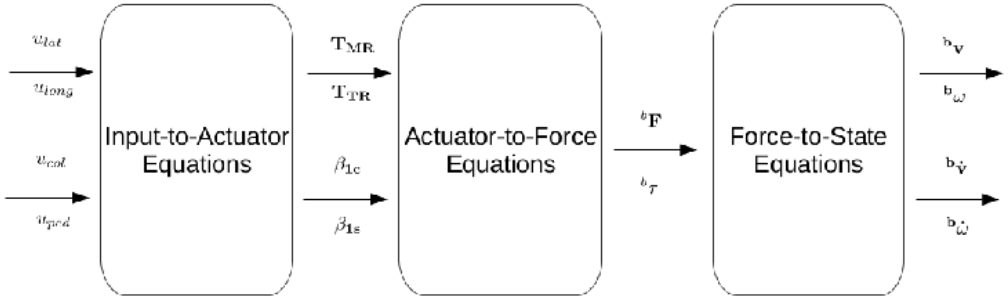

Figure 3.1: Three levels of modelling

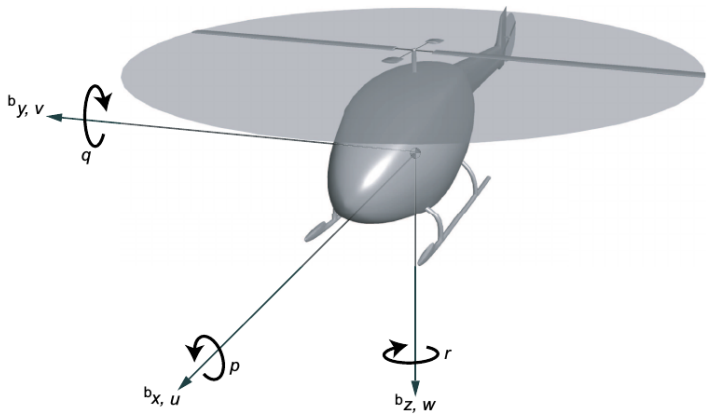

Figure 3.2: Helicopter axis illustration

u_{ped} describes the pedal inputs that control the yaw motion of the helicopter. The thrust of the tail rotor is linked to that of the main rotor, but less or more thrust is added by the input on the pedals to allow the tail of the helicopter to pivot around the $z-$axis, thus producing a yaw motion [10].

The outputs of the first level of modelling are the actuator dynamics. The thrusts of the main and tail rotors are given by T_{MR} and T_{TR} respectively. The TPP angles influence the direction of the thrust relative to the axes of the airframe. These angles are described within figure 3.3.

The second level converts those actuator dynamics into forces and torques along the BF. These forces act in the directions of the $x-$, $y-$ and $z-$axes, while the torques occur about these axes. The torques are produced by moments about the centre of mass of the helicopter airframe. The moment arms are described within figure 3.4.

The third level obtains the system states from the force and torque inputs. The system states are the velocities and angular velocities ${}^{\mathbf{b}}\mathbf{v}$ and ${}^{b}\boldsymbol{\omega}$ as well as their derivatives ${}^{\mathbf{b}}\dot{\mathbf{v}}$ and ${}^{\mathbf{b}}\dot{\boldsymbol{\omega}}$.

Since it is the states that need to be controlled, it is often valuable to begin the derivation of the model from the third level of figure 3.1. This third level models the interconnection between states and the motion produced by forces acting on the rigid body. The interconnection between states of an aircraft model tend to be produced by

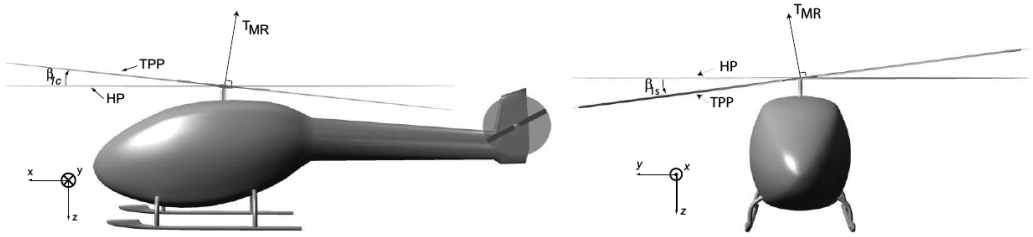

(a) A side view of the helicopter depicts β_{1c} used to denote the longitudinal flapping (angle between the HP and TPP).

(b) A front view of the helicopter depicts β_{1s} used to denote the lateral flapping (angle between the HP and TPP).

Figure 3.3: Illustration of the longitudinal and vertical TPP angles [10]

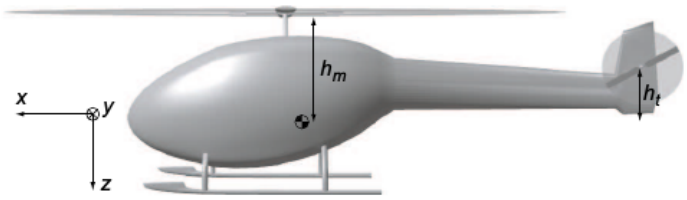

(a) Side view of the helicopter. h_m is the distance from COG to the main rotor, and h_t is the distance from COG to the tail rotor (both along the z axis).

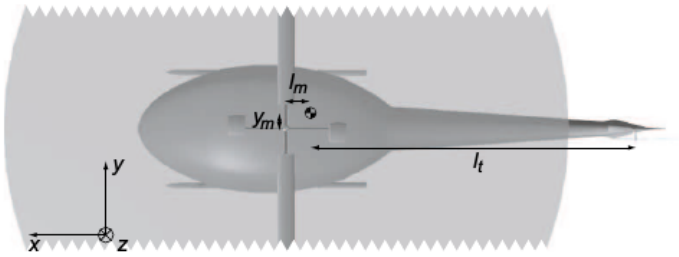

(b) Top view of the helicopter. l_m is the distance from COG to the main rotor, and l_t is the distance from COG to the tail rotor (both along the x axis). y_m is the distance from COG to the main rotor along the y axis.

Figure 3.4: Illustration of the moment arm distances of ${}^{b}\tau$ [10]

gyroscopic forces and the Coriolis effect. If these effects are ignored, the rigid body equations are wholly based on Newton's laws of motion. The choice of whether to include these effects depends on the choice of the designer, but the general trend is to incorporate at least the Coriolis effect for any flying body [9–11, 32].

3.2 GYROSCOPIC FORCES AND THE CORIOLIS EFFECT

Ultimately, the designer may choose to include gyroscopic forces in the model, but within most literature sources, they tend to be ignored [10, 11, 30]. For this reason, and because the total rotational inertia term for the test helicopter was not known, this effect was ignored within this study.

While gyroscopic forces are not typically modelled, the Coriolis effect is included in many models of RWUAVs and especially so for helicopter models. This effect is observed because of the rotating EF below the BF and SF of the RWUAV. From space, it would seem that the RWUAV would be flying in a curved path relative to the earth, even though its inputs only aim for a straight flight path. Figure 3.5 illustrates this concept.

To show the relevance of the Coriolis effect, the model that is derived in section 3.3 below was tested both with the presence of the Coriolis effect and without it, for the same inputs. Figure 3.6 shows the difference in flight position for the two cases. This test was done for a regular quick-stop manoeuvre. For other manoeuvres, one may often find that the Coriolis effect is even more pronounced.

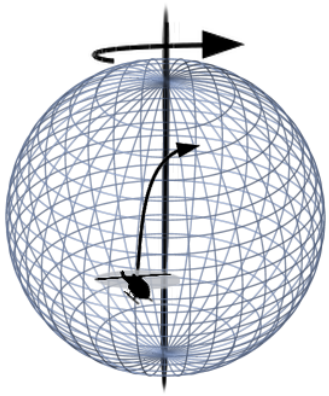

Figure 3.5: The Coriolis effect

The matrix in (3.1) models the Coriolis effect. The configuration variables for the model are the velocities ${}^{\mathbf{b}}\mathbf{v} = \begin{bmatrix} {}^{b}u & {}^{b}v & {}^{b}w \end{bmatrix}^{\mathsf{T}}$ of the centre of mass in the BF and the rotational velocities ${}^{\mathbf{b}}\boldsymbol{\omega} = \begin{bmatrix} {}^{b}p & {}^{b}q & {}^{b}r \end{bmatrix}^{\mathsf{T}}$ of the airframe about the centre of mass in the BF . The I_{ii} terms represent the rotational inertias about the various Cartesian axes, while m represents the mass. The right side of the equation shows a compact notation that is commonly found in literature. Also note how this equation forms part of (3.1) which describes the force-to-state model of the aircraft in (3.2). The matrix $\mathbf{C}(\omega, \dot{\mathbf{x}})$ will later be used within (3.8) to help accommodate the Coriolis effect within the port-Hamiltonian forms of the rigid body equations.

$$\underbrace{\begin{bmatrix} 0 & 0 & 0 & 0 & m\,{}^{b}w & -m\,{}^{b}v \\ 0 & 0 & 0 & -m\,{}^{b}w & 0 & m\,{}^{b}u \\ 0 & 0 & 0 & m\,{}^{b}v & -m\,{}^{b}u & 0 \\ 0 & 0 & 0 & 0 & I_{zz}\,{}^{b}r & -I_{yy}\,{}^{b}q \\ 0 & 0 & 0 & -I_{zz}\,{}^{b}p & 0 & I_{xx}\,{}^{b}p \\ 0 & 0 & 0 & I_{yy}\,{}^{b}q & -I_{xx}\,{}^{b}p & 0 \end{bmatrix}}_{\mathbf{C}(\omega,\dot{\mathbf{x}})} \begin{bmatrix} {}^{b}u \\ {}^{b}v \\ {}^{b}w \\ {}^{b}p \\ {}^{b}q \\ {}^{b}r \end{bmatrix} = \begin{bmatrix} {}^{\mathbf{b}}\boldsymbol{\omega} \times (m \cdot {}^{\mathbf{b}}\mathbf{v}) \\ {}^{\mathbf{b}}\boldsymbol{\omega} \times (\boldsymbol{I_{rr}} \cdot {}^{\mathbf{b}}\boldsymbol{\omega}) \end{bmatrix} \tag{3.1}$$

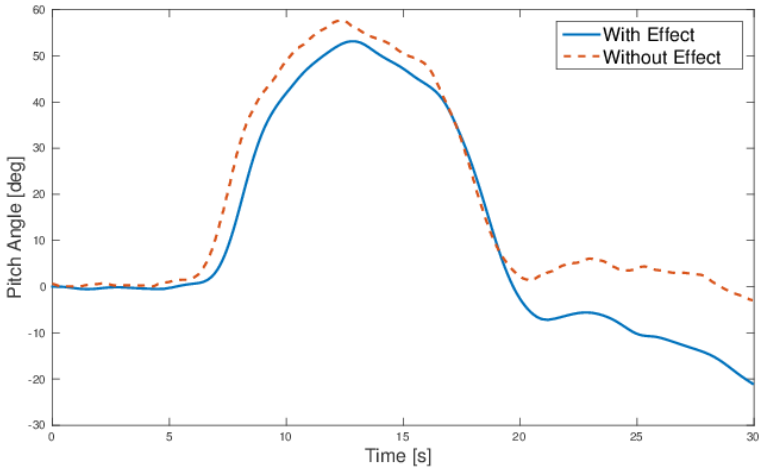

Figure 3.6: Prominence of the Coriolis effect

3.3 FORCE-TO-STATE EQUATIONS

The force-to-state equations are given by

$$\begin{bmatrix} m & 0 & 0 & 0 & 0 & 0 \\ 0 & m & 0 & 0 & 0 & 0 \\ 0 & 0 & m & 0 & 0 & 0 \\ 0 & 0 & 0 & I_{xx} & 0 & 0 \\ 0 & 0 & 0 & 0 & I_{yy} & 0 \\ 0 & 0 & 0 & 0 & 0 & I_{zz} \end{bmatrix} \begin{bmatrix} {}^b\dot{u} \\ {}^b\dot{v} \\ {}^b\dot{w} \\ {}^b\dot{p} \\ {}^b\dot{q} \\ {}^b\dot{r} \end{bmatrix} + \underbrace{\begin{bmatrix} {}^{\mathbf{b}}\boldsymbol{\omega} \times (m \cdot {}^{\mathbf{b}}\mathbf{v}) \\ {}^{\mathbf{b}}\boldsymbol{\omega} \times (\boldsymbol{I} \cdot {}^{\mathbf{b}}\boldsymbol{\omega}) \end{bmatrix}}_{\textit{equation 3.1}} = \begin{bmatrix} {}^bf_x \\ {}^bf_y \\ {}^bf_z \\ {}^b\tau_{xx} \\ {}^b\tau_{yy} \\ {}^b\tau_{zz} \end{bmatrix}, \quad (3.2)$$

with m the total mass of the helicopter in kg and I_{ii} the rotational inertia term about the i-axis in kg $\cdot$ m^2. f_i is the sum of the forces along the $i-$axis, measured in N , while τ_{jj} is the torque about the j-axis, measured in N $\cdot$ m.

Readers will note that these equations are obtained simply with Newton's second law which may be written in general notation as $f = m \cdot \dot{v}$ for translational dynamics and $\tau = I \cdot \dot{\omega}$ for rotational dynamics. Of course, as noted before, the conceptual force of the Coriolis effect from (3.1) is added to account for the rotation of the EF below the aircraft.

(3.2) may be used to model the motion of any form of aircraft from an aeroplane to a quadrotor to a blimp. In the various cases, only the body forces and torques, denoted by ${}^b\mathbf{f}$ and ${}^b\boldsymbol{\o}$ respectively, will differ according to the dynamics of the actuators of each airframe.

3.4 ACTUATOR-TO-FORCE EQUATIONS

To model the forces acting on the airframe in terms of the actuator dynamics, the second level of modelling is used. Specifically for the helicopter, the forces ${}^b\mathbf{F}$ and torques ${}^b\boldsymbol{\o}$ are divided into contributions by the main and tail rotors. The forces generated by the main rotor are given by

$${}^b\mathbf{F_M} = \begin{bmatrix} {}^bf_{x\,M} \\ {}^bf_{y\,M} \\ {}^bf_{z\,M} \end{bmatrix} = \begin{bmatrix} -T_M \sin(\beta_{1c}) \\ T_M \sin(\beta_{1s}) \\ -T_M \cos(\beta_{1s}) \cos(\beta_{1c}) \end{bmatrix},$$

where T_M is the thrust of the main rotor. β_{1s} and β_{1c} are the TPP angles in the lateral and longitudinal directions respectively. They are described within figure 3.3.

The forces contributed by the tail rotor are simpler. The tail rotor acts only in the $y-$direction without any associated angle as in the case of the main rotor.

$${}^b\mathbf{F_T} = \begin{bmatrix} {}^bf_{x\,T} \\ {}^bf_{y\,T} \\ {}^bf_{z\,T} \end{bmatrix} = \begin{bmatrix} 0 \\ T_T \\ 0 \end{bmatrix}.$$

The torques about the axes of the aircraft should take into account various moment arm distances as defined in figure 3.4. The torque contribution by the main rotor is

given by (3.3). Note that a common alternative symbol for the torques, namely L, M and N, are included for the reader's reference.

$$ {}^{b}\boldsymbol{\tau}_{M} = \begin{bmatrix} {}^{b}\tau_{xx\,M} \\ {}^{b}\tau_{yy\,M} \\ {}^{b}\tau_{zz\,M} \end{bmatrix} = \begin{bmatrix} {}^{b}L_{M} \\ {}^{b}M_{M} \\ {}^{b}N_{M} \end{bmatrix} = \begin{bmatrix} {}^{b}f_{y\,M}\,h_{m} - {}^{b}f_{z\,M}\,y_{m} \\ -{}^{b}f_{x\,M}\,h_{m} - {}^{b}f_{z\,M}\,l_{m} \\ {}^{b}f_{x\,M}\,y_{m} + {}^{b}f_{y\,M}\,l_{m} \end{bmatrix}. \tag{3.3} $$

The torques by the tail rotor are given by

$$ {}^{b}\boldsymbol{\tau}_{T} = \begin{bmatrix} {}^{b}\tau_{xx\,T} \\ {}^{b}\tau_{yy\,T} \\ {}^{b}\tau_{zz\,T} \end{bmatrix} = \begin{bmatrix} {}^{b}L_{T} \\ {}^{b}M_{T} \\ {}^{b}N_{T} \end{bmatrix} = \begin{bmatrix} {}^{b}f_{y\,T}\,h_{t} \\ 0 \\ -{}^{b}f_{y\,T}\,l_{t} \end{bmatrix}. $$

The torque equations also include an aerodynamic drag component on the rotors. Because the drag on the tail rotor is considered negligible, it is not included here. For the majority of models, these torques are modelled in a simplified manner by multiplying an aerodynamic drag constant A_{Q} with a function of the torque of the appropriate rotor. To this is added a constant initial drag B_{Q} that is present when the blade pitch is zero.

The main rotor drag is given by

$$ Q_{M} = -(A_{Q\,M}\,T_{M}^{1.5} + B_{Q\,M}). $$

This drag torque can be decomposed into torques about the various axes.

$$ {}^{b}\boldsymbol{\tau}_{MD} = \begin{bmatrix} {}^{b}\tau_{xx\,MD} \\ {}^{b}\tau_{yy\,MD} \\ {}^{b}\tau_{zz\,MD} \end{bmatrix} = \begin{bmatrix} {}^{b}L_{MD} \\ {}^{b}M_{MD} \\ {}^{b}N_{MD} \end{bmatrix} = \begin{bmatrix} Q_{M}\sin(\beta_{1c}) \\ -Q_{M}\sin(\beta_{1s}) \\ Q_{M}\cos(\beta_{1s})\cos(\beta_{1c}) \end{bmatrix}. $$

In this way, the forces and torques acting on the aircraft may be given by (3.4). Note the addition of the gravitational force mgz, with g being the gravitational acceleration. This may be modelled differently if one assumes that the direction of the $z-$axis of the BF will differ significantly from that of the EF. If the helicopter performs aggressive manoeuvres, this will indeed be the case. This would require that the gravitational force be described in orthogonal components in the $x-$, $y-$ and $z-$directions of the BF. Of course, it will always be acting in the $z-$direction of the EF.

For the decomposition of the forces into the orthogonal components, the Euler angles are used. The Euler angles may be obtained from the rotational velocity vector ${}^{\mathbf{b}}\dot{\boldsymbol{\omega}}$. A reference frame transformation as described by section **2.1.4** of chapter 2 is required. (3.4) describes the forces for very small pitch and roll angles. These would be the conditions for hover or near-hover flight. (3.5) shows the same forces while making use of the Euler angles. This equation may be used for more aggressive manoeuvres.

$$ \begin{bmatrix} {}^{b}f_{x} \\ {}^{b}f_{y} \\ {}^{b}f_{z} \\ {}^{b}\tau_{xx} \\ {}^{b}\tau_{yy} \\ {}^{b}\tau_{zz} \end{bmatrix} = \begin{bmatrix} -T_{M}\sin(\beta_{1c}) \\ T_{M}\sin(\beta_{1s}) + T_{T} \\ -T_{M}\cos(\beta_{1s})\cos(\beta_{1c}) + mg \\ {}^{b}f_{y\,M}\,h_{m} - {}^{b}f_{z\,M}\,y_{m} + {}^{b}f_{y\,T}\,h_{t} + Q_{M}\sin(\beta_{1c}) \\ -{}^{b}f_{x\,M}\,h_{m} - {}^{b}f_{z\,M}\,l_{m} - Q_{M}\sin(\beta_{1s}) \\ {}^{b}f_{x\,M}\,y_{m} + {}^{b}f_{y\,M}\,l_{m} - {}^{b}f_{y\,T}\,l_{t} + Q_{M}\cos(\beta_{1s})\cos(\beta_{1c}) \end{bmatrix}. \tag{3.4} $$

$$\begin{bmatrix} {}^{b}f_x \\ {}^{b}f_y \\ {}^{b}f_z \\ {}^{b}\tau_{xx} \\ {}^{b}\tau_{yy} \\ {}^{b}\tau_{zz} \end{bmatrix} = \begin{bmatrix} -T_M \sin(\beta_{1c}) - mg \sin(\theta) \\ T_M \sin(\beta_{1s}) + T_T + mg \sin(\phi) \cos(\theta) \\ -T_M \cos(\beta_{1s}) \cos(\beta_{1c}) + mg \cos(\phi) \cos(\theta) \\ {}^{b}f_{y\,M}\, h_m - {}^{b}f_{z\,M}\, y_m + {}^{b}f_{y\,T}\, h_t + Q_M \sin(\beta_{1c}) \\ -{}^{b}f_{x\,M}\, h_m - {}^{b}f_{z\,M}\, l_m - Q_M \sin(\beta_{1s}) \\ {}^{b}f_{x\,M}\, y_m + {}^{b}f_{y\,M}\, l_m - {}^{b}f_{y\,T}\, l_t + Q_M \cos(\beta_{1s}) \cos(\beta_{1c}) \end{bmatrix}. \quad (3.5)$$

3.5 INPUT-TO-ACTUATOR EQUATIONS

The input-to-actuator equations comprise the third level of modelling. These relate the inputs that the pilot gives on the controls to outputs of thrusts and TPP angles. This is the most complex level of modelling. Hald et al. [10] even included a recursive definition of the main rotor thrust. The flapping of the control-rotor is also a complex procedure which includes the mixing of two sets of parameters derived from the swash plate dynamics. For reference, figure 3.7 graphically illustrates the mixer system. Because these equations are so complex and because they are not used within this work, the specific equations are not discussed here. Instead, interested readers are referred to the work of Hald et al. [10].

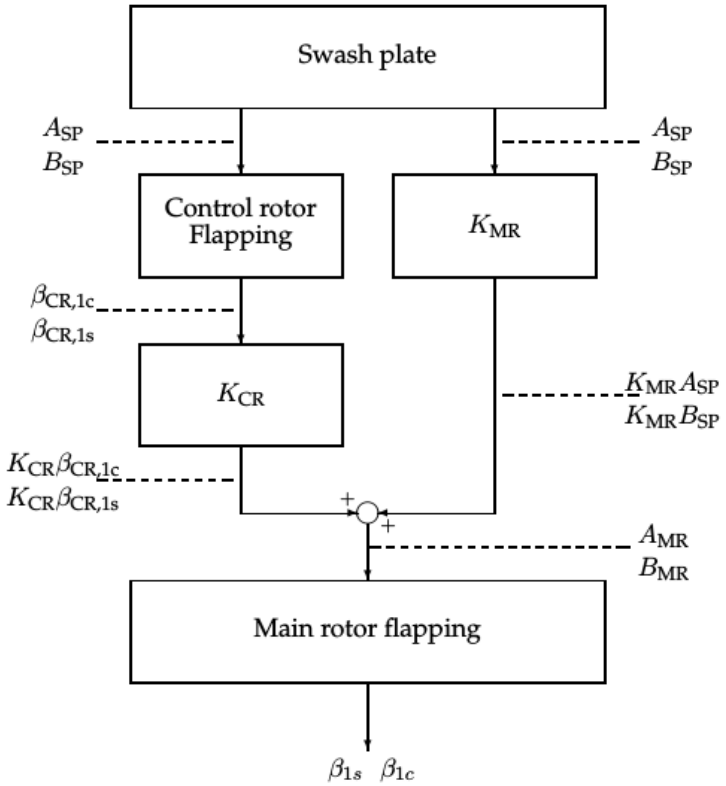

Figure 3.7: Flapping equation mixing within [10]

3.6 RESTRUCTURING OF MODEL

Within the port-Hamiltonian representation of a system, the state vector $\mathbf{x}$ contains both the position variables $\mathbf{q}$ and momentum variables $\mathbf{p} = \boldsymbol{I} \cdot \dot{\mathbf{q}}$. The other important difference adaptation is the use of the Hamiltonian function. In this case of a mechanical system, it consists of the kinetic and potential energies of the system. For the helicopter system, this is given by

$$\begin{aligned} H(\mathbf{x}) &= \frac{1}{2}\mathbf{p}^{\mathsf{T}}\mathbf{M}\mathbf{p} + x\,mg\sin(\theta) - y\,mg\sin(\phi)\cos(\theta) - z\,mg\cos(\phi)\cos(\theta) \quad (3.6) \\ &= \frac{1}{2}\left[\; u^2m + v^2m + w^2m + p^2I_{xx} + q^2I_{yy} + r^2I_{zz} \;\right] \\ &\quad + x\,mg\sin(\theta) - y\,mg\sin(\phi)\cos(\theta) - z\,mg\cos(\phi)\cos(\theta). \quad (3.7) \end{aligned}$$

In a compact notation, the port-Hamiltonian form of (3.2) would then be described by

$$\underbrace{\begin{bmatrix} \dot{\mathbf{q}} \\ \dot{\mathbf{p}} \end{bmatrix}}_{\dot{\mathbf{x}}} = \underbrace{\begin{bmatrix} \mathbf{O_{6x6}} & \mathbf{I_{6x6}} \\ -\mathbf{I_{6x6}} & -\mathbf{C}(\omega, \dot{\mathbf{x}}) \end{bmatrix}}_{\mathbf{Q}(\mathbf{x})} \frac{\partial H}{\partial \mathbf{x}}(\mathbf{x}) + \underbrace{\begin{bmatrix} \mathbf{O_{6x1}} \\ \mathbf{I_{6x1}} \end{bmatrix}}_{\mathbf{g}(\mathbf{x})} \mathbf{u}. \quad (3.8)$$

Here $\mathbf{I_{6x6}}$ represents the 6×6 identity matrix while $\mathbf{0_{6x6}}$ represents the 6×6 zero-matrix. Note the presence of the matrix $\mathbf{C}(\omega, \dot{\mathbf{x}})$ that helps to model the Coriolis equations within $\mathbf{Q}(\mathbf{x})$. The rest of the $\mathbf{Q}(\mathbf{x})-$matrix is simply the identity-matrix and zero-matrix elements. Readers will note that the states are then included within the term $\frac{\partial H}{\partial \mathbf{x}}(\mathbf{x})$, which is given by

$$\begin{aligned} \frac{\partial H}{\partial \mathbf{q}}(\mathbf{x}) &= \begin{bmatrix} mg\sin(\theta) & -mg\sin(\phi)\cos(\theta) & -mg\cos(\phi)\cos(\theta) & 0 & 0 & 0 \end{bmatrix}^{\mathsf{T}} \quad (3.9) \\ \frac{\partial H}{\partial \mathbf{p}}(\mathbf{x}) &= \begin{bmatrix} u & v & w & p & q & r \end{bmatrix}^{\mathsf{T}}. \quad (3.10) \end{aligned}$$

3.7 CONCLUSIONS TO MODELLING APPROACH

3.7.1 *Presence of Euler angles within the Hamiltonian function*

The reader will note the presence of the Euler angles ϕ, θ, and ψ within the Hamiltonian function of the system. Within many models, these angles will also be implemented as states. However, for the purposes of this model, the Euler angles will be considered as a special form of the angular positions within the BF. Within a simulation, this is not difficult to implement, but for notation purposes in this work, it will be both confusing and tedious to indicate Euler angles as transformations of the rotational positions.

Readers may feel that the Euler angles could rather have been included within the input vector $\mathbf{u}$ because they are associated solely with force terms like the rest of the input vector. However, the gravitational terms are included within the Hamiltonian function because of their association with the potential energy of the system.

3.7.2 *Position coordinates within the Earth Reference Frame*

Readers should take note of the fact that the positions of the helicopter should be described relative to a point within a fixed reference frame like the EF. Because of

the conventions with the data used for validation in chapter 6, the EF defined as an East-North-Down coordinate system. Thus, the x-positions point in East, even though the BF x-velocity u points toward the front of the aircraft as given in figure 3.2. These two different conventions sound counter-intuitive, but are necessary to accomodate the model as well as the data supplied for this project.

3.7.3 *Complexity of model*

It is clear that the rigid body equations discussed within section 3.3 are not complex. Also, they are not specific to a helicopter system. It is only within the force equations of section 3.4 that the model becomes specifically a helicopter model. However, only the rigid body equations, or force-to-state equations, are used within the control system design of chapter 5. Thus, the designed control system would be applicable to all forms of aircraft, but would require an interface between the control system signals and the actuators of the aircraft. This was deemed acceptable for the purposes of this study since various forms of actuation exist, even for helicopters. As mentioned within the scope of this project in chapter 1, the purpose of this project is only to evaluate the suitability of IDA-PBC for helicopter control and not necessarily to implement it on a physical system. However, to evaluate the suitability specifically for a helicopter system, the state, mass and rotational inertia terms within 3.2 for an actual helicopter system will be used within the validation tests of chapter 6.

4

FOUNDATIONAL THEORY OF IDA-PBC

Using the port-Hamiltonian representation of the model of Chapter 3, one may embark on the design of a IDA-PBC controller. However, it is important to understand the difference between regular IDA-PBC and trajectory tracking IDA-PBC. Trajectory tracking IDA-PBC is more suited for the purposes of variable-trajectory control. This makes it ideal for helicopter control. It is also an extension of the regular IDA-PBC, and for this reason, the regular method is discussed in detail. Thereafter, the trajectory tracking modifications are presented.

This chapter delves deeper into the literature than Chapter 2. It focuses on the applications of IDA-PBC rather than the mathematical proof of the technique. Stability proofs are not included here. However, a concerted effort is made to include all the practical computations necessary to understand the application of IDA-PBC to control problems. While an understanding of the basic state-space representations of systems and the computation of partial derivatives are assumed, the reader does not require any prior experience in the solution of Partial Differential Equation (PDE)s. Neither is an understanding of Hamiltonian mechanics required. An effort is made to discuss all the practical theory within the sections below. Readers who are interested in additional properties and proofs for this technique are encouraged to study [21, 23, 24, 34].

4.1 REGULAR IDA-PBC

IDA-PBC is based upon the port-Hamiltonian representation of systems. This is simply an alternative representation of the linear or non-linear state-space system as given by:

$$\dot{\mathbf{x}} = \mathbf{F}(\mathbf{x}) + \mathbf{G}(\mathbf{x})\mathbf{u}. \tag{4.1}$$

Instead, the equations of motion are described by:

$$\dot{\mathbf{x}} = [\mathbf{J}(\mathbf{x}) - \mathbf{R}(\mathbf{x})]\frac{\partial H}{\partial \mathbf{x}}(\mathbf{x}) + \mathbf{g}(\mathbf{x})\mathbf{u} \tag{4.2}$$

where:

$\mathbf{x}$ is the state vector.

$\mathbf{J}(\mathbf{x})$ is called the interconnection matrix used to indicate the interconnection between states; it is typically but not always composed of the terms -1, 0 or 1.

$\mathbf{R}(\mathbf{x})$ represents the damping matrix and includes all the dissipation terms, usually in the form of resistances or damping constants.

$\frac{\partial H}{\partial \mathbf{x}}(\mathbf{x})$ is the gradiet of the Hamiltonian function. The Hamiltonian function is composed of the sum of the energies of the system.

$\mathbf{g}(\mathbf{x})$ is the regular input gain matrix.

$\mathbf{u}$ is the regular input matrix.

Note that $\mathbf{J}(\mathbf{x}) - \mathbf{R}(\mathbf{x})$ will be represented as $\mathbf{Q}(\mathbf{x})$ for ease of presentation of the equations.

The simplest way to understand the port-Hamiltonian representation of a system is to review an example of a system modelled in this form. Readers are encouraged to study the modelling of the RLC circuit and MAGLEV system examples in [24]. Readers may also view [13], which is included in part III of this dissertation.

With this basic understanding of the port-Hamiltonian framework for modelling system, one is able to progress to IDA-PBC theory. The theory has developed significantly over the past fifteen years, but it may also be summarized as the author will attempt to do. For that purpose, a good place to start is the basic design objective that IDA-PBC aims to achieve.

4.1.1 *Basic design objectives*

The idea behind the mathematics of IDA-PBC is to match the regular dynamics of a system to a set of desired dynamics by changing the inputs to that system. This design procedure is achieved through matching equations.

Stated differently, the objective of the matching equations of IDA-PBC is to add control terms to the system given by (4.2) in the form of the new input $\mathbf{fi}(\mathbf{x})$. The integrated system can then demonstrate new, desired behaviour. This objective is stated as:

$$\mathbf{Q}(\mathbf{x})\frac{\partial H}{\partial \mathbf{x}}(\mathbf{x}) + \mathbf{g}(\mathbf{x})\mathbf{fi}(\mathbf{x}) \quad = \quad \mathbf{Q_d}(\mathbf{x})\frac{\partial H_d}{\partial \mathbf{x}}(\mathbf{x}). \tag{4.3}$$

The desired forms of the terms, namely $\mathbf{J_d}$ and $\mathbf{R_d}$ which are captured within $\mathbf{Q_d} = \mathbf{J_d} - \mathbf{R_d}$ on the right side of the above equation, serve to assign specific qualities to the interconnection and damping structures. Also, the desired Hamiltonian is chosen to have at least an isolated local minimum at the desired equilibrium point $\mathbf{x}_*$ [6, 23, 24]. This choice of $\frac{\partial H_d}{\partial \mathbf{x}}(\mathbf{x})$ will become more apparent when considering controller stability, but it is sufficient to note here that this is the basis of the excellent stability characteristics offered by IDA-PBC.

4.1.2 *Matching equations*

Based upon the basic design objective of (4.3), the matching equations have been developed even further to make them applicable to a larger range of systems. This applicability is mostly facilitated by additional DOFs that may be added to the equations. The reader will notice that (4.3) is a PDE on account of the $\frac{\partial H_d}{\partial \mathbf{x}}(\mathbf{x})$ term on its right hand side. Solving the PDE is one of the most pertinent challenges of IDA-PBC design [21], but the additional DOFs can be of help to the designer in this regard. The procedure to add these additional DOFs is described in detail below.

In order to alter the inherent Hamiltonian characteristics of the system from $H(\mathbf{x})$ to the new $H_d(\mathbf{x})$, an additional function $H_a(\mathbf{x})$ is added to $H(\mathbf{x})$. This additional function will form part of the term $\mathbf{fi}(\mathbf{x})$. The modification begins with the definition $H_d(\mathbf{x}) \triangleq H(\mathbf{x}) + H_a(\mathbf{x})$. For the sake of simplicity, one may also substitute $\mathbf{J_d}(\mathbf{x}) \triangleq \mathbf{J}(\mathbf{x})$ and $\mathbf{R_d}(\mathbf{x}) \triangleq \mathbf{R}(\mathbf{x})$ into (4.3), such that:

$$[\mathbf{Q}(\mathbf{x}))]\frac{\partial H}{\partial \mathbf{x}}(\mathbf{x}) + \mathbf{g}(\mathbf{x})\beta(\mathbf{x}) \quad = \quad [\mathbf{Q}(\mathbf{x}))]\frac{\partial H}{\partial \mathbf{x}}(\mathbf{x}) + [\mathbf{Q}(\mathbf{x}))]\frac{\partial H_a}{\partial \mathbf{x}}(\mathbf{x}).$$

The terms $[\mathbf{Q}(\mathbf{x}))]\,\frac{\partial H}{\partial \mathbf{x}}(\mathbf{x})$ cancel, resulting in an equation that is specifically used for IDA-PBC design in two of the examples in [24].

$$\mathbf{g}(\mathbf{x})\beta(\mathbf{x}) \quad = \quad [\mathbf{Q}(\mathbf{x})]\,\frac{\partial H_a}{\partial \mathbf{x}}(\mathbf{x}). \tag{4.4}$$

This equation, however, applies to a very simple case. Instead, being able to select $\mathbf{J_d}(\mathbf{x}) \neq \mathbf{J}(\mathbf{x})$ and $\mathbf{R_d}(\mathbf{x}) \neq \mathbf{R}(\mathbf{x})$ allows for additional DOFs when solving for $\beta(\mathbf{x})$. Indeed, the MAGLEV example from [24] illustrates that in some cases, the unmodified interconnection matrix will cause the controller to be unstable; the freedom to chose $\mathbf{J_d}(\mathbf{x}) \neq \mathbf{J}(\mathbf{x})$ is vital for their controller design. One may therefore recognize that it would be valuable to extend upon (4.4) to obtain more freedom.

The energy-shaping objective is not altered if one were to set $\mathbf{J_d}(\mathbf{x}) \neq \mathbf{J}(\mathbf{x})$ and $\mathbf{R_d}(\mathbf{x}) \neq \mathbf{R}(\mathbf{x})$. If one sets $\mathbf{J_d}(\mathbf{x}) \triangleq \mathbf{J}(\mathbf{x}) + \mathbf{J_a}(\mathbf{x})$ and $\mathbf{R_d}(\mathbf{x}) \triangleq \mathbf{R}(\mathbf{x}) + \mathbf{R_a}(\mathbf{x})$, then (4.3) may be simplified as given by (4.5).

$$\begin{aligned}
[\mathbf{Q}(\mathbf{x})]\,\frac{\partial H}{\partial \mathbf{x}}(\mathbf{x}) + \mathbf{g}(\mathbf{x})\beta(\mathbf{x}) \quad &= \quad [\mathbf{Q}(\mathbf{x}) - \mathbf{Q_a}(\mathbf{x})]\,\frac{\partial H_d}{\partial \mathbf{x}}(\mathbf{x}), \\
[\mathbf{Q}(\mathbf{x})]\,\frac{\partial H}{\partial \mathbf{x}}(\mathbf{x}) + \mathbf{g}(\mathbf{x})\beta(\mathbf{x}) \quad &= \quad [\mathbf{Q}(\mathbf{x}) - \mathbf{Q_a}(\mathbf{x})]\left[\frac{\partial H}{\partial \mathbf{x}}(\mathbf{x}) + \frac{\partial H_a}{\partial \mathbf{x}}(\mathbf{x})\right], \\
\mathbf{g}(\mathbf{x})\beta(\mathbf{x}) - [\mathbf{Q_a}(\mathbf{x})]\,\frac{\partial H}{\partial \mathbf{x}}(\mathbf{x}) \quad &= \quad [\mathbf{Q}(\mathbf{x}) - \mathbf{Q_a}(\mathbf{x})]\,\frac{\partial H_a}{\partial \mathbf{x}}(\mathbf{x}).
\end{aligned} \tag{4.5}$$

One may conclude that one needs to understand how to select the appropriate $\mathbf{J_a}(\mathbf{x})$, $\mathbf{R_a}(\mathbf{x})$ and $H_a(\mathbf{x})$ terms to design an IDA-PBC system with this technique. Within the literature, three methodologies have been explicitly defined for selecting these parameters. However, these methodologies are often implemented on forms of the matching equations that have been defined with other conditions to prove stability of the controller. For this reason, the stability conditions and control law are discussed first. The section on the methodologies solving these equations will be discussed in section 4.1.5.

4.1.3 *Formal proposition for stable controllers*

Given a system of the form

$$\dot{\mathbf{x}} = [\mathbf{Q}(\mathbf{x})]\,\frac{\partial H}{\partial \mathbf{x}}(\mathbf{x}) + \mathbf{g}(\mathbf{x})\mathbf{u}$$

with each variable except $\mathbf{u}$ and $\dot{\mathbf{x}}$ known, it is assumed that the system is desired to reach an equilibrium state at a known $\mathbf{x}_*$. If one is able to find variables $\mathbf{J_a}(\mathbf{x})$, $\mathbf{R_a}(\mathbf{x})$ and $\mathbf{fi}(\mathbf{x})$ such that

$$\mathbf{J}(\mathbf{x}) + \mathbf{J_a}(\mathbf{x}) \quad = \quad -[\mathbf{J}(\mathbf{x}) + \mathbf{J_a}(\mathbf{x})]^\intercal \geq 0$$

as well as

$$\mathbf{R}(\mathbf{x}) + \mathbf{R_a}(\mathbf{x}) \quad = \quad -[\mathbf{R}(\mathbf{x}) + \mathbf{R_a}(\mathbf{x})]^\intercal \geq 0$$

and one is able to find a vector function $K(\mathbf{x})$ that satisfies

$$[\mathbf{Q}(\mathbf{x}) + \mathbf{Q_a}(\mathbf{x})]\,K(\mathbf{x}) \quad = \quad \mathbf{g}(\mathbf{x})\mathbf{fi}(\mathbf{x}) - [\mathbf{Q_a}(\mathbf{x})]\,\frac{\partial H}{\partial \mathbf{x}}(\mathbf{x})$$

which is matching equation of (4.5), then one should be able to solve for $\mathbf{u} = \beta(\mathbf{x})$.

If the integrability, equilibrium assignment, and Lyapunov stability conditions listed below hold, then the closed-loop system defined by

$$\dot{\mathbf{x}} = [\mathbf{Q}(\mathbf{x})] \frac{\partial H}{\partial \mathbf{x}}(\mathbf{x}) + \mathbf{g}(\mathbf{x})\beta(\mathbf{x})$$

will be a port-controlled Hamiltonian system with dissipation and will also be described by the equation

$$\dot{\mathbf{x}} \quad = \quad [\mathbf{Q_d}(\mathbf{x})] \frac{\partial H_d}{\partial \mathbf{x}}(\mathbf{x})$$

as stated by (4.3). Note that $\mathbf{J_d}(\mathbf{x}) \triangleq \mathbf{J}(\mathbf{x}) + \mathbf{J_a}(\mathbf{x})$, $\mathbf{R_d}(\mathbf{x}) \triangleq \mathbf{R}(\mathbf{x}) + \mathbf{R_a}(\mathbf{x})$ and $H_d(\mathbf{x}) \triangleq H(\mathbf{x}) + H_a(\mathbf{x})$. Also

$$\frac{\partial H_a}{\partial \mathbf{x}}(\mathbf{x}) \quad = \quad K(\mathbf{x}).$$

The equilibrium $\mathbf{x}_*$ of the closed-loop system will be at least locally stable. If the largest invariant set under the closed-loop dynamics contained in

$$\left\{ \mathbf{x} \in \mathbb{R}^n \cap B \mid \left[\frac{\partial H_d}{\partial \mathbf{x}}(\mathbf{x}) \right]^\intercal \mathbf{R_d}(\mathbf{x}) \frac{\partial H_d}{\partial \mathbf{x}}(\mathbf{x}) = 0 \right\}$$

equals $\mathbf{x}_*$, then the equilibrium $\mathbf{x}_*$ will be asymptotically stable.

The integrability, equilibrium assignment, and Lyapunov stability conditions mentioned above are respectively given by:

1. $K(\mathbf{x})$ should be the gradient of a scalar function so that

$$\frac{\partial K}{\partial \mathbf{x}}(\mathbf{x}) \quad = \quad \left[\frac{\partial K}{\partial \mathbf{x}}(\mathbf{x}) \right]^\intercal.$$

2. $K(\mathbf{x})$, at $\mathbf{x}_*$, should verify

$$K(\mathbf{x}_*) \quad = - \quad \frac{\partial H}{\partial \mathbf{x}}(\mathbf{x}_*).$$

3. The Jacobian of $K(\mathbf{x})$, at $\mathbf{x}_*$, should satisfy the bound

$$\frac{\partial K}{\partial \mathbf{x}}(\mathbf{x}_*) \quad > \quad -\frac{\partial^2 H}{\partial \mathbf{x^2}}(\mathbf{x}_*).$$

□

This proposition first appeared in [24]. Proof for this proposition was later given in [23]. [23] also expanded on these conditions to state that, if one were to fix $\mathbf{J_a}(\mathbf{x})$ and $\mathbf{R_a}(\mathbf{x})$ or even set them equal to zero, which is a common strategy, one can attempt to employ the Moore-Penrose inverse and left-annihilator of $\mathbf{g}(\mathbf{x})$ to set up two PDEs that allow one to solve for the control law. These two PDEs are given by:

$$-\mathbf{g}(\mathbf{x})^\dagger [\mathbf{Q_a}(\mathbf{x})] \frac{\partial H}{\partial \mathbf{x}}(\mathbf{x}) = \mathbf{g}(\mathbf{x})^\dagger [\mathbf{Q}(\mathbf{x}) + \mathbf{Q_a}(\mathbf{x})] \frac{\partial H_a}{\partial \mathbf{x}}(\mathbf{x}) \tag{4.6}$$

$$\beta(\mathbf{x}) \quad = \quad [\mathbf{g}(\mathbf{x})^\intercal \mathbf{g}(\mathbf{x})]^{-1} \mathbf{g}(\mathbf{x})^\intercal \left\{ [\mathbf{Q_d}(\mathbf{x})] \frac{\partial H_a}{\partial \mathbf{x}}(\mathbf{x}) + [\mathbf{Q_a}(\mathbf{x})] \frac{\partial H}{\partial \mathbf{x}}(\mathbf{x}) \right\}. \tag{4.7}$$

The reader may notice that these equations are wholly based on (4.5). Here the left annihilator $\mathbf{g}(\mathbf{x})^\dagger$ of $\mathbf{g}(\mathbf{x})$ is defined such that $\mathbf{g}(\mathbf{x})^\dagger \mathbf{g}(\mathbf{x}) = 0$. For instance

$$\mathbf{g}(\mathbf{x})^\dagger \mathbf{g}(\mathbf{x}) = \begin{bmatrix} 0 & 1 & 0 \end{bmatrix} \begin{bmatrix} 0 \\ 0 \\ 1 \end{bmatrix} = 0,$$

but so also

$$\mathbf{g}(\mathbf{x})^\dagger \mathbf{g}(\mathbf{x}) = \begin{bmatrix} 1 & 1 & 0 \end{bmatrix} \begin{bmatrix} 0 \\ 0 \\ 1 \end{bmatrix} = 0.$$

Clearly, $\mathbf{g}(\mathbf{x})^\dagger$ is not uniquely determined by $\mathbf{g}(\mathbf{x})$ for most systems and one may expect that a different left annihilator may produce a slightly different solution to these equations [21].

Also, to solve for the control law $\beta(\mathbf{x})$, one will need to make use of the Moore-Penrose inverse given by $[\mathbf{g}(\mathbf{x})^\intercal \mathbf{g}(\mathbf{x})]^{-1} g(x)^\intercal$. This form is used as opposed to the regular matrix inverse since $\mathbf{g}(\mathbf{x})$ is rarely a square matrix.

[23] note that powerful solution techniques exist for linear PDEs such as (4.6). This makes (4.6) and (4.7) a worthwhile consideration for designing a control system. However, a very similar set of equations have been developed in [21] to extend the applicability of these equations. With these new equations, one no longer needs to fix $\mathbf{J_a}(\mathbf{x})$ and $\mathbf{R_a}(\mathbf{x})$. Instead, the three methodologies discussed in section 4.1.5 may be used to solve for the control law.

4.1.4 *Definition of the control law*

To develop this definition, it is necessary to restate the original design objective of (4.3).

$$[\mathbf{Q}(\mathbf{x})] \frac{\partial H}{\partial \mathbf{x}}(\mathbf{x}) + \mathbf{g}(\mathbf{x})\mathbf{fi}(\mathbf{x}) = [\mathbf{Q_d}(\mathbf{x})] \frac{\partial H_d}{\partial \mathbf{x}}(\mathbf{x}). \tag{4.8}$$

Again employing the left-annihilator and the Moore-Penrose inverse, one can define two PDEs. Both [6] and [20] refer to these as the non-actuated and fully-actuated matching equation

$$\mathbf{g}(\mathbf{x})^\dagger [\mathbf{Q}(\mathbf{x})] \frac{\partial H}{\partial \mathbf{x}}(\mathbf{x}) \quad = \quad \mathbf{g}(\mathbf{x})^\dagger [\mathbf{Q_d}(\mathbf{x})] \frac{\partial H_d}{\partial \mathbf{x}}(\mathbf{x}) \tag{4.9}$$

$$\beta(\mathbf{x}) \quad = \quad \mathbf{g}(\mathbf{x})^{-1} \left\{ [\mathbf{Q_d}(\mathbf{x})] \frac{\partial H_d}{\partial \mathbf{x}}(\mathbf{x}) - [\mathbf{Q}(\mathbf{x})] \frac{\partial H}{\partial \mathbf{x}}(\mathbf{x}) \right\} \tag{4.10}$$

[21] states that if $\mathbf{J_d}(\mathbf{x}) = -\mathbf{J_d}(\mathbf{x})^\intercal$, $\mathbf{J_d}(\mathbf{x}) = -\mathbf{J_d}(\mathbf{x})^\intercal$, $\mathbf{R_d}(\mathbf{x}) = \mathbf{R_d}(\mathbf{x})^\intercal \geq 0$ and $H_d(\mathbf{x}, \mathbf{x_d}) : \mathbb{R}^n \to \mathbb{R}$ such that (4.9) is satisfied and

$$\min H_d(\mathbf{x}) \quad at \quad \mathbf{x} = \mathbf{x_d},$$

where $\mathbf{x_d} \in \mathbb{R}^n$ is the desired equilibrium point where the system should be stabilized, one can design a closed-loop controlled system

$$\dot{\mathbf{x}} \quad = \quad \mathbf{F}(\mathbf{x}) + \mathbf{G}(\mathbf{x})\beta(\mathbf{x}).$$

The control law is given by (4.10) and the closed loop system will be port-controlled Hamiltonian system where

$$\dot{\mathbf{x}} \quad = \quad [\mathbf{Q_d}(\mathbf{x})] \frac{\partial H_d}{\partial \mathbf{x}}(\mathbf{x})$$

applies. $\mathbf{x_d}$ will be at least a locally stable equilibrium. If $\mathbf{x_d}$ is an isolated minimum of $H_d(\mathbf{x})$ and if the largest invariant set under the above dynamics contained in the set

$$\left\{ \mathbf{x} \in \mathbb{R}^n | \left[\frac{\partial H_d}{\partial \mathbf{x}}(\mathbf{x}) \right]^\mathsf{T} \mathbf{R_d}(\mathbf{x}) \frac{\partial H_d}{\partial \mathbf{x}}(\mathbf{x}) = \mathbf{0} \right\}$$

indeed equals $\{\mathbf{x_d}\}$, then the system dynamics will be asymptotically stable. One can also estimate the domain of attraction for these dynamics. The domain is contained in the largest bounded level set $\left\{ \mathbf{x} \in \mathbb{R}^n | \frac{\partial H_d}{\partial \mathbf{x}}(\mathbf{x}) \leq c \right\}$.

4.1.5 *Three methodologies for solving matching equations*

[21] discussed three methodologies to go about selecting the $\mathbf{J_a}(\mathbf{x})$, $\mathbf{R_a}(\mathbf{x})$ matrices and the $H_a(\mathbf{x})$-vector. Each methodology produces a different controller in the majority of cases. The three methodologies for selecting appropriate free parameters are the *parametrized IDA*, the *non-parametrized IDA* and the *algebraic IDA* methodologies [21]. Each may be applied to some form of the above equations.

Within the parametrized IDA methodology, the desired energy function is bound to a specific class of functions. This focuses the $H_d(\mathbf{x})$-term and constrains the $\mathbf{J_d}(\mathbf{x})$ and $\mathbf{R_d}(\mathbf{x})$ terms, at least narrowing down the options that are available to choose from. The class of functions that the energy functions are bound to, is decided based upon prior knowledge of the system.

Within the non-parametrized methodology, the designer fixes the $\mathbf{J_d}(\mathbf{x})$ and $\mathbf{R_d}(\mathbf{x})$ terms as well as the left-annihilator $\mathbf{g}(\mathbf{x})^\dagger$. The designer then solves for the $H_d(\mathbf{x})$ that satisfies the conditions for these particular matrices. From this family of solutions, he then selects one that also satisfies

$$\min H_d(\mathbf{x}, \mathbf{x_d}) \quad at \quad \mathbf{x} = \mathbf{x_d}.$$

Quite the opposite of the non-parametrized method, is the algebraic IDA method. In this case, the designer fixes the function $H_d(\mathbf{x})$ and algebraically solves for $\mathbf{J_d}(\mathbf{x})$, $\mathbf{R_d}(\mathbf{x})$ and $\mathbf{g}(\mathbf{x})^\dagger$.

With all of these methodologies it is important that the choice of $\mathbf{J_d}(\mathbf{x})$, $\mathbf{R_d}(\mathbf{x})$, $H_d(\mathbf{x})$ and $\mathbf{g}(\mathbf{x})^\dagger$ verify the PDE (4.9).

4.2 TRAJECTORY TRACKING IDA-PBC

The problem of formulating a trajectory tracking IDA-PBC technique has been primarily investigated by Wang and Goldsmith [34, 35], Fujimoto *et al.* [**Fujimoto2001**, 8] and Souza *et al.* [30]. Although [30] does not discuss new theory about this technique, they make specific use of [34] for the purpose of controlling four DOFs of a quadrotor. For this reason, their work is very applicable to this study.

Wang and Goldsmith were able to adapt the definition of section 4.1.4 to apply to the trajectory tracking problem. This is the formulation that is used in Chapter 5 for the design of the controller for the helicopter system.

The derivation of the control law for the trajectory tracking problem is an adaptation of the matching equation seen in (4.3). The derivation begins with actual dynamics and the desired dynamics of the controlled system. These are respectively given by

$$\dot{\mathbf{x}} = \mathbf{f}(\mathbf{x}) + \mathbf{g}(\mathbf{x})\mathbf{fi}(\mathbf{x}, \mathbf{x_d}) \quad \text{and}$$

$$\dot{\mathbf{e}} = [\mathbf{Q_d}(\mathbf{x})] \frac{\partial H_d}{\partial \mathbf{e}}(\mathbf{x}, \mathbf{x_d}). \tag{4.11}$$

The desired dynamic equation is the primary difference within trajectory tracking control. Through this form, the problem of controlling a system so that $\mathbf{e} \to \mathbf{0}$ becomes a "stabilisation" effort.

Manipulating the above equations and setting them equal to zero will allow one to come to the following :

$$\mathbf{f}(\mathbf{x}) + \mathbf{g}(\mathbf{x})\mathbf{fi}(\mathbf{x}, \mathbf{x_d}) - \dot{\mathbf{x}} = [\mathbf{Q_d}(\mathbf{x})] \frac{\partial H_d}{\partial \mathbf{e}}(\mathbf{x}, \mathbf{x_d}) + \dot{\mathbf{e}}.$$

This may then be solved for (4.12), which is given as equation (81) in [34].

$$\mathbf{f}(\mathbf{x}) + \mathbf{g}(\mathbf{x})\beta(\mathbf{x}, \mathbf{x_d}) = [\mathbf{Q_d}(\mathbf{x})] \frac{\partial H_d}{\partial \mathbf{e}}(\mathbf{x}, \mathbf{x_d}) + \dot{\mathbf{x}}_\mathbf{d} \tag{4.12}$$

Algebraically solving for $\beta(\mathbf{x}, \mathbf{x_d})$ will confirm that

$$\beta(\mathbf{x}, \mathbf{x_d}) = [\mathbf{g}^\intercal(\mathbf{x})\mathbf{g}(\mathbf{x})]^{-1} \mathbf{g}^\intercal(\mathbf{x}) \quad [\mathbf{Q_d}(\mathbf{e})] \frac{\partial}{\partial \mathbf{e}} H_\mathbf{d}(\mathbf{x}, \mathbf{x_d}) + \dot{\mathbf{x}}_\mathbf{d} - \mathbf{f}(\mathbf{x}). \tag{4.13}$$

It may not seem immediately apparent that this control law serves the trajectory tracking control problem. To clearly show what this control law achieves, it is necessary to digress to (4.12). Also assume that $H_d(\mathbf{x}, \mathbf{x_d})$ is chosen such that

$$\dot{\mathbf{e}} = [\mathbf{Q_d}(\mathbf{x})] \frac{\partial H_d}{\partial \mathbf{e}}(\mathbf{x}, \mathbf{x_d}) \to \mathbf{0},$$

as $t \to k$. $k < \infty$ is an arbitrary time that depends on the system and control parameters. Then from (4.11),

$$\dot{\mathbf{x}} = \mathbf{f}(\mathbf{x}) + \mathbf{g}(\mathbf{x})\mathbf{fi}(\mathbf{x}) \quad \to \quad \mathbf{0} + \dot{\mathbf{x}}_\mathbf{d},$$

which is precisely what one desires of the controller. One may therefore expect the control law of (4.13) to be legitimate for any system that satisfies the requirements of the *Corollary 1* in [34]. These conditions basically state that $\mathbf{J_d}(\mathbf{x}) = -\mathbf{J_d}(\mathbf{x})^\intercal$, $\mathbf{J_d}(\mathbf{x}) = -\mathbf{J_d}(\mathbf{x})^\intercal$, $\mathbf{R_d}(\mathbf{x}) = \mathbf{R_d}(\mathbf{x})^\intercal \geq 0$ and $H_d(\mathbf{x}, \mathbf{x_d}) : R^n \to R$ such that following condition that stems from (4.12) is satisfied:

$$\mathbf{g}(\mathbf{x})^\dagger \mathbf{f}(\mathbf{x}) = \mathbf{g}(\mathbf{x})^\dagger \left\{ [\mathbf{Q_d}(\mathbf{x})] \frac{\partial H_d}{\partial \mathbf{e}}(\mathbf{x}, \mathbf{x_d}) + \dot{\mathbf{x}}_\mathbf{d} \right\}.$$

Of course, the full rank left annihilator $\mathbf{g}(\mathbf{x})^\dagger$ must exist. Also,

$$\min H_d(\mathbf{x}, \mathbf{x_d}) \quad at \quad \mathbf{x} = \mathbf{x_d},$$

which was the case for $H_d(\mathbf{x})$ in section 4.1.2 also. It implies that at least an isolated minimum exists at the desired equilibrium point.

4.3 CONCLUSIONS TO THE FOUNDATIONAL THEORY

For the purposes of the control system design in chapter 5, the trajectory tracking equations of section 4.2 will be used. This choice is motivated by the fact that the trajectory data for an aircraft system will be dynamic as opposed to the fixed reference point that would be used for a MAGLEV system. For certain purposes, an aircraft may be controlled for a fixed reference point. This approach was followed in the work of Secchi et al. [29]. However, the purpose of this control system was similar to the work of Souza et al. [30] who made use of the trajectory-tracking equations presented above.

Readers who want to do similar designs are encouraged to become familiar with regular IDA-PBC design before progressing to trajectory-tracking IDA-PBC. It is for that reason that the regular IDA-PBC equations are presented first. From the discussion above, it should be plain to see that the trajectory-tracking equations are an extension of the regular IDA-PBC equations. It is believed that once the reader has mastered regular IDA-PBC design, the trajectory-tracking approach will be simple to apply.

5

IDA-PBC DESIGN OF A HELICOPTER CONTROL SYSTEM

The controller design follows directly on the theory of Chapter 4. The chapter begins with an introduction to the notation used below. It also recites the model derived within Chapter 3 for ease of reference. Thereafter, terms within the matching equations are selected such that the requirements for a stable controller design are satisfied. The reasoning for the choice of the kinetic and potential energy terms, which is the most difficult part of the design, is clearly illustrated. Once the terms for the Hamiltonian function are selected, simple algebraic manipulation is used to solve for the control law.

The chapter is ended with a discussion of damping assignment for the controller as well as several conclusions about pitfalls and testing procedures. The conclusions also discuss the procedure for determining the free-parameter gains that are introduced into the Hamiltonian function.

5.1 INTRODUCTION

As introduction to this chapter, it is of value to describe the form of notation used within the following sections. For the purposes both of writing out the equations by hand as well as within a software program such as Maple™, it makes sense to divide the twelve state equations into two sets of six equations. Maple™ is able to display matrices as large as 10×10 quite readily. However, larger matrices must be viewed as a table within a pop-up window. Matrices of size 6×6 are easily manageable in both handwritten and computer formats. For this reason, it is often easier to divide matrices such as the 12×12 interconnection matrix of chapter 3 into four 6×6 sections.

The modelling equations from chapter 3 easily separate into a set of six homogeneous equations and six non-homogeneous equations. The reader should take careful note that each of these sets have intrinsic value. The homogeneous equations solve for the kinetic energy terms of the desired Hamiltonian function, while the non-homogeneous equations solve for the control law.

A reader who seeks to understand the process described within the following sections is strongly encouraged to write out the equations that are supplied in vector form within this chapter. The reader should find that seeing the complete matrices is valuable, especially when not entirely comfortable with such concise notation. To assist the reader with this, the equations are noted with a superscript to differentiate between the configuration variables and the momentum variables. Those state equations associated with the first six states are indicated with a left superscript $\mathbf{q}$ while the final six equations that described the momentum states are indicated with a left superscript $\mathbf{p}$. As an example, the input vector associated with the configuration variables is indicated as ${}^{\mathbf{q}}\mathbf{g}$. This should not be confused with the reference frame indication which does not make use of bold symbols. The velocity within the BF coordinate system ${}^{b}\mathbf{v}$ is such an example.

Chapter 3 gave the complete model for the helicopter. It is repeated here for reference. Note that $\mathbf{I_{6x6}}$ represents the 6×6 identity matrix while $\mathbf{0_{6x6}}$ represents the 6×6 zero-matrix.

$$\underbrace{\begin{bmatrix} {}^{b}\dot{\mathbf{q}} \\ {}^{b}\dot{\mathbf{p}} \end{bmatrix}}_{\dot{\mathbf{x}}} = \underbrace{\begin{bmatrix} \mathbf{O_{6x6}} & \mathbf{I_{6x6}} \\ -\mathbf{I_{6x6}} & -\mathbf{C}(\omega, \dot{\mathbf{x}}) \end{bmatrix}}_{\mathbf{Q}(\mathbf{x})} \frac{\partial H}{\partial \mathbf{x}}(\mathbf{x}) + \underbrace{\begin{bmatrix} \mathbf{O_{6x1}} \\ \mathbf{I_{6x1}} \end{bmatrix}}_{\mathbf{g}(\mathbf{x})} \mathbf{u} \tag{5.1}$$

with $\frac{\partial H}{\partial \mathbf{x}}(\mathbf{x}) = \begin{bmatrix} \frac{\partial H}{\partial \mathbf{q}}(\mathbf{x}) & \frac{\partial H}{\partial \mathbf{p}}(\mathbf{x}) \end{bmatrix}^{\mathsf{T}}$ given by:

$$\begin{aligned} \frac{\partial H}{\partial \mathbf{q}}(\mathbf{x}) &= \begin{bmatrix} mg\,sin(\theta) & -mg\,sin(\phi)\,cos(\theta) & -mg\,cos(\phi)\,cos(\theta) & 0 & 0 & 0 \end{bmatrix}^{\mathsf{T}} \\ \frac{\partial H}{\partial \mathbf{p}}(\mathbf{x}) &= \begin{bmatrix} {}^{b}u & {}^{b}v & {}^{b}w & {}^{b}p & {}^{b}q & {}^{b}r \end{bmatrix}^{\mathsf{T}}. \end{aligned}$$

The Coriolis matrix $\mathbf{C}(\omega, \dot{\mathbf{x}})$ within (5.1) is described within:

$$\begin{bmatrix} {}^{\mathbf{b}}\boldsymbol{\omega} \times (m \cdot {}^{\mathbf{b}}\mathbf{v}) \\ {}^{\mathbf{b}}\boldsymbol{\omega} \times (\boldsymbol{I_{rr}} \cdot {}^{\mathbf{b}}\boldsymbol{\omega}) \end{bmatrix} = \underbrace{\begin{bmatrix} 0 & 0 & 0 & 0 & m\,{}^{b}w & -m\,{}^{b}v \\ 0 & 0 & 0 & -m\,{}^{b}w & 0 & m\,{}^{b}u \\ 0 & 0 & 0 & m\,{}^{b}v & -m\,{}^{b}u & 0 \\ 0 & 0 & 0 & 0 & I_{zz}\,{}^{b}r & -I_{yy}\,{}^{b}q \\ 0 & 0 & 0 & -I_{zz}\,{}^{b}p & 0 & I_{xx}\,{}^{b}p \\ 0 & 0 & 0 & I_{yy}\,{}^{b}q & -I_{xx}\,{}^{b}p & 0 \end{bmatrix}}_{\mathbf{C}(\omega, \dot{\mathbf{x}})} \begin{bmatrix} {}^{b}u \\ {}^{b}v \\ {}^{b}w \\ {}^{b}p \\ {}^{b}q \\ {}^{b}r \end{bmatrix}. \tag{5.2}$$

$\boldsymbol{I_{rr}} = \begin{bmatrix} I_{xx} & I_{yy} & I_{zz} \end{bmatrix}^{\mathsf{T}}$ represents the rotational inertias about the various axes. ${}^{e}\dot{\mathbf{q}}$ and ${}^{b}\dot{\mathbf{p}}$ are the time-derivatives of the configuration and momentum variables referenced within theEF and BF respectively. m is the mass of the aircraft. g is the constant gravitational acceleration. ${}^{b}\mathbf{v} = {}^{b}\dot{\mathbf{q}}$ is the velocity of the helicopter. ${}^{\mathbf{b}}\dot{\boldsymbol{\omega}}$ is the rotational velocities about the body axes.

5.2 SATISFYING IDA-PBC REQUIREMENTS

Chapter 4 noted several requirements that need to be considered for the design of a stable trajectory tracking controller. These are primarily discussed within Corollary 1 of [35]. These form the starting point of the controller design within this chapter.

The first requirements relate to the interconnection and damping matrices. Note that these matrices are a function of the error of the states as the dependent variable, where $\mathbf{e} = \mathbf{x} - \mathbf{x_d}$.

$$\begin{aligned} \mathbf{J_d}(\mathbf{e}) &= -\mathbf{J_d}(\mathbf{e})^{\mathsf{T}} \\ \mathbf{R_d}(\mathbf{e}) &= \mathbf{R_d}(\mathbf{e})^{\mathsf{T}} \geq 0 \end{aligned}$$

These conditions are true for $\mathbf{J}(\mathbf{x})$ and $\mathbf{R}(\mathbf{x})$ and it will be assumed for the purposes of this design that $\mathbf{J_d}(\mathbf{e}) \triangleq \mathbf{J}(\mathbf{x})$ and $\mathbf{R_d}(\mathbf{e}) \triangleq \mathbf{R}(\mathbf{x})$.

It is also assumed that a function $H_d(\mathbf{x}, \mathbf{x_d}) : R^{12} \rightarrow R$ exists. This function will be required to verify the PDE

$$\mathbf{g}^{\dagger}(\mathbf{x})\mathbf{f}(\mathbf{x}) \quad = \quad \mathbf{g}^{\dagger}(\mathbf{x}) \left\{ [\mathbf{Q_d}(\mathbf{e})] \frac{\partial}{\partial \mathbf{e}} \mathbf{H_d}(\mathbf{x}, \mathbf{x_d}) + \dot{\mathbf{x}}_\mathbf{d} \right\}.$$

$H_d(\mathbf{x}, \mathbf{x_d})$ is chosen such that $\min H_d(\mathbf{x}, \mathbf{x_d})$ occurs at $\mathbf{x} = \mathbf{x_d}$. With these requirements satisfied, the solution for the control law will ensure at least a locally stable equilibrium at the point where the error signal $\mathbf{e} = \mathbf{0}$. This has been discussed thoroughly within section 4.1.4 of chapter 4. This condition is also discussed within [34].

As a matter of interest, the reader is made attentive to the fact that Wang and Goldsmith [35] indicate the error as $\mathbf{e} = \mathbf{x} - \mathbf{x_d}$ within the latter section of their article. Souza *et al*. [30] make use of the notation $\bar{\mathbf{x}} = \mathbf{x} - \mathbf{x_d}$ which is used for a general case in the former part of [35]. Generally, the symbol $\mathbf{e}$ is more conspicuous within equations as opposed to $\bar{\mathbf{x}}$, which is easily confused with $\mathbf{x}$ or $\dot{\mathbf{x}}$ when read quickly. For this reason, the same notation as seen in the later part of [35] is used here.

5.3 HOMOGENEOUS AND NON-HOMOGENEOUS EQUATIONS

From chapter 3, it may be seen that the input gain matrix $\mathbf{g}(\mathbf{x})$ is given by

$$\mathbf{g}(\mathbf{x}) = \begin{bmatrix} {}^{\mathbf{q}}\mathbf{g} \\ {}^{\mathbf{p}}\mathbf{g} \end{bmatrix} \quad = \quad \begin{bmatrix} \mathbf{0_{6x1}} \\ \mathbf{I_{6x1}} \end{bmatrix}.$$

By substituting this into the matching equation

$$\mathbf{g}(\mathbf{x})\beta(\mathbf{x}, \mathbf{x_d}) \quad = \quad [\mathbf{Q_d}(\mathbf{e})] \frac{\partial}{\partial \mathbf{e}} H_\mathbf{d}(\mathbf{x}, \mathbf{x_d}) + \dot{\mathbf{x}}_\mathbf{d} - \mathbf{f}(\mathbf{x}), \tag{5.3}$$

it is clear that the first six equations will be a homogeneous set of equations. As noted above, these may be used to solve for the kinetic energy terms. The second set of six equations solves for the control law $\beta(\mathbf{x}, \mathbf{x_d})$. Conveniently, the six-state notation separates these sets from one another.

5.4 SOLUTION OF HOMOGENEOUS EQUATIONS

Note that within the six homogeneous equations $\mathbf{f}(\mathbf{x}) = \dot{\mathbf{q}}$. Thus, the first six equation of (5.3) are given as

$$\mathbf{0} \quad = \quad [{}^{\mathbf{q}}\mathbf{Q_d}(\mathbf{e})] \frac{\partial}{\partial \mathbf{e}} H_\mathbf{d}(\mathbf{x}, \mathbf{x_d}) + \dot{\mathbf{q}}_\mathbf{d} - \dot{\mathbf{q}}.$$

In section 5.1, it was mentioned that the kinetic energy terms of desired Hamiltonian function can be solved for using these homogeneous equations. This is done by simplifying the above equation as follows:

$$\begin{aligned} -\frac{\partial}{\partial \mathbf{p_e}} H_d(\mathbf{x}, \mathbf{x_d}) \quad &= \quad -\dot{\mathbf{q}}_\mathbf{e} \\ \frac{\partial}{\partial \mathbf{p_e}} H_d(\mathbf{x}, \mathbf{x_d}) \quad &= \quad \mathbf{M_d^{-1}} \mathbf{p_e}. \end{aligned}$$

By integrating the above equations, it is clear that $H_d(\mathbf{x}, \mathbf{x_d}) = \frac{1}{2} \mathbf{p_e^T} \mathbf{M_d}^{-1} \mathbf{p_e}$, which is the desired kinetic energy equations for a rigid-body aircraft. From the literature [21, 30, 34], this form for the kinetic energy is a very intuitive result for mechanical systems.

5.5 POTENTIAL ENERGY TERMS

Based upon the intuitive nature of the above solution for the kinetic energy terms of the Hamiltonian function, it may be reasoned that the potential energy of the system will take a similarly intuitive form. The design within [30] also seems to indicate the validity of this approach. Therefore, the potential energy terms are selected as

$$H_d(\mathbf{x}, \mathbf{x_d}) = \frac{1}{2}\mathbf{K_p}\mathbf{q_e^2}, \tag{5.4}$$

where $\mathbf{K_p}$ is a diagonal gain matrix that adds an additional DOFs to the controller design. Because this is a set of desired dynamics that is projected onto the system by the means of a controlled input, these gains may be made variable.

Note also that regular potential energy functions do not tend to contain the square of a position variable, but instead are of the form $H_d(\mathbf{x}, \mathbf{x_d}) = \mathbf{K_p}\mathbf{q_e}$. This form of (5.4) is introduced here to assign a definite minimum to the derivative of potential energy function. A similar approach was followed by Souza et al. [30].

5.6 SOLUTIONS TO MATCHING EQUATIONS

The matching equation is derived from the following equality. The objective with this equation is to solve for $\beta(\mathbf{x}, \mathbf{x_d})$.

$$\mathbf{f}(\mathbf{x}) + \mathbf{g}(\mathbf{x})\mathbf{fi}(\mathbf{x}, \mathbf{x_d}) = [\mathbf{Q_d}(\mathbf{x})]\frac{\partial H_d}{\partial \mathbf{e}}(\mathbf{x}, \mathbf{x_d}) + \dot{\mathbf{x}}_\mathbf{d}$$

For the first six states, that is to say the configuration states, this equation simplifies to

$$\begin{bmatrix} x \\ y \\ z \\ i \\ j \\ k \end{bmatrix} = \begin{bmatrix} x_e + x_d \\ y_e + y_d \\ z_e + z_d \\ i_e + i_d \\ j_e + j_d \\ k_e + k_d \end{bmatrix}.$$

Note that this is inherently true because $\mathbf{x_e} = \mathbf{x} - \mathbf{x_d}$. Also note that due to the nature of the matrix $\mathbf{g}(\mathbf{x})$, the control law $\beta(\mathbf{x}, \mathbf{x_d})$ is not influenced by these first six equations.

The next six state equations for the system includes the Coriolis effect. For the purposes of this design, the dynamics were not confined to hover conditions. (3.9) from Chapter 3 is used for for the standard system Hamiltonian because it includes the gravitational potential energy along the $x-$, $y-$ and $z-$axes of the BF.As such, these equations evaluate to

$$\mathbf{A} = \begin{bmatrix} -mwq_e + mvr_e + R_{d\,22}u_e - k_{p1}x_e + \dot{u}_d m \\ mwp_e - mur_e + R_{d\,22}v_e - k_{p2}y_e + \dot{v}_d m \\ -mvp_e + muq_e + R_{d\,22}w_e - k_{p3}z_e + \dot{w}_d m \\ I_{yy}qr_e - I_{xx}rq_e + R_{d\,22}p_e - k_{p4}i_e + \dot{p}_d m \\ -I_{xx}pr_e + I_{zz}rp_e + R_{d\,22}q_e - k_{p5}j_e + \dot{q}_d m \\ I_{xx}pq_e - I_{yy}qp_e + R_{d\,22}r_e - k_{p6}k_e + \dot{r}_d m \end{bmatrix}$$

with

$$\mathbf{A} = \begin{bmatrix} -mg\,sin(\theta) - m\,wq + m\,vr + \beta_1\,(\mathbf{x}, \mathbf{x_d}) \\ mg\,sin(\phi)\,cos(\theta) + m\,wp - m\,ur + \beta_2\,(\mathbf{x}, \mathbf{x_d}) \\ mg\,cos(\phi)\,cos(\theta) - m\,vp + m\,uq - m\,g + \beta_3\,(\mathbf{x}, \mathbf{x_d}) \\ I_{yy}\,qr - I_{zz}\,rq + \beta_4\,(\mathbf{x}, \mathbf{x_d}) \\ -I_{xx}\,pr + I_{zz}\,rp + \beta_5\,(\mathbf{x}, \mathbf{x_d}) \\ I_{xx}\,pq - I_{yy}\,qp + \beta_6\,(\mathbf{x}, \mathbf{x_d}) \end{bmatrix}.$$

Now, by solving for the β-terms and remembering that $\mathbf{x_d} = \mathbf{x} - \mathbf{x_e}$, one finds that

$$\beta\,(\mathbf{x}, \mathbf{x_d}) = \begin{bmatrix} mwq_d - mvr_d + R_{d\,22}k_{v1}u_e - k_{p1}x_e + \dot{u}_d m + mg\,sin(\theta) \\ -mwp_d + mur_d + R_{d\,22}k_{v2}v_e - k_{p2}y_e + \dot{v}_d m - mg\,sin(\phi)\,cos(\theta) \\ mvp_d - muq_d + R_{d\,22}k_{v3}w_e - k_{p3}z_e + \dot{w}_d m - mg\,cos(\phi)\,cos(\theta) \\ -I_{yy}qr_d + I_{xx}rq_d + R_{d\,22}k_{v4}p_e - k_{p4}i_e + \dot{p}_d m \\ I_{xx}pr_d - I_{zz}rp_d + R_{d\,22}k_{v5}q_e - k_{p5}j_e + \dot{q}_d m \\ -I_{xx}pq_d + I_{yy}qp_d + R_{d\,22}k_{v6}r_e - k_{p6}k_e + \dot{r}_d m \end{bmatrix} \tag{5.5}$$

Note that by solving for the control law vector $\beta\,(\mathbf{x}, \mathbf{x_d})$, the terms that model the Coriolis effect now change from containing error values to containing only desired values. For example, within the first equation, the following algebraic calculations occur:

$$\begin{aligned} -mwq_e + mvr_e - (-m\,wq + m\,vr) &= mw(-q_e + q) + mv(r_e - r) \\ &= mwq_d - mvr_d. \end{aligned}$$

5.7 DAMPING ASSIGNMENT

When the is working correctly, damping is typically not required for "stable" trajectory tracking. However, when the simulation diagrams are not set up correctly, damping can have a very real impact on the apparent response of the sysem. When a mistaken signal flow connection amplified the error during initial tests of the above control system, additional damping made a significant difference to the quality of the tracking. This was also the case for incorrect initial conditions. The effect of poor damping during an oscillation at the beginning of the roll-reversal manoeuvre is shown in figure 5.1. In this case, the damping constant was changed from $R_{22} = 1$ to $R_{22} = 200$. Note how the poorly damped response oscillates by the approximate size of the initial oscillation about the desired trajectory that the damped response ultimately follows. This same effect is observed for incorrect initial conditions. If the initial conditions are incorrect by 20 m, the poorly damped system oscillates by ± 20 m about the reference trajectory.

To include damping in the system dynamics, the desired damping matrix $\mathbf{R_d}$ is adjusted. Note that the conditions for IDA-PBC as discussed in section 5.2 should still be satisfied. Therefore, the general method of adding damping to a system that was previously under-damped is to let

$$\mathbf{R_d} = \begin{bmatrix} \mathbf{0_{6x6}} & \mathbf{0_{6x6}} \\ \mathbf{0_{6x6}} & \mathbf{R_{d\,22}} \end{bmatrix}.$$

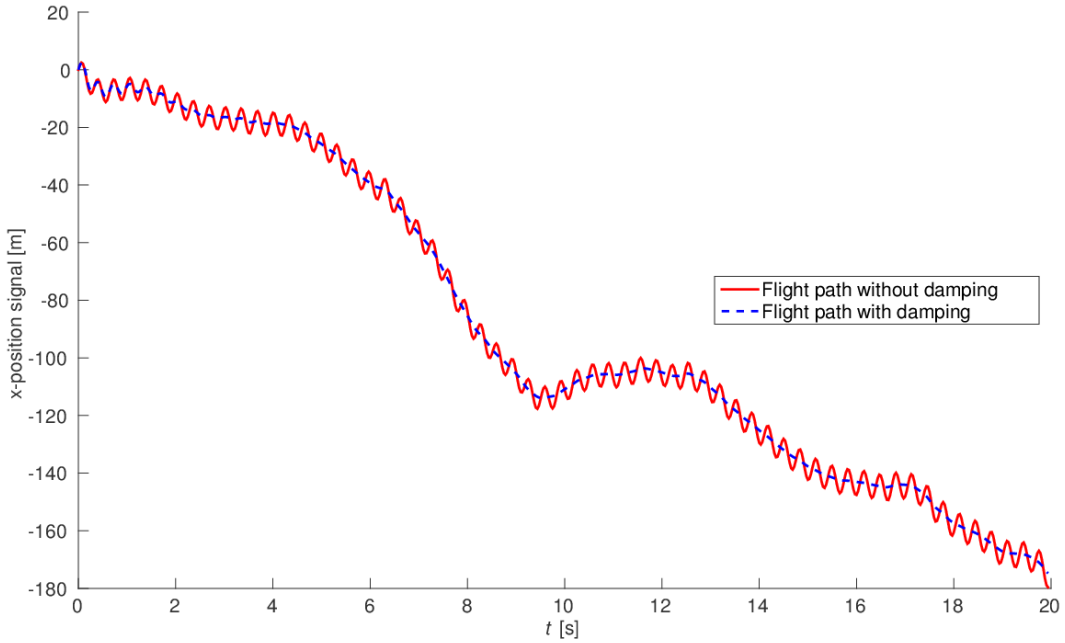

Figure 5.1: Effect of damping for incorrect initial conditions

In this way, the damping constant can be set as desired by the control system designer. The damping matrix will influence some terms within the matrix $\mathbf{C}(\omega, \dot{\mathbf{x}}, R_{22})$ in (5.2). Within the rigid body model of (5.1), $\mathbf{C}(\omega, \dot{\mathbf{x}}, R_{22})$ will be given by

$$\mathbf{C}(\omega, \dot{\mathbf{x}}, R_{22}) = \begin{bmatrix} R_{22} & 0 & 0 & 0 & m\,{}^b w & -m\,{}^b v \\ 0 & R_{22} & 0 & -m\,{}^b w & 0 & m\,{}^b u \\ 0 & 0 & R_{22} & m\,{}^b v & -m\,{}^b u & 0 \\ 0 & 0 & 0 & R_{22} & I_{zz}\,{}^b r & -I_{yy}\,{}^b q \\ 0 & 0 & 0 & -I_{zz}\,{}^b p & R_{22} & I_{xx}\,{}^b p \\ 0 & 0 & 0 & I_{yy}\,{}^b q & -I_{xx}\,{}^b p & R_{22} \end{bmatrix}.$$

5.8 CONCLUSIONS TO CONTROLLER DESIGN PROCEDURE

5.8.1 *Pitfalls*

In conclusion, the reader should be attentive to the fact that the equations should be completely evaluated and then separated into the first and last six equations. The matrix computations will require this, but confusion can occur when incorrect matrix operations are implemented when writing out the state equations.

5.8.2 *Simulation of error dynamics*

Readers who are interested in testing the developed controller within a simulation environment would do well to simulate the system using the proposed dynamics of (5.6).

$$\mathbf{e} = [\mathbf{J_d}(\mathbf{e}) - \mathbf{R}(\mathbf{e})] \frac{\partial}{\partial \mathbf{e}} H_d(\mathbf{x}, \mathbf{x_d}). \tag{5.6}$$

It is possible to test the control system by simulating only this equation to see if the choice of $H_d(\mathbf{x}, \mathbf{x_d})$ was made correctly. This equation is often simpler to implement within a MATLAB® SimuLink™ diagram. It provides a base of comparison when simulating the effects of the control law on the model. If the results for (5.6) are not the same as for the implementation of (5.5), at least one of the simulations has been implemented incorrectly. Most often, the fault resides in the implementation of the control law, since those equations are significantly more complex to implement than (5.6). The more complex simulation diagrams allow for more mistakes to creep in.

5.8.3 *Testing the system*

During the implementation of the control law of (5.5), it was discovered that it is significantly more efficient to gradually add complexity to the simulation models. For this reason, a simulation was first set up to test one DOF while ignoring all Coriolis effect terms. The Coriolis effect was added to the 1-DOF model once the initial test results proved to be satisfactory. To accommodate the other state variables that determine the Coriolis effect, state outputs measured on practical systems were used as inputs to the model. To do this, one would want to make the assumption that all those state inputs to the model are indeed correct for the simulation conditions. However, the implementation of the control law showed that this is not necessarily true. On more than one occasion, mistaken transformation or incorrect interpretations of the data were discovered. This would have an effect if the simulation diagram is set up correctly. However, readers will notice that 5.5 implements the exact inverse of the Coriolis effect among the control terms. Thus, when the simulation diagram is set up correctly, all Coriolis effect terms are cancelled by the control law. In this case, even incorrect inputs to the simulation diagram will not show a noticeable deviation in flight path. Of course, within a practical system, one would notice such deviations.

When each of these simulations have proved the control strategy to be successful, a 6-DOF model may be set up. This allows outputs from the model to be used as inputs to the Coriolis effect equations. This is, of course, the most realistic implementation of the model.

5.8.4 *Compensation for the Coriolis effect in low-level control*

Readers should be aware of the general approach for including compensation for the Coriolis effect within a low level control system like this one. Because the Coriolis effect represents a perceived force, it will typically be compensated for within a trajectory planning stage. The reason why it is incorporated here is to show how the controller design will address this issue. In this case, the solution is simply an inverse compensation of the terms that introduce the effect. This is seen in (5.5) where the inverse of the Coriolis effect equations are implemented in the control law.

If the system were to be applied to a helicopter system where the Coriolis effect is already taken into account during the trajectory planning, the compensation for the effect may easily be removed. In this case, the control law will be given by (5.7). The control system developed within this chapter still follows the input trajectory, regardless of whether the Coriolis effect is taken into account or not.

$$\begin{bmatrix} \beta_1(\mathbf{x}, \mathbf{x_d}) \\ \beta_2(\mathbf{x}, \mathbf{x_d}) \\ \beta_3(\mathbf{x}, \mathbf{x_d}) \\ \beta_4(\mathbf{x}, \mathbf{x_d}) \\ \beta_5(\mathbf{x}, \mathbf{x_d}) \\ \beta_6(\mathbf{x}, \mathbf{x_d}) \end{bmatrix} = \begin{bmatrix} R_{d\,22}k_{v1}u_e - k_{p1}x_e + \dot{u}_d m + mg\,sin(\theta) \\ R_{d\,22}k_{v2}v_e - k_{p2}y_e + \dot{v}_d m - mg\,sin(\phi)\,cos(\theta) \\ R_{d\,22}k_{v3}w_e - k_{p3}z_e + \dot{w}_d m - mg\,cos(\phi)\,cos(\theta) \\ R_{d\,22}k_{v4}p_e - k_{p4}i_e + \dot{p}_d m \\ R_{d\,22}k_{v5}q_e - k_{p5}j_e + \dot{q}_d m \\ R_{d\,22}k_{v6}r_e - k_{p6}k_e + \dot{r}_d m \end{bmatrix} \tag{5.7}$$

5.8.5 *Selecting control-law gains*

Unfortunately, no literature sources seem to discusses a mathematical approach to choosing the gains that produce an optimal response. Instead, the gains for this controller are tuned by trial-and-error. This was also the method applied by [29]. Some literature sources do not explicitly discuss how the gains had been selected, as is the case within [30]. Therefore, the trial-and-error approach is considered to be acceptable for the purposes of this study.

Two main goals guide the tuning procedure. The first is the objective of accurate trajectory tracking. The general impression during tuning is that smaller gains slow down the rate of error-correction between the desired and actual trajectories. However, it is also clear that higher gains produce diminishing returns. At a certain maximum value dependant on the system parameters, the trajectory tracking is not visibly improved even for increased gain values.

From a practical perspective, higher gains need to be implemented using operational amplifiers. With larger gains come larger voltage inputs to the amplifiers, which increases power consumption. To this end, the goal is to keep the gains as small as possible. In general, the gains for controller simulations were selected such that the gains were selected as small as practical without diminishing the trajectory tracking accuracy of the controller.

Governed by these two objectives, the gains were adjusted within a while-loop that selected a minimal ITAE pefromance index for five simulations, each with a different gain. The difference between the gains were narrowed until the ITAE value for two simulation loops differed by less than or equal to 2 units.

For completeness, the calculation of the ITAE performance index as described within [6] is given below. Not that several performance indices exist, but the ITAE index was chosen because of its sharp minimum characteristic compared to the other indices. Other indices would also serve the purpose, but would require a smaller constraint than the 2 units selected for the ITAE index. The ITAE index is also described as being less sensitive to large initial errors while emphasizing errors later in the response. However, this benefit is not relevant to this particular set of data.

$$ITAE = \int_0^T t\,|e(t)|\,dt$$

Readers will agree that this is a very simple procedure. It is not a fool-proof procedure, because there do exist local minimums within the function that relates the ITAE index to the gains. It is quite possible for the loop to drive the gain towards a local instead of a global minimum. For this reason, the selected gain must be reviewed, but

Parameter	*Value*	*Parameter*	*Value*
$k_{p\,x} = k_{p\,y} = k_{p\,z}$	2.6423×10^6	$k_{v\,x} = k_{v\,y} = k_{v\,z}$	-64.8
$k_{p\,\phi}$	2.307×10^7	$k_{v\,\phi} = k_{v\,\theta} = k_{v\,\psi}$	-2000
$k_{p\,\theta}$	8×10^8	R_{22}	200
$k_{p\,\psi}$	5×10^8	I_{yy}	$55\,800\ \mathrm{kg \cdot m^2}$
m	7 200 kg	I_{zz}	$55\,200\ \mathrm{kg \cdot m^2}$
I_{xx}	$12\,200\ \mathrm{kg \cdot m^2}$		

Table 5.1: Controller parameters and gains

it proved accurate during most tests. The procedure also does lack the analytical impression of linear design approaches like Ackerman's formula [6]. In this respect, the literature on IDA-PBC was found to be lacking, but the difficulty of monolithic design theory for non-linear systems is well understood [22].

In conclusion, Table 5.1 summarizes the values for the controller gains and other parameters that are used to test the controller designed within this chapter.

6 VALIDATION OF THE CONTROL SYSTEM

Having designed a control system that seems to show much promise during the preliminary testing, the question now needs to be answered whether the system will function well within its typical working conditions. This chapter proposes to deliver sufficient results to convince the reader that it indeed will.

The chapter begins with a comparison of validation methodologies from the literature. For validation of the system within this work, a combination of simulation and practical data measurement is implemented. This discussion is followed by a description of a preliminary validation procedure that proved valuable for finding various coding errors within the simulation program. This procedure provided a method to test the system quickly, but had several shortcomings. To address these shortcomings, three alternative procedures are proposed. One is selected and implemented. The validation tests are then shown for one of four manoeuvres for which data had been recorded for a piloted helicopter. The recorded data provided a realistic base of cross-coupling between the helicopter states.

In the conclusion section, several relevant observations about the validation procedure are discussed. One regards the use of gyroscope measurements for determining position and velocity trajectory data. The other discussed an anomaly that was observed during the validation procedure which could be explained by additional investigation of the data.

6.1 PROPOSED VALIDATION PROCEDURE

Table 6.1 shows a comparison of validation methods from several sources in the literature. All of these sources evaluated control systems, albeit not necessarily PBC systems. Of course, the ultimate goal for the new control system design also contributes to the choice of the validation methods. Take for instance [25] where the aim was to produce a more computationally efficient model predictive control scheme. To validate the efficiency, practical testing on a micro-controller certainly makes excellent sense. Also, a comparison of the new controller to a former implementation suited this investigation. However, table 6.1 also indicates that both [27] and [29] evaluated their control systems within simulation only. The limitations of available resources of this research project also required predominantly a simulation-based approach. However, the simulation also makes use of data from practical tests of a real-world helicopter. This ensures that the six DOFs are realistically cross-coupled and illustrate actual manoeuvres.

The approach selected for the validation is illustrated in figure 6.1. The idea focussed on deriving a realistic reference trajectory from real-world data of actual helicopter test flights. These reference trajectories for each of the six DOFs were used as inputs to the controller. The controller in turn produced inputs to the model and the model supplied expected trajectories that could be compared to the reference trajectories. In between, the inputs to the model from the control system were also compared to the same inputs within the real world data.

Source	*Simulation*	*Comparison*	*Practical Testing*	*Goal*
Rabbath [25]	X	X	X	Efficiency improvement
Schafroth *et al.* [28]	X		X	Performance evaluation
Vilchis *et al.* [33]	X		X	Robustness evaluation
Das *et al.* [5]	X	X		Performance evaluation
Souza *et al.* [30]	X	X		Performance evaluation
Roy *et al.* [27]	X			Performance evaluation
Secchi *et al.* [29]	X			Performance evaluation

Table 6.1: Comparison of validation methods within literature

6.2 MEASURED DATA AS REFERENCE TRAJECTORIES

For preliminary validation tests, the measured flight trajectories from the data were used as input reference trajectories to the control system. This proved to be a valuable approach because it pointed to faults within the control system without much additional work being done on generating an appealing trajectory. Section 6.3 discusses some concerns with this approach, but it should be mentioned that corrections to the control system could already be made from the results of using the measured data as reference trajectory inputs.

The faults within the control system were not found within the design, but within the implementation of the system within MATLAB® SimuLink™. The original implementation made use of differentiators within the simulation diagram to produce velocity and acceleration data from a position trajectory. However, these differentiators influenced the solving capabilities of SimuLink™ for that particular simulation diagram. When all velocity and acceleration data were integrated or differentiated in separate diagrams, they could simply be imported to the simulation diagram. When this was done, considerably better trajectory tracking performance was observed. Note that the results for this simulation is not presented here because it does not show relevant information. With the correct gains, the simulation shows excellent trajectory tracking, just as it does within section 6.5, even though the measured data does not give an entirely realistic flight reference trajectory. As the reader will see within the

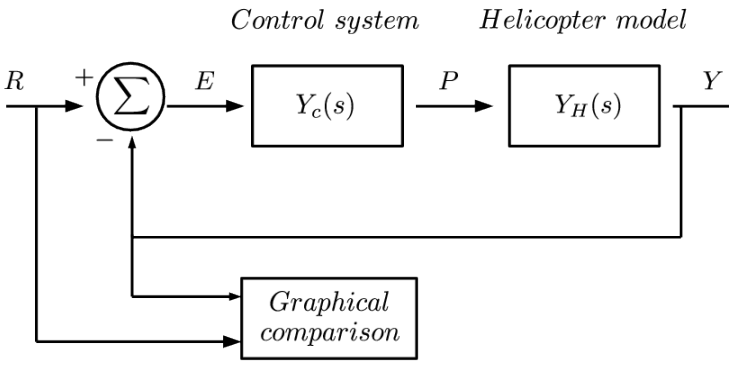

Figure 6.1: Illustration of selected validation procedure

following sections, some small alterations are required to generate a more realistic reference trajectory that may be used as input to the control system.

6.3 REALISTIC REFERENCE TRAJECTORIES

It was mentioned within section 6.1 that the object of the validation approach was to input realistic trajectories to the designed control system. There were some proposed shortcomings to the use of measured data for reference trajectory. The pilot and helicopter dynamics would have some influence on the actual flight trajectory. It would therefore be inaccurate to assume that a realistic reference trajectory would look exactly the same as the actual flight trajectory.

If one were to consider the step response of a control system, one can rarely, if ever, expect the control system to track the step input 100% accurately. Instead, some high frequency damping takes place. The control system shows a settling time and, quite possibly, a percentage overshoot. When making use of measured data, the control has already been implemented. One would be making use of the output data of a real world system as an input, as opposed to the reference trajectory that the pilot considered.

If one were to consider real world systems, one could ascertain that an actual helicopter system will have mechanical linkages. Inputs from the pilot will not produce an immediate response in the trajectory. However small, there is some delay in system response. In this case, the data seems to indicate a delay of approximately 500 ms. The model of the helicopter proposed in chapter 3 does not take such delays into account. Of course, it is not difficult to add such delays within a SimuLink™ simulation, but it begs the question whether more such delays should be considered for a realistic reference trajectory input.

These two considerations point toward shortcomings in making use of the measured data for a reference trajectory. Instead, the reference trajectory that the pilot tried to follow for each test flight should be used as an input to the control system. The difficulty is that such reference trajectories are not recorded for the data that was available to this project. When a pilot performed a "roll-reversal" manoeuvre as the one used within the experiments to be discussed, he simply tested the helicopter for a dramatic roll to the one direction and then to the other. There was no specific roll angle that the pilot necessarily attempted to achieve. The same is true for every other manoeuvre that this control system was tested for. Thus, the only solution would be to approximate the reference trajectory from the data that was available.

Several possible solutions to the above problem could be proposed. One of these was to take into account that a human pilot might avoid jerked responses, especially for the planned reference trajectory. To that end, a moving-average filter could be used to remove sharp peaks from the measured data. However, this still does not address the problem of mechanical delays and high frequency damping that the system would have added to that measured data to obtain an inverse of such unmodelled effects. A moving-average filter will not add high-frequency information to the reference trajectory that the system could damp out.

A second proposition would be to test the step response of the control system. This is indeed a dramatic test for which no project-specific specifications had been developed, but it would give realistic measurement of a standard among other control systems.

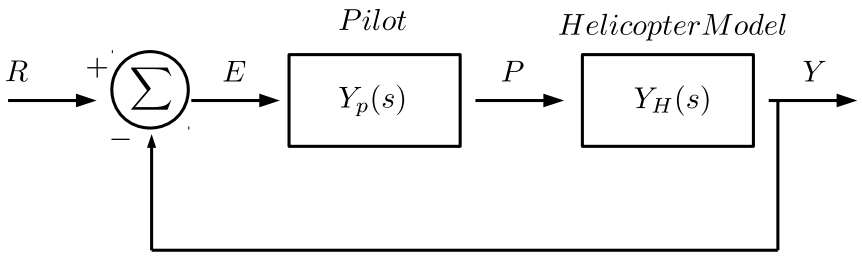

Figure 6.2: Illustration of a typical helicopter control loop

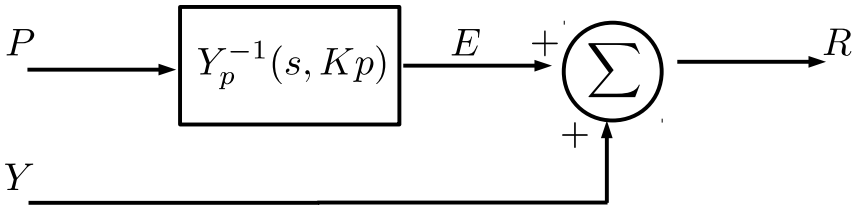

Figure 6.3: Illustration of trajectory generation procedure

A third option would be to deduct some information about the trajectories from the pilot inputs on the system controls. Although a system-specific model for these inputs is not available, one could attempt to derive some form of a trajectory from the four DOFs offered by the helicopter controls. Of course, the under-actuated characteristics of the system would present a challenge to this approach.

6.4 ESTIMATION OF REFERENCE TRAJECTORIES

Based upon the three options, the final one was selected. If one considers figure 6.2 as a starting point, the reasoning follows that if one is able to obtain a transfer function for the response of a typical pilot as given by $Y_p(s)$, then the inverse of that transfer function could lead one to obtain a conceptual reference trajectory R that is completely based on the inputs P. These are the inputs that the pilot supplied to the helicopter system. This procedure is more directly described by figure 6.3. Readers will be able to relate how figure 6.3 is derived from figure 6.2 if one assumes that the actual flight trajectory Y and the pilot inputs P are known.

Of course one needs to make certain assumptions and accept certain inaccuracies, but one would be able to obtain a reference trajectory that is only influenced by the pilot's premonition of system delays and the accuracy with which he judges the error E. Within the control loop of figure 6.2, one would be one step closer to the reference trajectory source when one works from the signal P. One only needs to estimate the dynamics of the pilot. The reader can compare this to the use of Y as well as the dynamics of both the helicopter $Y_H(s)$ and the pilot $Y_p(s)$. Also, the concern about high-frequency damping within the system dynamics is now more adequately addressed; there is the possibility that high frequency information that had been damped by the pilot's perception would now be added back into the conceptual reference trajectory by the inverse transfer function $Y_p^{-1}(s)$.

6.4.0.1 *Assumptions*

One necessary assumption would be that this "human pilot transfer function" is sufficiently descriptive of the pilot who performed the test flights. Also, one needs to assume that the input-to-output relationships are linear for the flight test conditions. Thus, a movement of 5 mm on the cyclic stick will have the same effect on the helicopter for all flights, regardless of the initial position of the stick.

One must assume that forward or backward acceleration is induced by a pitch motion, while right and left acceleration along the y-axis of the body is induced by a roll motion. This assumption is necessary because the system is under-actuated. Without this assumption, it is very difficult to attribute the pilot inputs to a pitch motion or a forward motion. To some degree, the inaccuracy of this assumption is addressed by the weighted gain factors K_p that are attributed to the pilot. These are assigned individually for each position, velocity and acceleration of each DOF of the model. However, this is an estimate. There is no way of knowing exactly what gain the pilot actually associated with each individual DOF. According to Roskam [26], who proposed the human pilot transfer function that was selected in section 6.4.0.2, K_p can be used for several different applications as long as it is weighted accordingly. Also, he specifically noted, that the magnitude of K_p "is consciously alterable." For the purpose of the trajectory estimation, it will be assumed that K_p is constant for each state during the entire flight.

6.4.0.2 *Human pilot transfer function*

From a quick survey of the literature, several approaches to modelling human pilot transfer function were found [16, 17, 26]. These models have varying degrees of complexity and accuracy. The transfer function selected from Roskam [26] provided a reasonable alternative between the complexity of the *Precision Pilot Model* and the simplicity of the *Crossover Pilot Model* discussed within [16]. Roskam's model is given by

$$Y_p(s) \quad = \quad K_p \cdot e^{-\tau s} \cdot \frac{T_{lead}s + 1}{T_{lag}s + 1} \cdot \frac{1}{T_n s + 1}.$$

Here, $e^{-\tau s}$ models the reaction delay time of the pilot. $T_{lead}s + 1$ models the lead constant used to compensate for the delay. $T_{lag}s + 1$ introduces a lag effect. Of course, K_p is the pilot gain that accommodates the difference between the input and output gains. $T_n s + 1$ represents a neuromuscular lag, but may be ignored when the pilot is considered to be athletic. In this case, it is known that the manoeuvres were performed by an experienced pilot and that the effect may indeed by neglected.

For simplicity of implementation, $e^{-\tau s}$ is approximated by the Pade approximation function

$$e^{-\tau s} \quad \approx \quad \frac{1 - \frac{\tau s}{2}}{1 + \frac{\tau s}{2}}.$$

This is acceptable for low frequency inputs. It will therefore be assumed that the pilot inputs will be supplied at 4 Hz frequencies at most.

The values of the various constants are selected as suggested within [26]. Since the pilot is an experienced test pilot, a reaction delay of $\tau = 0.1$ s is assumed. Although,

the lead constant can be consciously adjusted by the pilot, it is selected to introduce a lead of 0.1 s. To minimize the effect of the lag, it is selected to be ten times smaller than the lead effect. Note that the lag effect can be ignored, but this makes the implementation within a SimuLink™ transfer function block more difficult. It is not a problem when considering $Y_p(s)^{-1}$ because the inverse function has more poles than zeros, but when testing the transfer function itself, one would want to include the lag effect. As mentioned before, the neuromuscular lag was neglected.

6.4.0.3 *Successful implementation*

The difficulty with the approach outlined in figure 6.3 is the fact that there were three unknowns with two equations from the figure. These are given by

$$E = Y_p^{-1}(s, K_p)P. \tag{6.1}$$
$$R = E + Y. \tag{6.2}$$

Within these equations, K_p, E and R are unknown. A third equation is required to obtain a satisfactory solution for the reference trajectory. This equation is provided by placing a constraint on the value of the error signal.

$$-0.2Y \leq E \leq 0.2Y \tag{6.3}$$

This constraint allows for a several solutions to solve the inequality, but the most optimal solution can be selected by reasoning. In an effort to make the effect of the human pilot transfer function more prominent, the largest gain K_p that satisfied the above conditions, is selected. Within the areas where the signal approaches zero, a 20% error allows for more consistent results. With a 10% error margin, the constraints become too strict and force the K_p gain to evaluate to a very small value.

During the implementation of this procedure, it was noticed that the acceleration signals consistently required very small values for K_p to meet the 20% error constraint. To avoid cases where the pilot input P had negligible effect, its value was constrained to

$$K_p \leq 20.$$

This forces the system to accept a contribution from the pilot input P of at least $1/20^{th}$ or 5% of the final trajectory, regardless of whether the conditions of (6.3) are met. This rule only intervened in the trajectory tracking procedure for the generation of acceleration trajectories, which also proved less important for the testing of the controller. The position and velocity trajectories have a more pronounced effect due to the designer chosen gains.

The final results of the trajectory generation procedure are shown within figure 6.4. Readers will notice the relation of the estimated flight trajectory to the actual measured trajectory. The trajectory derived with this procedure is said to be "estimated" because their is no way to validate that this is indeed the trajectory that the pilot had in mind when he flew the manoeuvre. At best, it is an educated guess based upon the inputs that he provided on the helicopter controls. The reader will note, however, that the effect is most pronounced at the peaks extremities of the trajectory and areas where the rate of change was greater. This is precisely where the pilot would compensate for an error between the actual and estimated trajectories.

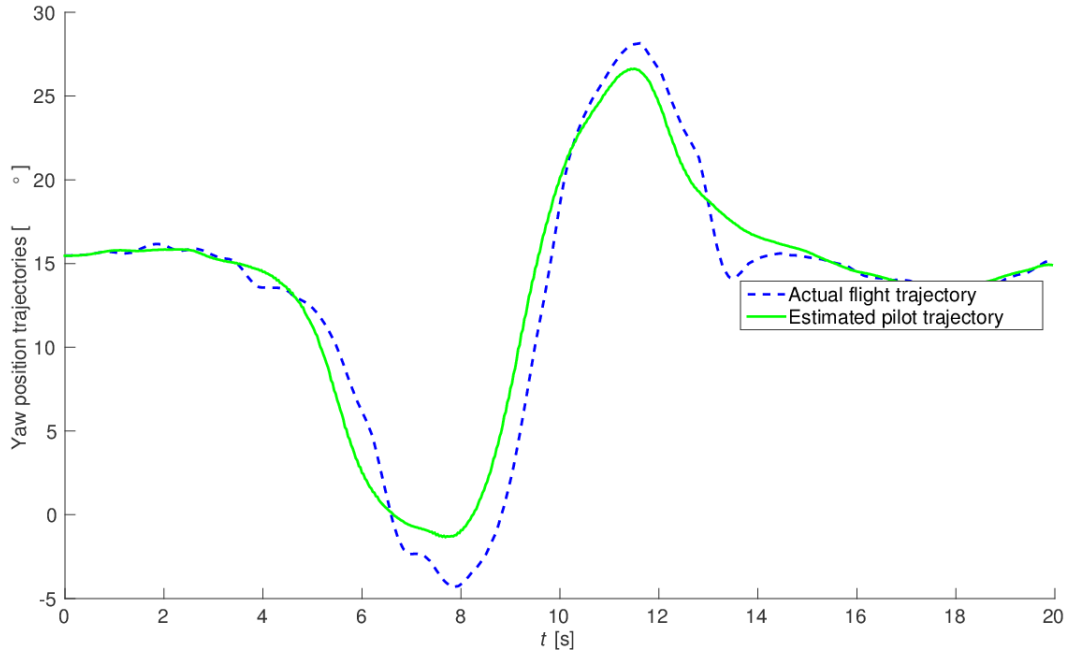

Figure 6.4: Difference between measured and estimated pilot trajectories

6.5 VALIDATION RESULTS

To show that the controller produces very accurate trajectory tracking, the reference trajectory and the output of the helicopter model for the controller inputs are plotted in figures 6.5 to 6.7. Each figure illustrates the position variables related to a specific axis. These include the linear positions along that EF axes, and the rotational position about the BF axes. While it may seem counter-intuitive to use two different reference frames, these are the positions directly described by the system states.

The results are shown for a roll-reversal manoeuvre. Results for three other manoeuvres are shown in part II. During the roll-reversal manoeuvre, the pilot or controller performs an aggressive roll, first to the right and then to the left. He then attempts to stabilise the helicopter at a roll angle of zero. The figures below show the rotational coordinates, not the Euler angles. For this reason, the drastic roll manoeuvre does not appear apparent in Figure 6.5, but readers will notice the roll effect within figure 6.8 of section 6.6.2.

Figures 6.5 and 6.6 show the helicopter is travelling in a north-westerly direction as shown by the negative trend of the x-position and the positive trend of the y-positions within the North-East-Down axes convention for the EF. It is also clear from figure 6.7 that the helicopter maintains its altitude around 700 m as it indeed should. The trajectory tracking is good for all six states, but one can see a slight oscillation at the beginning of the manoeuvre for the $x-$position. This oscillation is quickly damped by the presence of the damping term within the dissipation matrix.

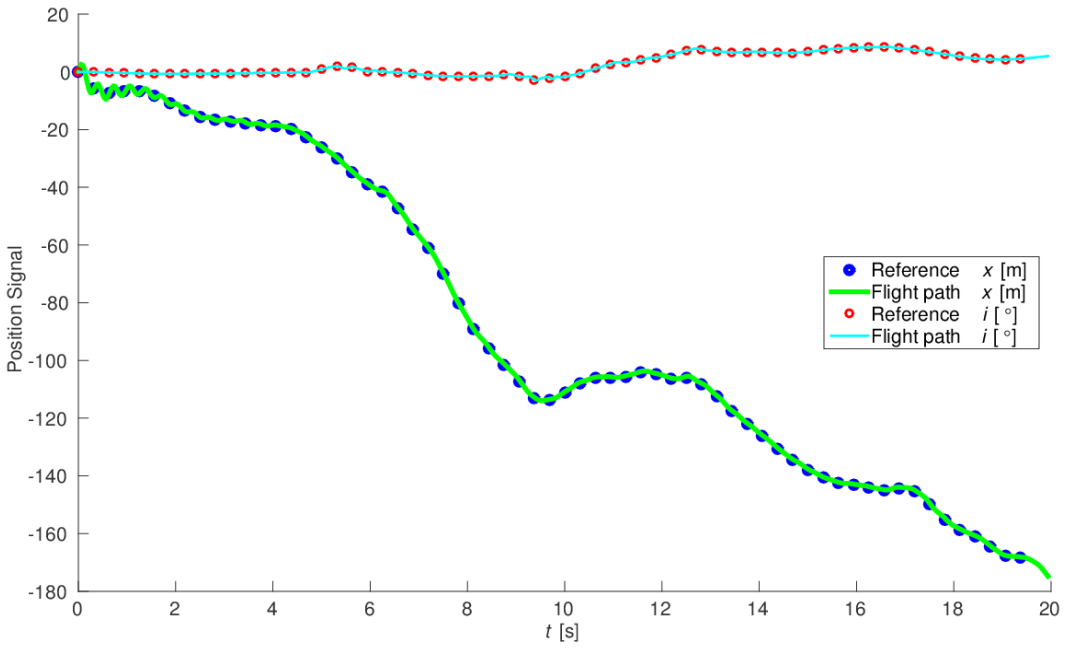

Figure 6.5: Validation results for positions about the $x-$axis

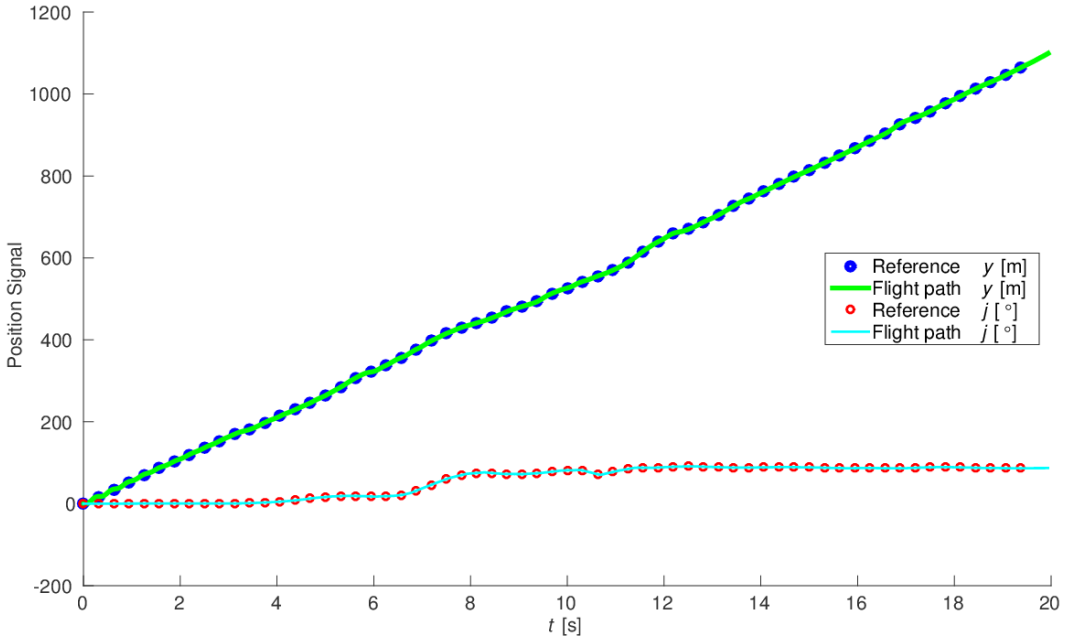

Figure 6.6: Validation results for positions about the $y-$axis

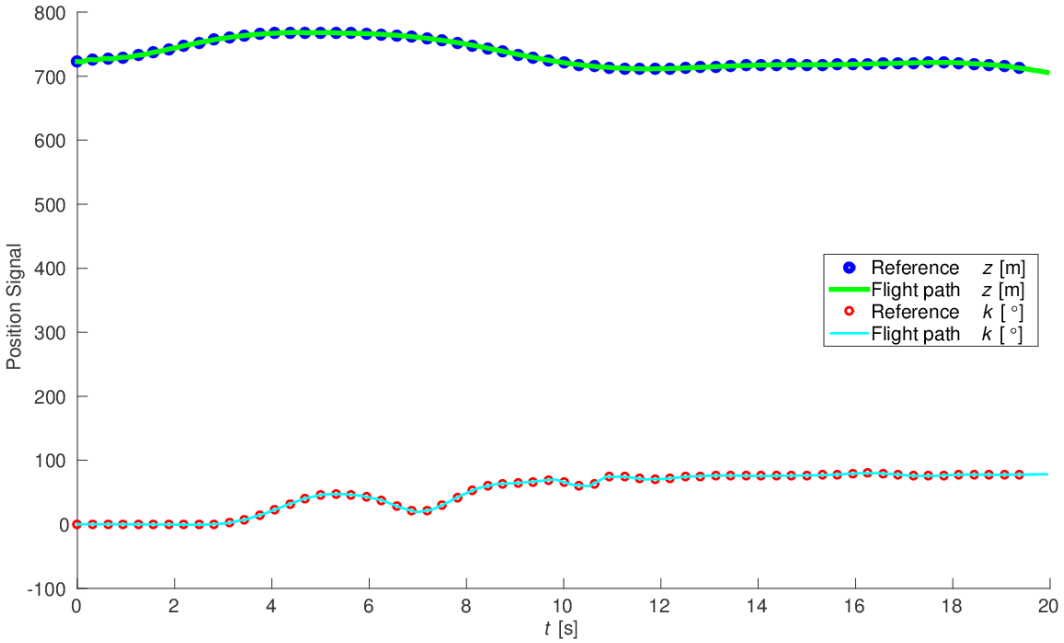

Figure 6.7: Validation results for positions about the $z-$axis

6.6 CONCLUSIONS

6.6.1 *Inaccuracies of gyroscope data*

During the initial stages of testing the controller, gyroscope data was integrated to obtain velocity and position measurements. Although the control system performed well for these inputs, it was only later recognized that the gyroscope data had been measured in g instead of m/s^2. When this mistake was corrected, the scale of position changes no longer seemed valid for the length of simulation time. The issue was mentioned to the engineer that supplied the data for the experiments and he confirmed that gyroscope drift makes the use of gyroscope signals very difficult for position and velocity measurements. Instead, he suggested that the latitude, longitude and altitude measurements be used to derive position and velocity measurements. An expert in the field of data transformation for flight paths helped to convert the latitude, longitude and altitude data to EF positions and BF velocities as required for the model of chapter 3. Readers may study the procedure for these transformations from the WGS-84 system to positions and velocities within [31].

6.6.2 *Deviations in estimated yaw angle trajectories*

During the trajectory estimation procedure described in section 6.4, a deviation was discovered in the yaw angle trajectories for both the quick-stop and the quick-stop-to-the-right manoeuvres. Interestingly, the estimated trajectories for the roll-reversal and wind-up turn manoeuvres were remarkably accurate. This effect can be seen in figure 6.9 and 6.8. This anomaly was immediately brought to the attention of the supplier of the data sets with one proposed explanation.

The hypothesis proposed that the pilot had tried to compensate for some yaw disturbances, possibly a cross wind or similar effect that was not modelled. The difficulty with proving this hypothesis is that the disturbance force would need to be measured

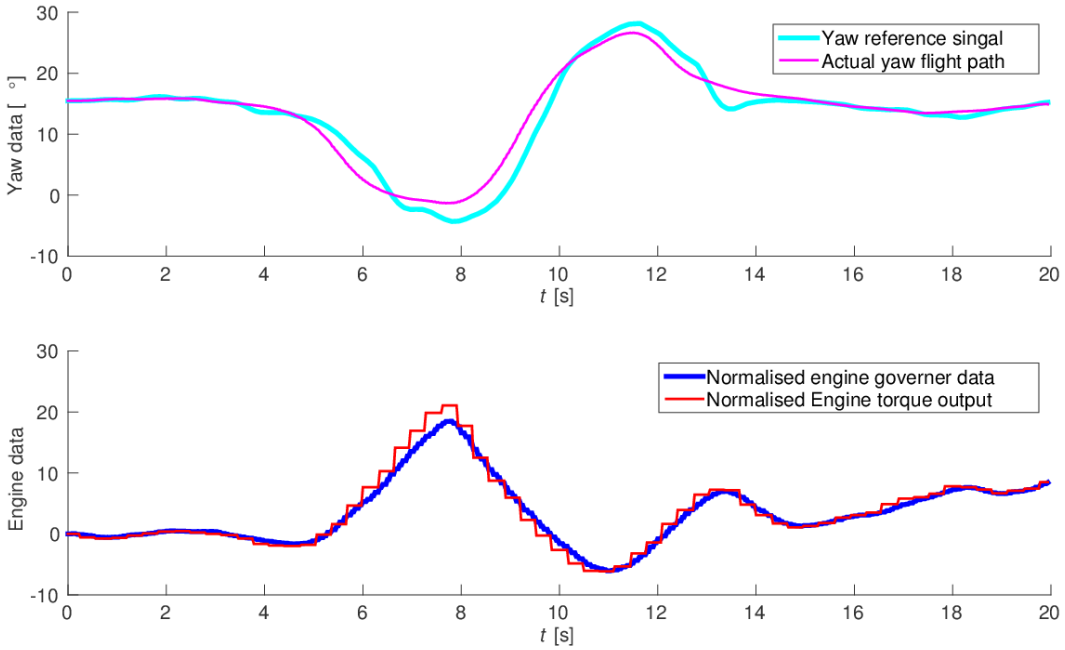

Figure 6.8: Engine governor vs. torque for roll-reversal manoeuvre

externally, which it was not. However, the supplier of the data posed an alternative hypothesis.

The supplier's first impression was that this phenomenon could indeed be caused by disturbances, but it was also possible that the drastic stop manoeuvre influenced the torque output of the engine, thus creating a yaw motion that had to be compensated for. The helicopter in question makes use of an engine governor that estimates the torque required on the rotors. However, there is a latency effect which could cause a difference in the required torque and the estimated torque. The drastic change in forward motion during the stop manoeuvres could cause such difference.

To prove this hypothesis, the engine torque and the engine governor data were normalized and plotted on the same axes. The normalization required a scaling of the data to be comparable. An offset was also added to both datasets so that the first data point would begin at zero. The purpose of this illustration is not to illustrate any unit of measurement, but to show the appropriate relationship between the trend of the estimated torque requirement versus the actual torque requirement.

Readers will notice that the difference between the engine governor and engine torque data is more pronounced at the end of the quick stop manoeuvres as illustrated in figure 6.9. Note that this phenomenon became apparent after the estimation of the trajectory that the pilot attempted to fly. The fact that it could be explained rationally led to increased confidence that the procedure of section 6.4 is indeed a valid approach.

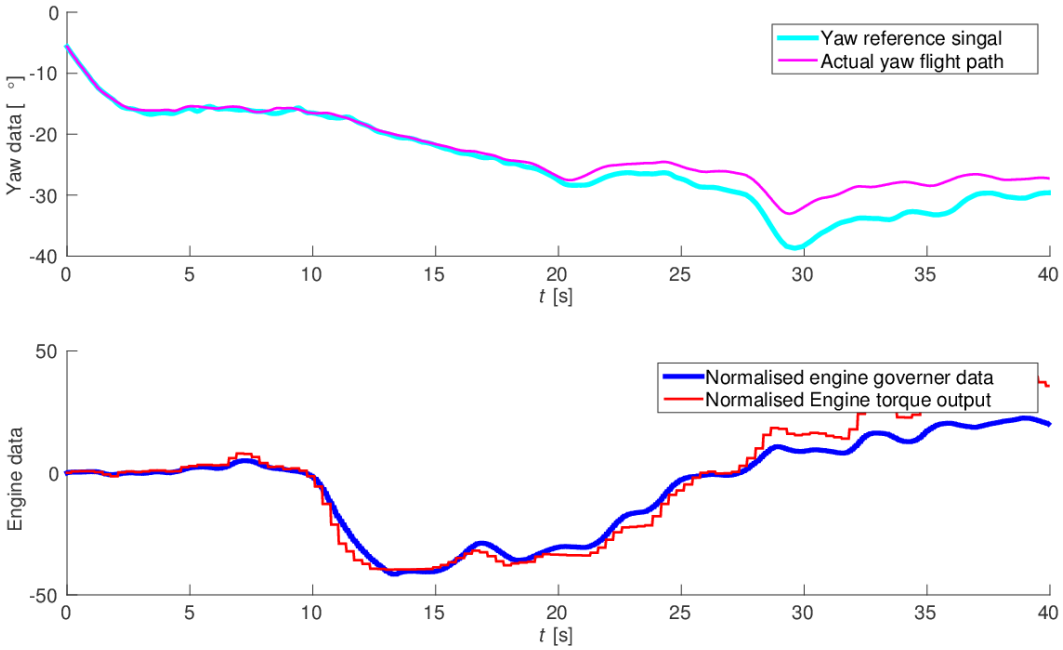

Figure 6.9: Engine governor vs. torque for quick-stop manoeuvre

7 CONCLUSIONS

This final chapter discusses three main areas of interest to the reader. Difficulties within the work are presented first. It is interesting to note that the difficulties with this project related more to the study of the literature and the validation of the control system than the design of the system itself. The discussion of these issue is followed by several recommendations for future work. The most important of these is the implementation of the designed control system on a physical helicopter platform. It is in this area that the most questions about the system remain unanswered.

The last discussion within this chapter relates the three questions about IDA-PBC systems for helicopters. These were mentioned within the problem statement of chapter 1 and relate specifically to the accuracy, stability and energy efficiency of the control system. Two additional sections are added to address additional conclusions. One is the reasoning for the ease with which the control system could be designed. Finally, some comments are also made about the comparison of the simulation results with the reference trajectories that were derived within chapter 6 as opposed to measured flight trajectory data.

7.1 DIFFICULTIES WITHIN THE WORK

7.1.1 *Understanding IDA-PBC*

Section 7.3.1 below discusses the fact that the design of chapter 5 is not a difficult procedure.However, it should also be mentioned that understanding IDA-PBC from the literature is less trivial. Perhaps readers with experience in non-linear control may find the learning curve less difficult, but for readers with only pre-graduate exposure to linear control systems, understanding IDA-PBC is not trivial. An effort is made within this work to ease that learning curve.

Part of the difficulty with understanding IDA-PBC design is that fact that mistakes creep into the literature. Take for instance the flagship work on IDA-PBC of Ortega and Van der Shaft [24]. The work contains two examples of IDA-PBC design, one for a simple RLC system and another for a MAGLEV system. The design of the RLC control system is relatively straight-forward. However, a mistake crept into the work during the recording of design for the MAGLEV system. For an inexperienced reader, the mistake may seem born of some understanding of the system that was not mentioned within [24]. However, it is within simulation of the control system that one will notice that the correction of the mistake dramatically improves the control of the system. Readers who are interested in repeating this procedure are encouraged to study [13] found within part III. Here, a detailed description of the mistake is given. The work also provides system parameters that may be used to reproduce the simulations that are presented in [13]. It is believed that the reader who studies this work will lay a firm foundation for better understanding of IDA-PBC design. For additional study, the

work by Dorlfer et al. [6] comes highly recommended. It is the comprehensiveness of this work that led to the discovery of the mistake within [24].

7.1.2 *Producing satisfactory validation results*

The second difficulty within this work, which was by far the most time-consuming, was to find a satisfactory method of producing validation results. The concerns with the reference trajectory inputs is thoroughly discussed within chapter 6. These concerns related primarly to the fact that the reference trajectory that the pilot had in mind when flying the manoeuvre and the actual flight path must differ at some point. This is based on the assumption that the pilot responds to a perceived error between the reference trajectory and the actual trajectory when he makes adjustments to the inputs like u_{col}, u_{lat} etc.

Two months of intensive work was put into finding a procedure that would provide sufficient confidence in the generated trajectory. Even then, the trajectories used for validation are still estimates and there is no way to validate that this is indeed the trajectory that the pilot had in mind. However, for the purposes of validating the trajectory tracking performance of the control system, the work is sufficient. This topic is expanded upon within section 7.3.3. It is sufficient to say here that the effort to produce the control system was considerably less than the effort necessary to produce a valid reference trajectory input.

7.2 RECOMMENDATIONS FOR FUTURE WORK

7.2.1 *Evaluation of the control system on a physical platform*

Within the project scope of chapter 1 it is specifically mentioned that it is not the purpose of this project to implement the designed technique on a physical system. It is also mentioned in section 3.7.3 of chapter 3 that the model for which the IDA-PBC design was implemented is not specifically a helicopter model. It is only within the Actuator-to-force equations that the model between other aircraft and a helicopter specifically, begin to differ.

Future work could focus on producing a system that can convert the force outputs of the designed control system to actuator signals for a physical platfrom. It would also be of great value to test the control system on such a platform to note the deviations between simulation results and practical tests. It is expected that such a work will comprise an entire master's degree study on its own. Of course, a physical platform must also be available for such a study. Designing a platform that would allow such testing would also be valuable future work.

7.2.2 *Aggressive testing*

Section 6.5 of chapter 6 states that the roll-reveral manoeuvre that the control system is tested for is an aggresive manoeuvre. This is indeed so. Also, the application of the of RWUAV will determine how important tracking of aggressive flight trajectories is. With more aggressive manoeuvres, higher control law gains are required, which is not always optimal.

That said, it is believed that the control system will be able to handle manoeuvres that are even more aggresive than the roll-reversal manoeuvre. The system functioned well for all trajectories that were tested. For this reason it would be good to do more aggressive testing within a simulation environment to see at what point the system is no longer able to meet the accuracy requirements. It is, however, also important to make sure that the manoeuvres remain realistic. Within this study, the control system is tested without constraints on the forces that the helicopter rotors are able to produce. For further investigation, it is important to take the system constraints into consideration.

7.2.3 *Improved gain optimisation*

In section 5.8.5 of chapter 5 the procedure for selecting the control law gains is described. It is noted there that this is by no means an optimal procedure and may be significantly improved. Such improvements may be valuable within future work. The optimal selection of control law gains is perhaps the most valuable contribution that can be made in within the field of IDA-PBC design.

If one were to consider the control law for the roll angle state as given in (5.7), then one can see the relation a Proportional-Integral-Derivative (PID) controller. When one bear's in mind that $\mathbf{p} = \mathbf{M} \cdot \dot{\mathbf{q}}$, then $R_{d\,22}$ represents the proportional constant, k_{p4} represents the integral constant and m represents the derivative constant.

Remember that $R_{d\,22}$, k_{v4} and k_{p4} are left to the choice of the designer. Also, m can be adjusted as desired as demonstrated within [29]. This makes the control law of (7.1) very similar to a PID control law. This also appliess to every state of (5.7).

$$\beta_4\left(\mathbf{x}, \mathbf{x_d}\right) \quad = \quad R_{d\,22} k_{v4} p_e - k_{p4} i_e + \dot{p}_d m \tag{7.1}$$

During testing of control system, the values of $R_{d\,22}$, k_{v4} and k_{p4} have a significant influence. An example of this is given in figure 5.1 in chapter 5 where the damping constant is varied. As such, while IDA-PBC may be considered an "optimal control technique" the selection of the control law gains may be far from optimal. Of course, the objective of the controller will also influence the values of the gains. Much work can be done to in the area of optimal control law gain selection.

7.2.4 *Redundancy of input signals*

One final recommendation for future work would be to investigate the extent to which the control system is able to function without some of the inputs. Some preliminary tests were performed during troubleshooting of the designed system, which showed some evidence that the system may have a certain level of redundancy. This would be a significant benefit in the event of a sensor failure. However, such investigations require significant additional work to determine under which conditions the system will continue to function normally.

7.3 EVALUATION OF FINAL RESULTS

7.3.1 *Ease of design*

Readers will recognise that the ultimate design of the control system as given within chapter 5 is not a difficult procedure. It requires simple application of the principles taught within chapter 4. The most difficult part of the design is the choice of the kinetic and potential energy functions. Readers who are not intimately familiar with the literature on IDA-PBC of mechanical systems may not have had the intuition to rewrite the solution to the homogenuous equations in terms of the momentum variables. This intuition develops with experience. The other difficult part of the design was the selection of the potential energy terms, which is indeed not intuitive before one realises the importance of a minimum within the desired energy function. Again, exposure to the literature on the topic, such as that of Souza et al. [30] helps to see that such a strange form of potential energy as $H_d(\mathbf{x}, \mathbf{x_d}) = \frac{1}{2}\mathbf{K_p}\mathbf{q_e^2}$ instead of $H_d(\mathbf{x}, \mathbf{x_d}) = \mathbf{K_p}\mathbf{q_e}$ is indeed a valid function.

Once such hurdles and the learning curve of IDA-PBC design are overcome, the design procedure is simple. Only a basic understanding of PDEs is necessary. With a good understanding of algebra, most readers should be able to reproduce the design with ease. Note, however, that IDA-PBC design will not always be so simple. If the model for the design included the Actuator-to-force equations of section 3.4, the design would be considerably more complicated. It is also very likely that special understanding will be required and that new interconnection and damping matrices may need to be assigned, as was the case for effective design of the MAGLEV controller in [24]. In that respect, the system designed for this work could be considered trivial as no special challenges presented themselves during the design procedure.

7.3.2 *Reference vs. actual trajectories*

Readers will notice that the validation results of figures 6.5, 6.6 and 6.7 show the trajectory tracking of the reference trajectory. No comparison was made with the measured flight trajectory that was included in the data for actual test flights. This was done because the measured data provides no valuable information. The simulated flight path will differ from the actual flight trajectory by as much as the reference trajectory differs. This difference for the yaw position trajectory is illustrated in figure 6.4 of chapter 6.

Since the reference trajectories that are used as inputs to the control system should represent the trajectories that the pilot had in mind, it is expected that a combination of human error, mechanical linkages, wind and other effects are responsible for the deviations between the reference trajectory and the actual trajectory. Of these it is only the human error that can definitely be removed from the factors that influence the flight path of the helicopter. During testing on a physical platform, it is expected that the flight trajectory will differ from the reference trajectory. However, it is also possible that the control system will be able to compensate for unmodelled effects because it adapts to the error between the inputs from sensors and the reference trajectory. Some preliminary tests do indicate that the system is capable of compensating for such effects.This was tested by removing the compensation for the Coriolis effect, while the effect was still included in the model. The control system compensated for this "perceived" inaccuracy and continued to follow the reference trajectory. This seems to

support the statement within section 5.8.4 of chapter 5 that the Coriolis effect should rather be compensated for during trajectory planning.

7.3.3 *Accuracy of control system*

Readers will agree that the trajectory tracking results presented in figures 6.5, 6.6 and 6.7 are excellent. The results within part II look similarly promising. Section 5.8.5 of chapter 5 makes mention of the ITAE performance index, but readers will notice that notice that no values are presented anywhere within this work. This is specifically done because the performance indexes present relatively little meaning. The tuning procedure could significantly improve the ITAE values by increasing the control gains, but the improved values do not show noticeably better trajectory tracking. Since the goal of the tuning procedure was to keep the control law gains as low as possible while ensuring accurate trajectory tracking, a good ITAE peformance index was sacrificed in favor or lower gains.

The ultimate accuracy of trajectory tracking will also depend on the sensors. The data provided to the control system was derived from GPS data which is known to have its associated inaccuracies. In flight applications where even better accuracy is required, more accurate sensors should be used. If the current control law gains prove insufficient, a new optimisation procedure may be developed or the control law gains may be tuned for the application. It is believed that the designed control system will indeed be able to serve such purposes.

7.3.4 *Stability of control systems*

The IDA-PBC system is an analytical technique backed by rigorous stability proofs. Though stability proofs may also be offered for non-analytical techniques like neural networks [9], the stability of the system is sometimes questioned because of the lack of transparency of the neural network training procedure. In this respect, the analytical approach of IDA-PBC design is a strong benefit.

It is encouraging to note that the control system proved to be stable for all tests that were conducted during this project, provided that the simulations were set up correctely. In all cases where the simulations showed unstable responses, there was some form of error within the set up of the simulation diagram that caused the instability. Often, a sign error was the cause.

In chapter 1, stability is mentioned as one of the main areas of investigation during this study. It can be confidently said that the designed system is stable even for aggressive manoeuvres. However, by the nature of the tests performed in chapter 6, the only basis of comparison is that of the test pilot. In that respect, the control system performs well, but no comment can be made about whether the control system is able to perform manoeuvres that a pilot is unable to fly.

7.3.5 *Energy efficiency of control system*

The question of energy efficiency of the control system is perhaps one of the most difficult to answer. In section 7.2.1 above, testing of the system on a physical platform is recommended as important future work for a subsequent study. Such testing will also provide the best basis for comparing the energy efficiency of the IDA-PBC system

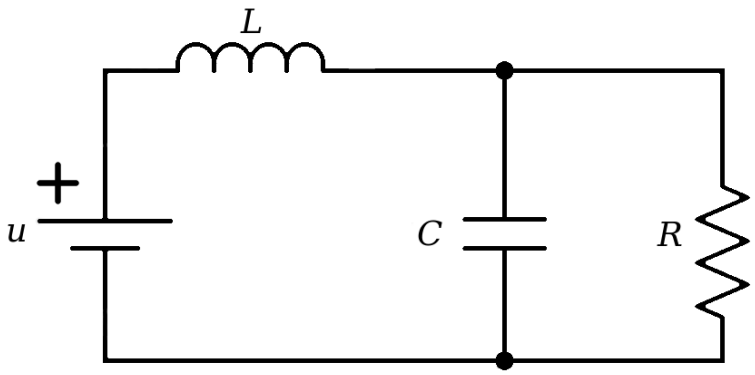

Figure 7.1: RLC system

with that of a PID or even another optimal control strategy. In this case, flight time will be the easiest form of evaluation as long as the same manoeuvres are performed using both systems. The alternative would be to measure fuel consumption or battery capacity after several manoeuvres. At this time, such information is not available.

Having said that, it is indeed possible to make some deductions about the energy efficiency of the system. For this purpose, the reader's attention is drawn to figure 7.2. It shows the energy consumption over time for an RLC system as described within [24] as well as [13]. The RLC system is shown in figure 7.1. From the figure, it is clear that the controlled system uses considerably less energy over time to maintain a specific voltage across the capacitor C. However, this is only an evaluation of a system with and without control. It illustrates that, in theory, more effective control may indeed provided better energy efficiency, but this is not only dependent on the control system. Factors such as the voltage source will also have an influence.

Partaining to the helicopter control, it is expected that the energy efficiency of the entire helicopter system will not be dependent on the control system but on the efficiency of the trajectory that the control system must follow. Frequent changes in direction will decrease efficiency. Of course, there is no point in producing a highly efficient trajectory plan if there is no control system to follow such a plan, but if two different control systems can follow a trajectory equally well, there should not be a significant difference in the energy consumption of the system.

Where one may find that the IDA-PBC system excells is during the control of very aggresive manoeuvres that incorporate non-linear dynamics. In those cases, a non-linear controller is expected to handle the trajectory tracking better than a linear controller. It is within these situations that one may indeed see improved energy efficiency. Sadly, such aggressive manoeuvres are not the norm. In the event of a quick avoidance manoeuvre, the system may provide good energy efficiency, but very few designers are concerned about energy efficiency during such a manoeuvre. In such cases, the stability of the system of much greater importance.

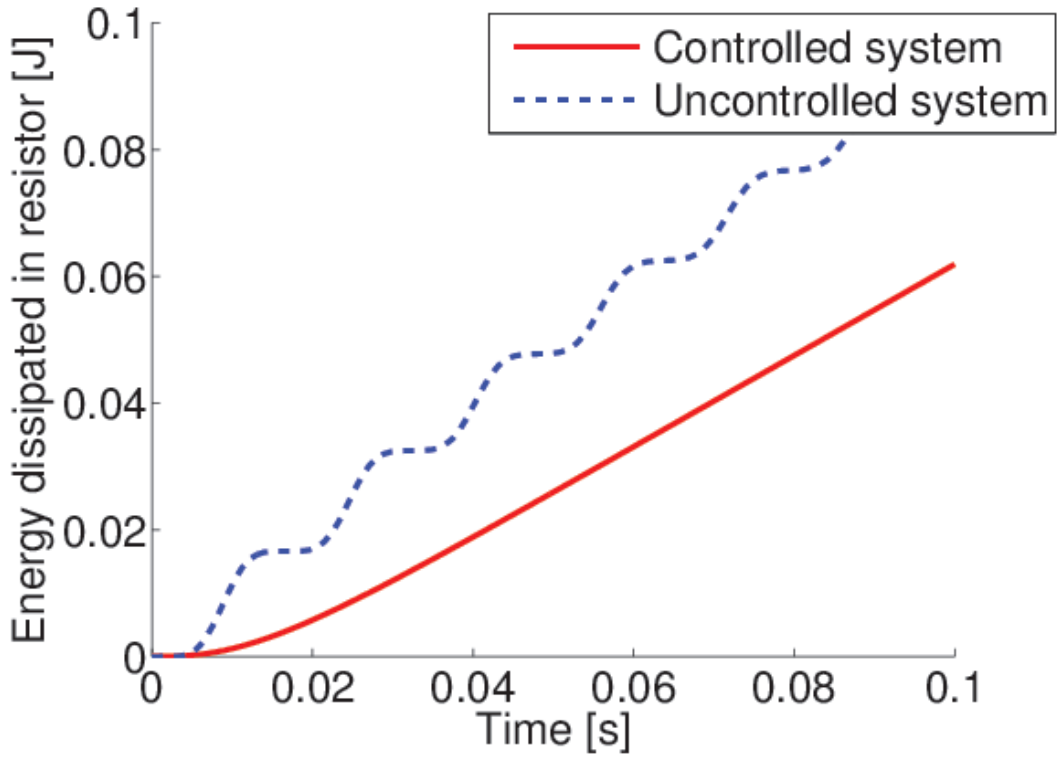

Figure 7.2: Energy consumption of an RLC system

Part II

APPENDIX I

The following three sections present the validation results for three additional manoeuvres, namely the quick-stop manoeuvre, the quick-stop-to-the-right manoeuvre and the wind-up turn manoeuvre. Each section contains a description of the manoeuvre. As in section 6.5 of chapter 6, the positions about the $x-$, $y-$ and $z-$axes are presented. An illustrations of the engine governer vs. torque is also presented together with a plot of the actual yaw trajectory and the estimated one. This will allow the readers to see how the engine governor makes incorrect estimates of the power required during the quick-stop manoeuvres.

A

QUICK-STOP MANOEUVRE

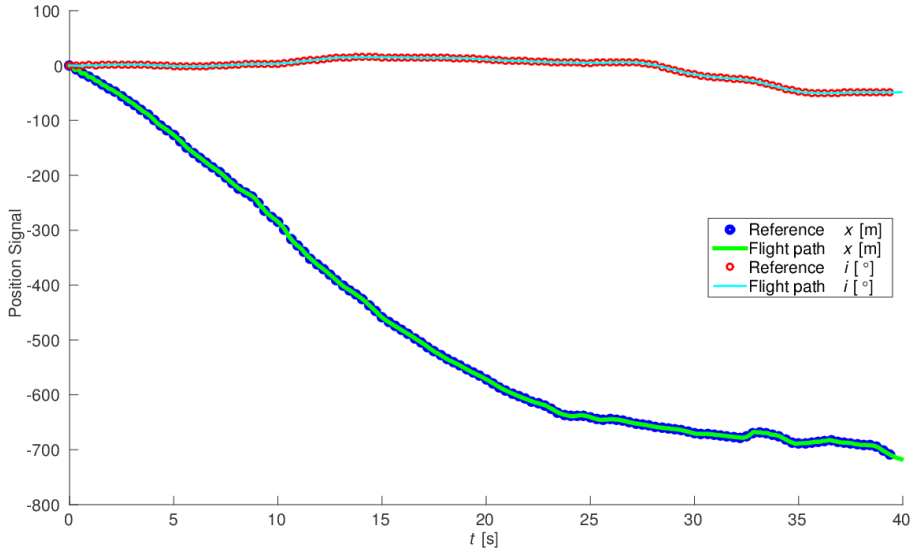

Figure A.1: Validation results for positions about the $x-$axis - QS

The quick-stop manoeuvre is a relatively simple manoeuvre. It requires the pilot to fly into the wind at speed and then perform a stop as quickly as possible.

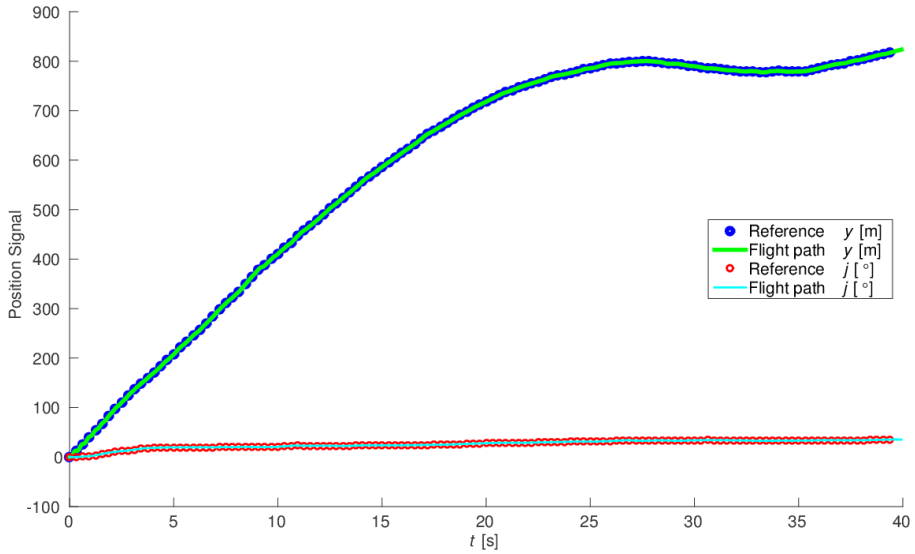

Figure A.2: Validation results for positions about the $y-$axis - QS

From figures A.1, the reader can see that the helicopter travels in a north-westerly direction. Both $x-$ and $y-$positions tend to remain constant toward the end of the manoeuvre, which is to be expected when the aircraft stops. The reader will also notice from figure A.3 that altitude is not maintained. Keeping the altitude constant is difficult during such a manoevre because the stop needs to take place so quickly. As discussed within section 6.6.2 of chapter 6, the engine governed attempts to estimate

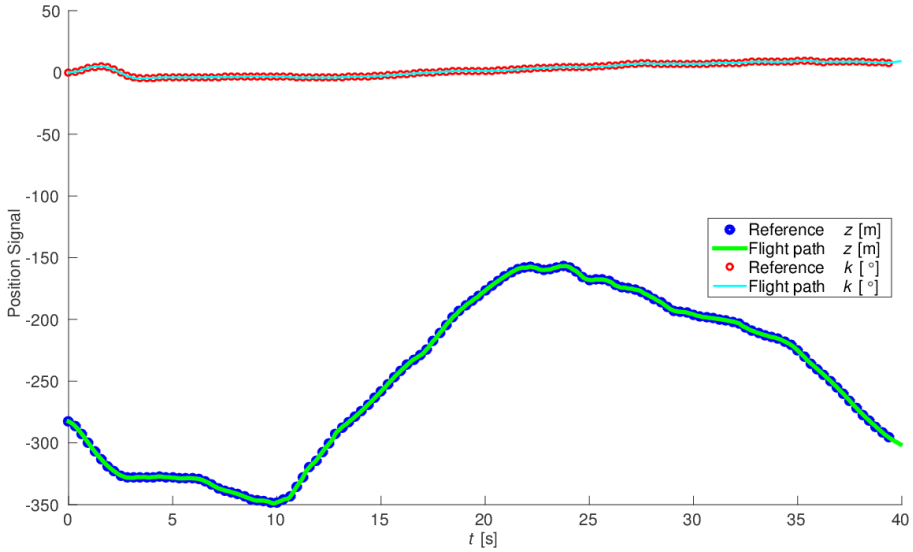

Figure A.3: Validation results for positions about the $z-$axis - QS

the power required, but this estimation becomes inaccurated during the quick-stop manoeuvres. This explains the deviation in the yaw angle within figure A.4. It is also to be expected that the pilot would need to make adjustments to the collective input of the helicopter to reduce the forward thrust. Such reduction is expected to influence the thrust in the upward direction also.

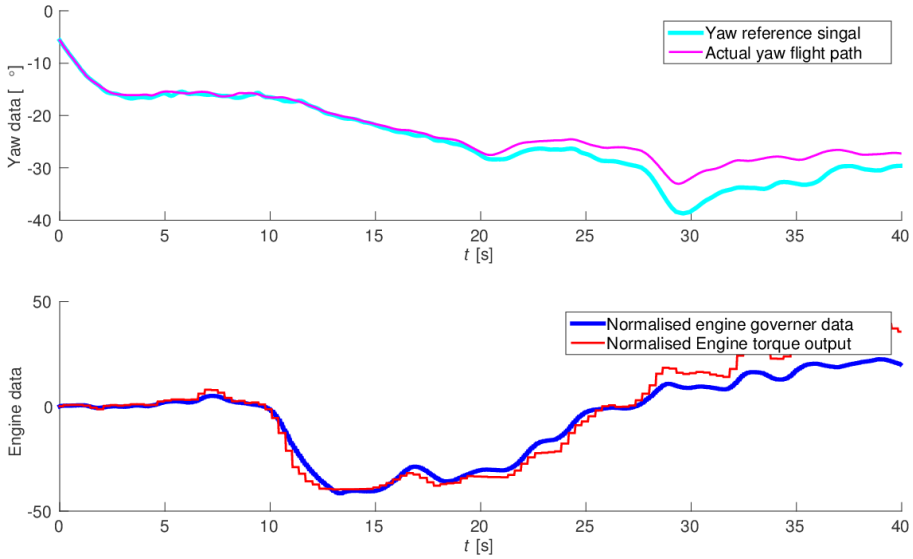

Figure A.4: Engine governor vs. torque - QS

B

QUICK-STOP-TO-THE-RIGHT MANOEUVRE

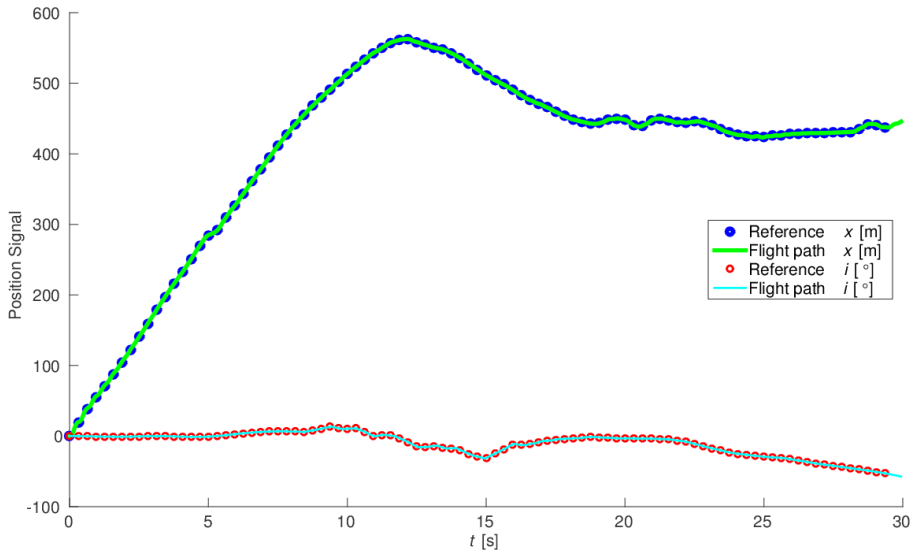

Figure B.1: Validation results for positions about the $x-$axis - QSR

The quick-stop-to-the-right manoeuvre is very similar to the quick-stop manoeuvre. However, the pilot does not start the manoeuvre by flying into the wind. Instead, he flies with the wind blowing across his path toward the left of the aircraft. He then initiates a stop while making a yaw to the right so that he faces into the wind at the end of the manoeuvre.

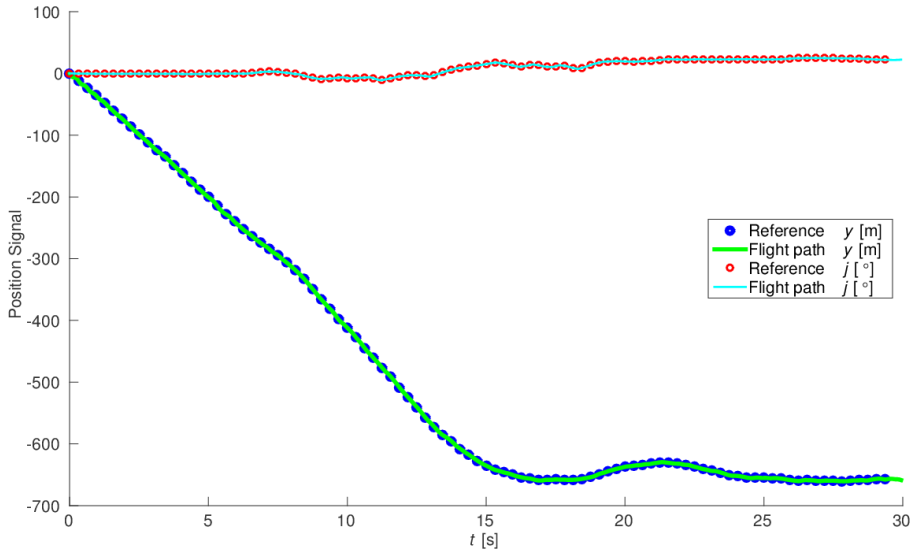

Figure B.2: Validation results for positions about the $y-$axis - QSR

Figures B.1 and B.2 show a south-easterly direction of travel. The fact that the helicopter progressed toward a hover is also apparent in this figure. Again, the $z-$position within figure B.3 shows that the altitude is difficult to control during a quick-stop man-

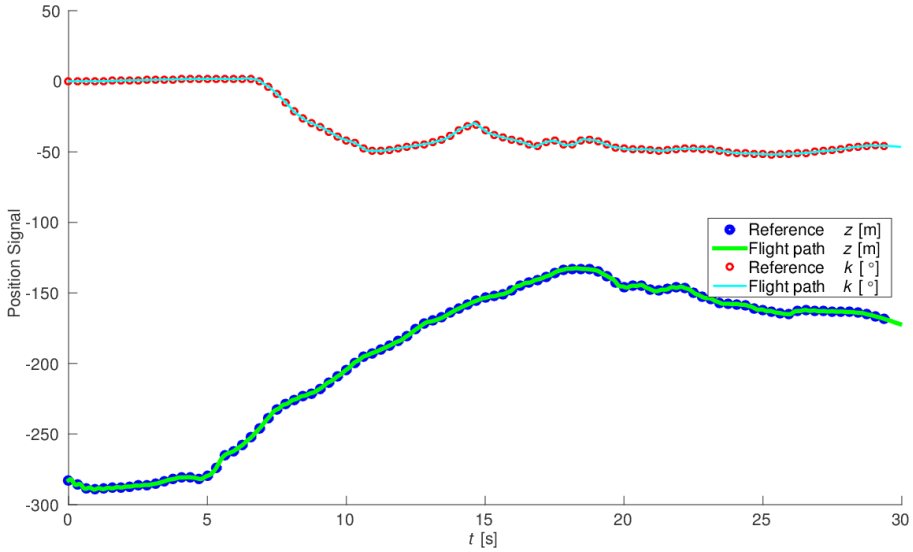

Figure B.3: Validation results for positions about the $z-$axis - QSR

oeuvre. Figure B.4 shows that engine governed does not estimate the required power correctly and therefore produces an undesired yaw motion that the pilot attempted to compensate for in order to maintain the direction of travel. In this case, the reader will also notice the positive yaw motion as the result of turning into the wind. This is not apparent in figure A.4 for the straight quick stop.

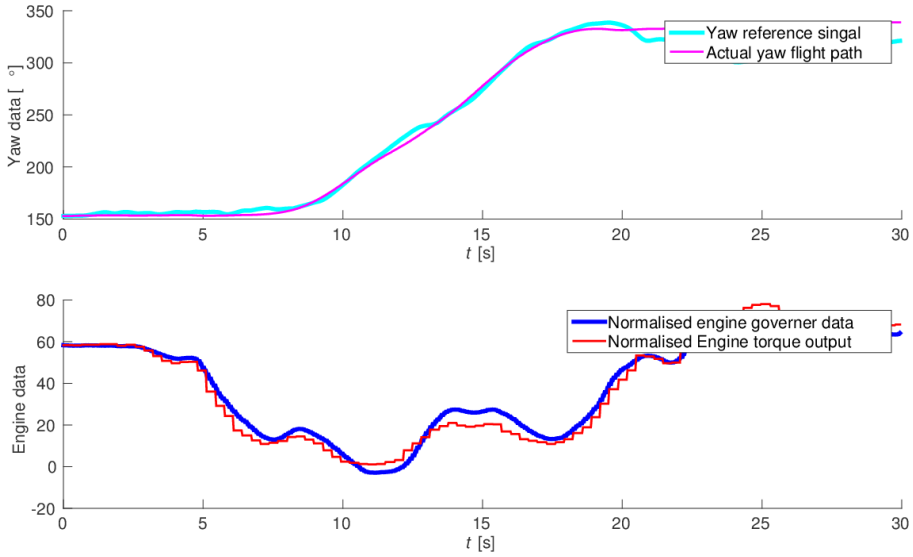

Figure B.4: Engine governor vs. torque - QSR

C

WIND-UP TURN MANOEUVRE

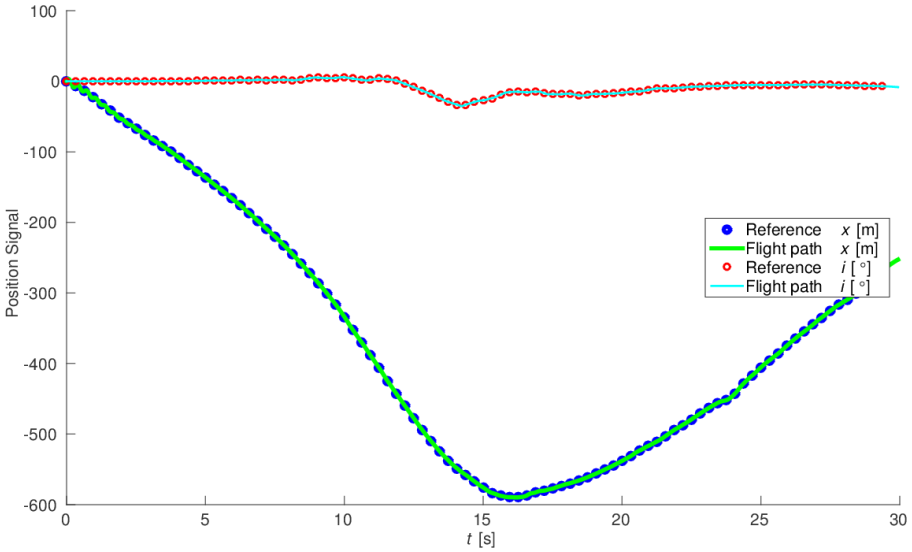

Figure C.1: Validation results for positions about the $x-$axis -WUT

According to the provider of the data, the definition of this wind-up turn is a turn of which the radius becomes smaller and smaller until the maximum allowable $z-$acceleration is achieved.

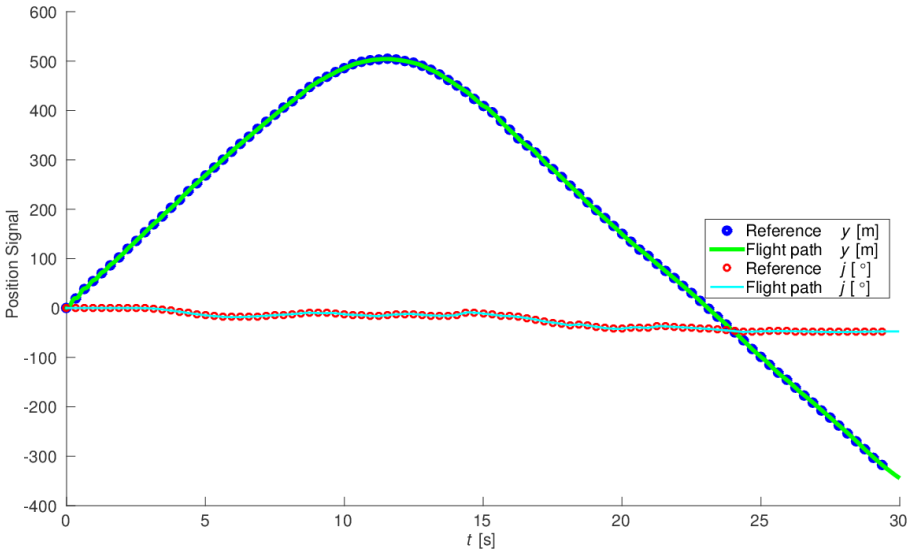

Figure C.2: Validation results for positions about the $y-$axis - WUT

Within figures C.1 and C.2, one can see the turning manoeuvre as indicated by the continually changing position. Figure C.4 also shows that the yaw angle makes a consistent turn from 355° to about 125°. The roll and pitch angles remain nearly constant at 0°. The $z-$position changes consistently as the pilot attempts to increase the acceleration during the turn. The motions for this manoeuvre are more consistent,

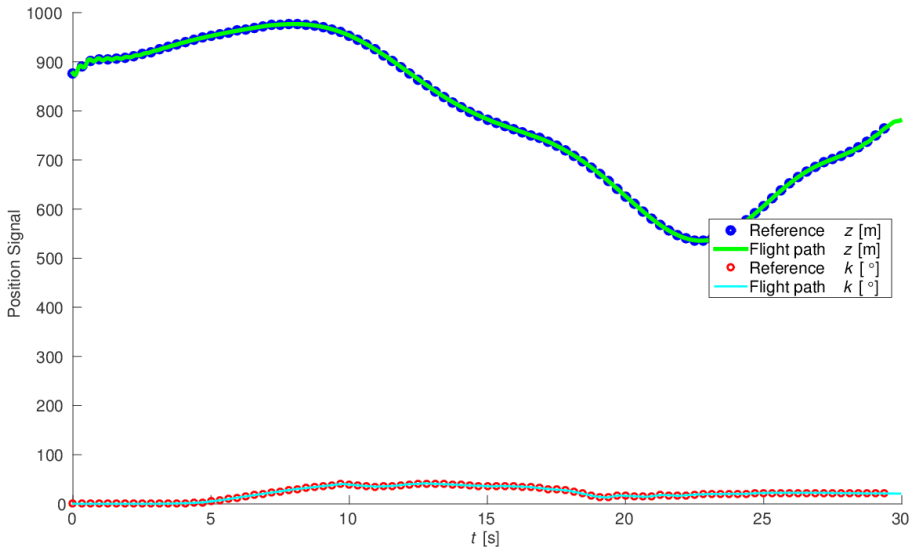

Figure C.3: Validation results for positions about the $z-$axis - WUT

which explains why the engine governor is able to estimate the power requirements more accurately.

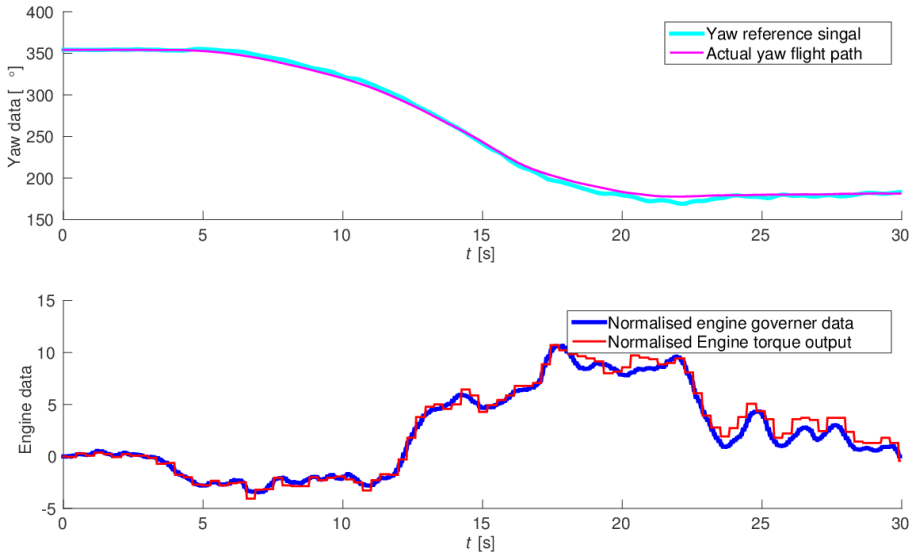

Figure C.4: Engine governor vs. torque - WUT

Part III

APPENDIX II

The following article was submitted to the SAIEE South African Universities Power Engineering Conference in 2014. The purpose of this article is to provide a layman's guide to IDA-PBC design. Within this article, two examples from the flagship work by Ortega and Van der Shaft [24] are discussed. One is an RLC example while the second is a MAGLEV example. A mistake within the IDA-PBC design of theMAGLEV example in [24] is brought to the attention of the readers. This mistake has the potential to confuse new researchers. For this reason, a detailed explanation is offered. To expand on the work of [24], simulation results for both examples are featured within this work. The system parameters for these simulation are also included to allow interested readers to reproduce the results.

DEMYSTIFYING INTERCONNECTION AND DAMPING ASSIGNMENT PASSIVITY-BASED CONTROL

P. J. Kruger* **K. R. Uren*** **and G. van Schoor†**

* *School of Electrical, Electronic and Computer Engineering, North-West University, Potchefstroom Campus, South Africa E-mails: krugerpetrus@gmail.com* and *kenny.uren@nwu.ac.za*

† *Unit for Energy Systems, North-West University, Potchefstroom Campus, South Africa E-mail: george.vanschoor@nwu.ac.za*

Abstract: Due to the vague description in the literature, the learning curve for Passivity-based control is particularly steep from an engineering perspective. In this article, the authors attempt to offer a layman's guide to Interconnection and Damping Assignment Passivity-based Control (IDA-PBC) that may ease the demystification of the techique for other researchers. Through thorough discussion, the application of this theory is demonstrated for a parallel RLC circuit and a magnetic levitation system. Both examples feature prominently within popular literature. This article is therefore meant to be a valuable companion guide to material on the subject of IDA-PBC. Simulation parameters and results are included for comparison by researchers who may be interested in duplicating the results. The simulation results for the RLC system show the quality of the controller as well the improved energy dissipation obtained by implementing the control. The MAGLEV system simulation shows how different response characteristics may be obtained with the free parameters in the control law.

Key words: IDA, PBC, examples, RLC, MAGLEV, nonlinear, control system.

1. INTRODUCTION

In the experience of the authors, the greatest challenge to Passivity-based control is the understanding and then reproducing of the controller design process. One reason for this challenge is the cryptic and sometimes mistaken description of certain critical steps within the calculation procedure as discussed in literature. Although many steps such as the solving of partial differential equations may seem relatively intuitive, the authors had spent much time understanding how the prominent researchers of IDA-PBC have worked toward the mathematical steps that were just briefly noted within articles. The authors also found it necessary to cross-reference between several articles before certain steps were completely understood. Motivated by this challenging experience with the understanding of the IDA-PBC technique, the authors have made it their goal to write a companion guide to material on the subject of IDA-PBC. It is expected that this material will be especially valuable to engineers who do not have the extensive experience with the application of partial differential equation solutions for control problems.

One of the primary reasons for the interest of the authors in this technique is its ability to control nonlinear systems. PBC is in fact known to simplify the controller development strategy. Ortega *et al.* [1] state that monolithic theory for the nonlinear control problem is simply too difficult for the vast and varied array of nonlinear systems. Passivity-based control has at least served for some form of unification for nonlinear control theory of passive systems. A vast array of systems have been controlled with Passivity-based control [1,2]. Control of these varied systems may at least be approached with a similar set of effective tools.

PBC also allows the designer to do the modelling and control from a framework that is commonly understood over various disciplines of engineering. Ortega and Van der Schaft [2] called energy concepts the *"lingua franca"* among various engineering disciplines. According to [2] and [3], the design of controllers become more intuitive when viewed from an energy-shaping perspective, which allows one to move away from approaching controllers as signal processors. In some cases, it can be beneficial to see how the controller effects the stability of the system when viewed as an energy-transforming system [2, 4]. The benefits of approaching the controller design from the energy system perspective over the energy processing perspective is elaborated upon in [2].

2. BASIC THEORY

2.1 Preliminary assumptions and recommendations

Since this article focuses on the applications of IDA-PBC rather than the mathematical proof of the technique, stability proofs are not included within this article. However, a concerted effort was made to include all the practical computations necessary to understand the application of IDA-PBC to control problems. While an understanding of the basic state-space representations of systems and the computation of partial derivatives are assumed, the reader does not require any prior experience in the solution of PDEs. Neither is an understanding of Hamiltonian mechanics required. An effort was made to discuss all the practical theory within the sections below. Researchers who are interested in additional properties and proofs for this technique are encouraged to study [2, 5, 6].

Both the RLC circuit example and the MAGLEV example are discussed within [2], albiet not with simulation results. The article does offer additional insight into theory that

could not be discussed within this article due to space constraints. Readers are also recommended to study the work in [7] for clear discussions and excellent examples.

2.2 Port-Hamiltonian representation

IDA-PBC is based upon the port-Hamiltonian representation of systems. This is simply an alternative representation of the a linear or non-linear state-space system as given by:

$$\dot{\mathbf{x}} = \mathbf{F}(\mathbf{x}) + \mathbf{G}(\mathbf{x})\mathbf{u}. \tag{1}$$

Instead, the equations of motion are described by:

$$\dot{\mathbf{x}} \quad = \quad [\mathbf{J}(\mathbf{x}) - \mathbf{R}(\mathbf{x})]\frac{\partial H}{\partial \mathbf{x}}(\mathbf{x}) + \mathbf{g}(\mathbf{x})\mathbf{u} \tag{2}$$

where:

- $\mathbf{x}$ is the state vector.
- $\mathbf{J}(\mathbf{x})$ is called the interconnection matrix used to indicate the interconnection between states; it is typically composed of the terms -1, 0 or 1.
- $\mathbf{R}(\mathbf{x})$ represents the damping matrix and includes all the dissipation terms, usually in the form of resistances or damping constants.
- $\frac{\partial H}{\partial \mathbf{x}}(\mathbf{x})$ is the gradient of the Hamiltonian function. The Hamiltonian function is composed of the sum of the energies of the system.
- $\mathbf{g}(\mathbf{x})$ is the regular input gain matrix.
- $\mathbf{u}$ is the regular input matrix.

The simplest way to understand the port-Hamiltonian representation of a system is to review an example of system modelled in this form. Readers are encouraged to study the modelling of the RLC circuit example in section 3 for a concise description that represents the intuitive nature of this representation.

2.3 IDA-PBC matching equations

As a preliminary, it is necessary to define the concept of the left annihilator and the Moore-Penrose inverse of the term $\mathbf{g(x)}$. The left annihilator $\mathbf{g}(\mathbf{x})^\dagger$ of $\mathbf{g}(\mathbf{x})$ is the solution to the equality $\mathbf{g}(\mathbf{x})^\dagger\mathbf{g}(\mathbf{x}) = \mathbf{0}$. $\mathbf{g}(\mathbf{x})^\dagger$ is not necessarily uniquely determined by $\mathbf{g}(\mathbf{x})$. This is illustrated in the two examples below. Suppose that $\mathbf{g}(\mathbf{x}) = \begin{bmatrix} 0 & 0 & 1 \end{bmatrix}^\intercal$, then:

$$\mathbf{g}(\mathbf{x})^\dagger\mathbf{g}(\mathbf{x}) = \begin{bmatrix} 0 & 1 & 0 \end{bmatrix}\mathbf{g}(\mathbf{x}) = \mathbf{0}, \text{ and}$$

$$\mathbf{g}(\mathbf{x})^\dagger\mathbf{g}(\mathbf{x}) = \begin{bmatrix} 1 & 1 & 0 \end{bmatrix}\mathbf{g}(\mathbf{x}) = \mathbf{0}.$$

Generally, to solve the matching equations defined below, the inverse of $\mathbf{g}(\mathbf{x})$ is required. However, $\mathbf{g}(\mathbf{x})$ is rarely a square matrix, and therefore a different form of the inverse is used. The Moore-Penrose inverse given by $[\mathbf{g}(\mathbf{x})^\intercal\mathbf{g}(\mathbf{x})]^{-1}\mathbf{g}(\mathbf{x})^\intercal$ is selected throughout [3, 5] and [6].

The objective of the matching equations of IDA-PBC is to add control terms in the form of $\beta(\mathbf{x})$ to the system given by (2) so that the integrated system demonstrates new behaviour. This objective is stated in:

$$[\mathbf{J}(\mathbf{x}) - \mathbf{R}(\mathbf{x})]\frac{\partial H}{\partial \mathbf{x}}(\mathbf{x}) + \mathbf{g}(\mathbf{x})\beta(\mathbf{x}) = [\mathbf{J_d}(\mathbf{x}) - \mathbf{R_d}(\mathbf{x})]\frac{\partial H_d}{\partial \mathbf{x}}(\mathbf{x}). \tag{3}$$

The desired forms of the terms on the right side of the above equation serve to assign specific qualities to the interconnection and damping structures. Also, the desired Hamiltonian should have at least an isolated local minimum at the desired equilibrium point $\mathbf{x}_*$ [2, 5, 7]. In order to alter the Hamiltonian of the system from $H(\mathbf{x})$ to $H_d(\mathbf{x})$ an additional function $H_a(\mathbf{x})$ is added to $H(\mathbf{x})$. Therefore, $H_d(\mathbf{x}) \triangleq H(\mathbf{x}) + H_a(\mathbf{x})$. One may substitute $\mathbf{J_d}(\mathbf{x}) \triangleq \mathbf{J}(\mathbf{x})$ and $\mathbf{R_d}(\mathbf{x}) \triangleq \mathbf{R}(\mathbf{x})$ into (3), such that:

$$[\mathbf{J}(\mathbf{x}) - \mathbf{R}(\mathbf{x})]\frac{\partial H}{\partial \mathbf{x}}(\mathbf{x}) + \mathbf{g}(\mathbf{x})\beta(\mathbf{x}) = [\mathbf{J}(\mathbf{x}) - \mathbf{R}(\mathbf{x})]\frac{\partial H}{\partial \mathbf{x}}(\mathbf{x}) + [\mathbf{J}(\mathbf{x}) - \mathbf{R}(\mathbf{x})]\frac{\partial H_a}{\partial \mathbf{x}}(\mathbf{x}), \tag{4}$$

The terms $[\mathbf{J}(\mathbf{x}) - \mathbf{R}(\mathbf{x})]\frac{\partial H}{\partial \mathbf{x}}(\mathbf{x})$ cancel, such that:

$$\mathbf{g}(\mathbf{x})\beta(\mathbf{x}) = [\mathbf{J}(\mathbf{x}) - \mathbf{R}(\mathbf{x})]\frac{\partial H_a}{\partial \mathbf{x}}(\mathbf{x}). \tag{5}$$

This is precisely the PDE that [2] posed to solve for $\beta(x)$. However, being able to select $\mathbf{J_d}(\mathbf{x}) \neq \mathbf{J}(\mathbf{x})$ and $\mathbf{R_d}(\mathbf{x}) \neq \mathbf{R}(\mathbf{x})$ allows for additional degrees of freedom when solving for $\beta(x)$. Indeed, the MAGLEV example from [2] illustrates that in some cases, the unmodified interconnection matrix will cause the controller to be unstable. The energy-shaping objective is not altered if one were to set $\mathbf{J_d}(\mathbf{x}) \neq \mathbf{J}(\mathbf{x})$ and $\mathbf{R_d}(\mathbf{x}) \neq \mathbf{R}(\mathbf{x})$. If one sets $\mathbf{J_d}(\mathbf{x}) \triangleq \mathbf{J}(\mathbf{x}) + \mathbf{J_a}(\mathbf{x})$ and $\mathbf{R_d}(\mathbf{x}) \triangleq \mathbf{R}(\mathbf{x}) + \mathbf{R_a}(\mathbf{x})$, then (3) may be simplified as given by (6).

$$[\mathbf{J}(\mathbf{x}) - \mathbf{R}(\mathbf{x})]\frac{\partial H}{\partial \mathbf{x}}(\mathbf{x}) + \mathbf{g}(\mathbf{x})\beta(\mathbf{x}) = [\mathbf{J}(\mathbf{x}) + \mathbf{J_a}(\mathbf{x}) - \mathbf{R}(\mathbf{x}) - \mathbf{R_a}(\mathbf{x})]\frac{\partial H_d}{\partial \mathbf{x}}(\mathbf{x}),$$

$$[\mathbf{J}(\mathbf{x}) - \mathbf{R}(\mathbf{x})]\frac{\partial H}{\partial \mathbf{x}}(x) + \mathbf{g}(\mathbf{x})\beta(\mathbf{x}) = [\mathbf{J}(\mathbf{x}) + \mathbf{J_a}(\mathbf{x}) - \mathbf{R}(\mathbf{x}) - \mathbf{R_a}(\mathbf{x})]\left[\frac{\partial H}{\partial \mathbf{x}}(\mathbf{x}) + \frac{\partial H_a}{\partial \mathbf{x}}(\mathbf{x})\right],$$

$$\mathbf{g}(\mathbf{x})\beta(\mathbf{x}) - [\mathbf{J_a}(\mathbf{x}) - \mathbf{R_a}(\mathbf{x})]\frac{\partial H}{\partial \mathbf{x}}(\mathbf{x}) = [\mathbf{J}(\mathbf{x}) + \mathbf{J_a}(\mathbf{x}) - \mathbf{R}(\mathbf{x}) - \mathbf{R_a}(\mathbf{x})]\frac{\partial H_a}{\partial \mathbf{x}}(\mathbf{x}). \tag{6}$$

With appropriate $\mathbf{J_a}(\mathbf{x})$, $\mathbf{R_a}(\mathbf{x})$ and $H_a(\mathbf{x})$ terms, one is able to solve for the control law $\mathbf{u} = \beta(\mathbf{x})$. These three free parameters are calculated from the definitions for $\mathbf{J_d}(\mathbf{x})$, $\mathbf{R_d}(\mathbf{x})$ and $H_d(\mathbf{x})$. One can conclude that one needs to understand how to select the desired matrices to design an

IDA-PBC with this technique.

2.4 Alternative form of matching equations

Dorfler *et al.* [7] make use of (3) together with the left-annihilator and Moore-Penrose inverse defined earlier to derive two alternative matching equations as defined in (7) and (8). These are included for the reader's reference, though they are not applied within this article.

$$g^{\dagger}(\mathbf{x})\left[\mathbf{J}(\mathbf{x})-\mathbf{R}(\mathbf{x})\right]\frac{\partial H}{\partial \mathbf{x}}(\mathbf{x}) = g^{\dagger}(\mathbf{x})\left[\mathbf{J_d}(\mathbf{x})-\mathbf{R_d}(\mathbf{x})\right]\frac{\partial H_d}{\partial \mathbf{x}}(\mathbf{x}) \quad (7)$$

$$\beta(\mathbf{x}) = \mathbf{g^{-1}}(\mathbf{x})\left(\left[\mathbf{J_d}(\mathbf{x})-\mathbf{R_d}(\mathbf{x})\right]\frac{\partial H_d}{\partial \mathbf{x}}(\mathbf{x})\right) - g^{-1}\left(\left[\mathbf{J}(\mathbf{x})-\mathbf{R}(\mathbf{x})\right]\frac{\partial H}{\partial \mathbf{x}}(\mathbf{x})\right) \quad (8)$$

2.5 Solving of the partial differential equations

The most complex task of the IDA-PBC design is to obtain an appropriate solution of $H_d(\mathbf{x})$ for the matching equations. The use of computational tools such as Maple™ greatly ease this process, but in many cases, Maple™ includes an arbitrary differential function $\_F(z)$ in the solution. Here z is a combination of several states. Any function of z will be sufficient as long as it is differentiable. However, very few functions will satisfy the additional requirements posed by the IDA-PBC technique.

In order to enforce passivity, IDA-PBC also requires that $H_d(\mathbf{x})$ has at least a local minimum, and preferably a global minimum, at the desired equilibrium point $\mathbf{x}_*$. Therefore, $\_F(z)$ should be selected such that $\frac{\partial H_d}{\partial \mathbf{x}}(\mathbf{x}_*) = \mathbf{0}$ is satisfied. The examples within this article will clearly illustrate how these conditions are met for the controller design. One final comment about $\_F(z)$ is necessary. Generally, the function $\_F(z)$ will be in one of two forms [7]:

$$\_F(z) = -\frac{K_p}{2}(z-z_d)^2+\phi \quad \text{or} \quad \_F(z) = K_p(z-z_d\ln z)+\phi. \quad (9)$$

Here, z_d has the same form as z, but instead of the states, z_d incorporates the desired value for each respective state. ϕ represents the additional terms necessary to ensure that $\frac{\partial H_d}{\partial \mathbf{x}}(\mathbf{x}_*) = \mathbf{0}$. The squared and ln forms are chosen specifically because they both have global minimums. The proportional constant K_p offers an additional degree of freedom. The z_d term provides the reference term necessary to force the minimum of $H_d(\mathbf{x})$ to occur at $\mathbf{x}_*$.

The final step in the design procedure is to write out the control law. The nature of the matrix $\mathbf{g}(\mathbf{x})$ from (2) introduces both zero and nonzero gain factors that are multiplied with the system input. For this reason, (5) will produce both homogeneous and nonhomogeneous matching equations. The nonhomogeneous matching equation will be used to solve for the control input $\beta(\mathbf{x})$ while the homogeneous equations are used to determine the arbitrary differential function $\_F(z)$. This will once again be illustrated best within the examples below.

2.6 General Algorithm

The general procedure for IDA-PBC design may now be summarised. Assuming that the system model is already in port-Hamiltonian form and that desired equilibrium point $\mathbf{x}_*$ is known:

1. *Determine the most appropriate form of the matching equations to be used. This may require trial and error.*
2. *Solve the homogeneous matching equation to determine the form of the arbitrary differential function* $\_F(z)$.
3. *Ensure that the choice of* $\_F(z)$ *satisfies the condition* $\frac{\partial H_d}{\partial \mathbf{x}}(\mathbf{x}_*) = \mathbf{0}$.
4. *Use the entire homogeneous solution to solve the nonhomogeneous matching equation for* $\beta(\mathbf{x})$.

The control input $\beta(\mathbf{x})$ may then be used within a simulation of the system.

3. RLC EXAMPLE

The port-Hamiltonian model of the circuit in Figure 1 is wholly based upon Kirchhoff's current and voltage laws. The important differences within this model are that the states are not the voltage and current of the circuit. Instead, they are the charge accumulated in the capacitor, q_C, and the flux flowing through the inductor, ϕ_L. Of course, flow of the charge, $\dot{q}_C$, is current. So is the term $\frac{1}{L}\phi_L$. Similarly, the flow of flux, $\dot{\phi}_L$, induces a voltage and the voltage across the capacitor terminals is given by $\frac{1}{C}q_C$. Therefore, the state-space model from KVL and KCL is given by (10).

$$\begin{aligned} \dot{x}_1 = \dot{q}_C &= -\frac{1}{RC}x_1+\frac{1}{L}x_2, \\ \dot{x}_2 = \dot{\phi}_L &= -\frac{1}{C}x_1+u. \end{aligned} \quad (10)$$

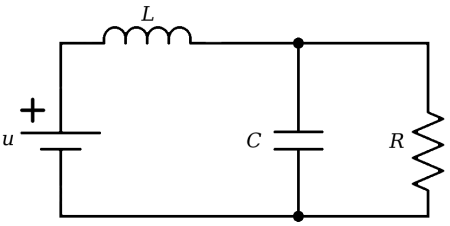

Figure 1: RLC circuit layout

To obtain the port-Hamiltonian model as defined by (12), the Hamiltonian should be defined as the sum of the individual energies:

$$H(\mathbf{x}) = \frac{1}{2C}x_1^2+\frac{1}{2L}x_2^2. \quad (11)$$

$$\dot{\mathbf{x}} = \left\{ \begin{bmatrix} 0 & 1 \\ -1 & 0 \end{bmatrix} - \begin{bmatrix} 1/R & 0 \\ 0 & 0 \end{bmatrix} \right\} \begin{bmatrix} \frac{\partial H}{\partial x_1}(\mathbf{x}) \\ \frac{\partial H}{\partial x_2}(\mathbf{x}) \end{bmatrix} + \begin{bmatrix} 0 \\ 1 \end{bmatrix} \mathbf{u}. \tag{12}$$

Readers may easily confirm that (10) and (12) represent the same system.

Ortega and Van der Schaft [2] started with the following matching equation:

$$[\mathbf{J}(\mathbf{x}) - \mathbf{R}(\mathbf{x})] \frac{\partial H_a}{\partial \mathbf{x}}(\mathbf{x}) = \mathbf{g}(\mathbf{x})\beta(\mathbf{x}). \tag{13}$$

From (12) the above matching equation may be expanded to:

$$\begin{aligned} -\frac{1}{R}\frac{\partial H_a}{\partial x_1}(\mathbf{x}) + \frac{\partial H_a}{\partial x_2}(\mathbf{x}) &= 0, \\ -\frac{\partial H_a}{\partial x_1}(\mathbf{x}) &= \beta(\mathbf{x}). \end{aligned} \tag{14}$$

The authors used Maple™ to obtain that:

$$H_a(\mathbf{x}) = \_F(Rx_1 + x_2), \tag{15}$$

with $\_F(\cdot) : \mathbb{R} \to \mathbb{R}$ is the differentiable function that is left to the choice of the designer. Let $(Rx_1 + x_2) = z$. For the purpose of passivity-based control $\_F(z)$ should be chosen such that $H_d(\mathbf{x})$ has a minimum at the desired equilibrium point $\mathbf{x}_*$. If the desired source input is given by u_* then $\mathbf{x}_* = \begin{bmatrix} Cu_* & \frac{L}{R}u_* \end{bmatrix}$ which may be readily confirmed by recalling the definitions for the charge in a capacitor and the flux in an inductor, $q_C = CV_C$ and $\phi_L = LI_L$ respectively.

From [2] it was shown that $\_F(z)$ was chosen to be a quadratic function such that:

$$H_a(z) = \frac{K_p}{2}[z - z_d]^2 - Ru_*z. \tag{16}$$

However, by substituting $H_a(z)$ into $H_d(\mathbf{x})$ and solving for $\frac{\partial H_d}{\partial \mathbf{x}}(\mathbf{x}_*)$, it may readily be seen that this form does not satisfy the equilibrium conditions:

$$\frac{\partial H_d}{\partial \mathbf{x}}(\mathbf{x}_*) = \begin{bmatrix} K_pR[(z_*) - (z_d)] - u_*R^2 + \frac{Cu_*}{C} \\ K_pR[(z_*) - (z_d)] - u_*R + \frac{\frac{L}{R}u_*}{L} \end{bmatrix} \neq \mathbf{0}. \tag{17}$$

Instead, a slightly different form for $H_a(z)$ is proposed:

$$H_a(z) = \frac{K_p}{2}[z - z_d]^2 - \frac{u_*}{R}z. \tag{18}$$

In this case, $\frac{\partial H_d}{\partial \mathbf{x}}(\mathbf{x}_*) = \mathbf{0}$ is satisfied:

$$\frac{\partial H_d}{\partial \mathbf{x}}(\mathbf{x}_*) = \begin{bmatrix} K_pR[(z_*) - (z_d)] - u_* + \frac{Cu_*}{C} \\ K_pR[(z_*) - (z_d)] - \frac{u_*}{R} + \frac{\frac{L}{R}u_*}{L} \end{bmatrix} = \mathbf{0}. \tag{19}$$

From (14) one can solve for the control law:

$$\beta(\mathbf{x}) = -K_pR[R(x_1 - x_{1*}) + (x_2 - x_2)] + R^2u_* - \frac{x_1}{C}. \tag{20}$$

4. MAGLEV SYSTEM

Due to space constraints the model for the MAGLEV system shown in Figure 2 is nog discussed in great detail here. Instead the reader is referred to [2] and [8]. It is believed that the reader will be able to confirm the port-Hamiltonian model. Kirchhoff's voltage law for the coil of the electromagnet and Newton's second law was used to derive the model. The coil has a resistance R and an inductance $L(\theta)$. The force of the electromagnet is given by (21):

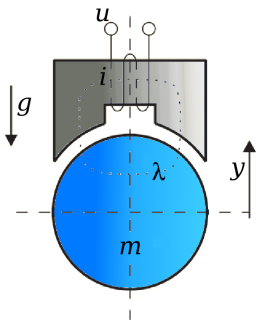

Figure 2: MAGLEV system layout

$$F = \frac{1}{2}\frac{\partial L}{\partial \theta}(\theta)i^2. \tag{21}$$

θ is the distance of the ball from the nominal position. The inductance may be suitably approximated with:

$$L(\theta) = \frac{k}{c - \theta}, \tag{22}$$

where the nominal position has been set equal to c and k is positive constant. This approximation is valid for the interval $-\infty < \theta < 1$.

If one selects the states as the flux through the electromagnet λ, θ and $m\dot{\theta}$, then $\mathbf{x} = \left[\lambda, \theta, \mathbf{m}\dot{\theta}\right]^\top$. Once again, the Hamiltonian is given by the sum of the system energies:

$$H(\mathbf{x}) = \frac{1}{2k}(c - x_2){x_1}^2 + \frac{1}{2m}{x_3}^2 + mgx_2.$$

The port-Hamiltonian model may then be stated as given in (23).

$$\dot{\mathbf{x}} = \left\{ \underbrace{\begin{bmatrix} R & 0 & 0 \\ 0 & 0 & 1 \\ 0 & -1 & 0 \end{bmatrix}}_{\mathbf{J}(\mathbf{x}) - \mathbf{R}(\mathbf{x})} \right\} \frac{\partial H}{\partial \mathbf{x}}(\mathbf{x}) - \underbrace{\begin{bmatrix} 1 \\ 0 \\ 0 \end{bmatrix}}_{\mathbf{g}(\mathbf{x})} u. \tag{23}$$

The chosen equilibrium points are selected to be $\mathbf{x}_* = \left[\sqrt{2kmg}, x_{2*}, 0\right]^\top$. x_{2*} is a setpoint that is left to the choice of the designer.

In [2] it is shown that by investigating the Hessian of $H_d(\mathbf{x})$ above, it may be shown the system is sign indefinite for

all $H_a(x_1)$. This will cause instability of the IDA-PBC controller. In order to solve the problem, which apparently stems from the lack of effective coupling between states, [2] propose a new form for $\mathbf{J}(\mathbf{x})$.

$$\mathbf{J}(\mathbf{x}) = \begin{bmatrix} 0 & 0 & -\alpha \\ 0 & 0 & 1 \\ \alpha & -1 & 0 \end{bmatrix},$$

where $\alpha > 0$ is a constant. Note that later within [2], a shuffling of the damping matrix $\mathbf{R}(\mathbf{x})$ is also done to simplify the control law. It is important to take note that such simplifications and adaptions may be made, but these adaptions are not the focus of this article.

The resulting matching equations for the new $\mathbf{J}(\mathbf{x})$ are then given by:

$$\begin{aligned} -R\frac{\partial H_a}{\partial x_1}(\mathbf{x}) &= \frac{\alpha}{m}x_3 + \beta(\mathbf{x}), \\ \frac{\partial H_a}{\partial x_3}(\mathbf{x}) &= 0, \\ \alpha\frac{\partial H_a}{\partial x_1}(\mathbf{x}) - \frac{\partial H_a}{\partial x_2}(\mathbf{x}) &= -\frac{\alpha}{k}(1-x_2)x_1. \end{aligned} \quad (24)$$

Solving the last of these in Maple™ results in a solution for $Ha(x_1, x_2)$:

$$H_a(x_1,x_2) = \frac{1}{6}\frac{{x_1}^3}{\alpha k} + \left(\frac{1}{2}\frac{x_2}{k} - \frac{1}{2k}\right){x_1}^2 + \_F1\left(\frac{x_1 + x_2\alpha}{\alpha}\right). \quad (25)$$

The arbitrary differentiable function $\_F1\left(\frac{x_1+x_2\alpha}{\alpha}\right)$ is given by [2] as (26).

$$\begin{aligned} \_F1\left(\frac{x_1 + x_2\alpha}{\alpha}\right) &= mg\left[-x_2 + x_{2d} - \frac{x_1 - x_{1d}}{\alpha}\right] \\ &\quad + mg\left[\frac{1}{2}b\left(x_2 - x_{2d} + \frac{x_1 - x_{1d}}{\alpha}\right)^2\right] \end{aligned} \quad (26)$$

By substituting (26) into (25) and then solving for $H_d(\mathbf{x}) = H(\mathbf{x}) + H_a(\mathbf{x})$, one can test whether the equilibrium conditions $\mathbf{x}_* = \left[\sqrt{2kmg}, x_{2*}, 0\right]^\top$ will satisfy the requirement that $\frac{\partial H_d}{\partial \mathbf{x}}(\mathbf{x}) = \mathbf{0}$.

Again, Maple™ was used to determine that

$$\frac{\partial H_d}{\partial \mathbf{x}}(\mathbf{x}) = \begin{bmatrix} mg\left(-\frac{1}{\alpha} + \frac{b}{\alpha}\left(\frac{x_1 - x_{1d}}{\alpha} + x_2 - x_{2d}\right)\right) + \frac{1}{2}\frac{{x_1}^2}{k\alpha} \\ mg + mg\left(-1 + b\left(\frac{x_1 - x_{1d}}{\alpha} + x_2 - x_{2d}\right)\right) \\ \frac{x_3}{m} \end{bmatrix}.$$

By substituting $\mathbf{x}_* = \left[\sqrt{2kmg}, x_{2*}, 0\right]^\top$ into the above, it may be seen that the choice of (26) is correct. It may be reasoned that with a little trial and error, the reader could also arrive at this choice of (26).

According to [2], both $\alpha, b > 0$. It was confirmed within the simulations that $\alpha < 0$ or $b < 0$ produce unbounded outputs.

The first condition from (24) was solved with Maple™ to produce the control law given by:

$$\begin{aligned} u &= -R\left(\frac{1}{2}\frac{{x_1}^2}{\alpha k} + \frac{(x_2 - 1)x_1}{k}\right) \\ &\quad + mgR\left(-\frac{1}{\alpha} + \frac{b}{\alpha}\left(x_2 - x_{2d} + \frac{x_1 - x_{1d}}{\alpha}\right)\right) - \frac{\alpha x_3}{m}. \end{aligned} \quad (27)$$

With some rearrangement of the terms as given below, one may arrive at the form of u given in [2].

$$\begin{aligned} u &= -\frac{R}{\alpha}\frac{{x_1}^2}{2k} + \frac{R}{k}(-x_2 + 1)x_1 \\ &\quad - mg\frac{-R}{\alpha} - \frac{mgRb}{\alpha}\left(x_2 - x_{2d} + \frac{1}{\alpha}x_1 - x_{1d}\right) - \frac{\alpha x_3}{m} \end{aligned} \quad (28)$$

Notice that K_p would then be set equal to $\frac{mgRb}{\alpha}$. The authors found that by simply selecting $K_p > 0$ as suggested by [2], the system would not necessarily stabilise for too large a value of K_p.

5. SIMULATION RESULTS AND DISCUSSION

5.1 RLC example

The systems described in sections 3 and 4 were simulated within MATLAB® SimuLink™ using the parameters as defined by:

$$\begin{aligned} u_d &= 12\text{ V} & R &= 200\ \Omega \\ C &= 625\ \mu\text{F} & L &= 10\text{ mH} \\ K_p &= 24.96 \end{aligned}$$

Figure 3 shows the response of the system for the capacitor charge q_C, both for the controlled and uncontrolled voltage sources. The values for R and C were specifically selected to produce a response with a poor damping constant so as to evaluate the controlled response. A strongly damped system will show considerably less difference between the controlled and uncontrolled responses.

Figure 4 displays the cumulative energy dissipation within the resistor of Figure 1. It may be clearly seen that the oscillatory response of the uncontrolled system adds excessive energy dissipation.

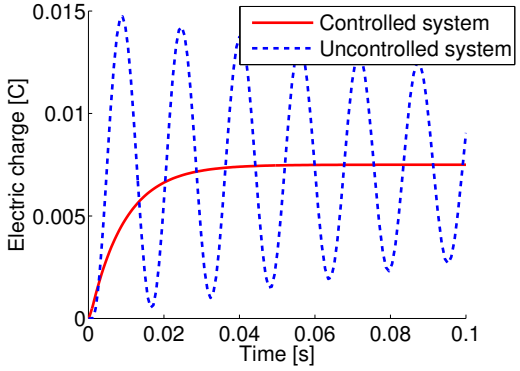

Figure 3: Capacitor charge over time

5.2 MAGLEV example

The MAGLEV example was simulated using the parameters from [8] as defined by:

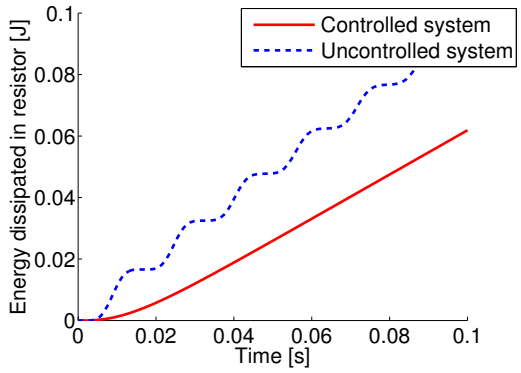

Figure 4: Energy dissipation of circuit over time

c	= 5×10^{-3} m	k	= 6.4042×10^{-5} H·m
R	= 2.52 Ω	m	= 0.0844 kg
K_p	= 3.16	g	= 9.81 m/s^2
x_{1d}	= 0.0103 Wb	x_{2d}	= -3×10^{-3} m

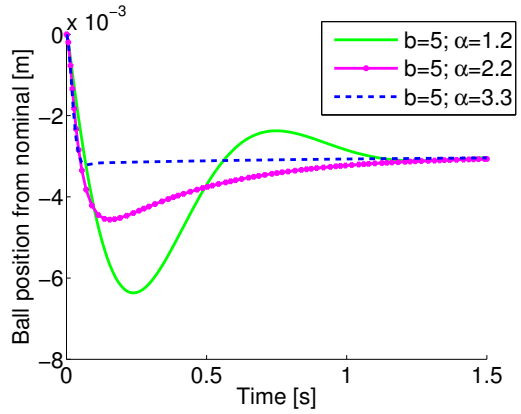

Figure 5: $H_{a1}(\mathbf{x})$: Sweep of the α-parameter, MAGLEV system

Figure 5 shows a sweep of the α parameter for the control law of (28). Sweeping the parameters in this way allowed the authors to change the response of the system to the reference input. The final simulation with the parameters $b = 5$ and $\alpha = 3.3$ allowed for the shortest settling time and least overshoot of the ball position from its reference point. The b parameter may be swept in a similar manner to obtain the response desired for the particular control problem.

6. CONCLUSIONS

Within this article, the port-Hamiltonian theory and matching equations that form an integral part of the IDA-PBC methodology have been discussed thoroughly. The authors have also given a clear discussion of two popular examples of IDA-PBC to control problems. Simulation results with practical system parameters were included to demonstrate the effect of the controllers produced with this technique.

The results for the above simulations should be simple for the reader to reproduce with the parameters given in sections 5.1 and 5.2. Working through these examples should give readers a clear introduction to the technique, allowing them to apply the principles to other control problems and further research.

Figures 3 to 5 show that high quality controllers may be developed with the IDA-PBC technique. Also, energy dissipation may be lowered. The system output may be controlled to stabilise at a set equilibrium point with minimal overshoot and a short settling time. When the control law contains several free parameters as in (28), the designer has more control over the shape of the response.

Testing the hypothesis that lowered energy dissipation will reduce maintenance costs in systems could constitute future work. Similarly, investigating the effect on energy dissipation of the various forms of the controlled response as for the MAGLEV system invites several more research questions. One would expect a more stringent response to dissipate more energy within the electromagnet, but initial investigations have proposed that the total energy dissipation of the system may be less for more stringent control laws even though the energy dissipation in the electromagnetic field may be larger.

REFERENCES

[1] R. Ortega, A. Loría, P. J. Nicklasson, and H. Sira-Ramírez, *Passivity-based Control of Euler-Lagrange Systems*, ser. Communications and Control Engineering. London: Springer London, 1998.

[2] R. Ortega and A. Van der Schaft, "Putting energy back in control," *Control Systems*, vol. 21, no. 2, pp. 18–33, 2001.

[3] J. A. Naudé, "Control Design Using Energy-Shaping Methods," Ph.D. dissertation, University of the Witwatersrand, 2012.

[4] A. Y. Mersha, R. Carloni, and S. Stramigioli, "Port-based Modeling and Control of Underactuated Aerial Vehicles," in *2011 IEEE International Conference on Robotics and Automation*, Shanghai, China, 2011, pp. 14–19.

[5] R. Ortega, A. V. D. Schaft, B. Maschke, and G. Escobar, "Interconnection and damping assignment passivity-based control of port-controlled Hamiltonian systems," *Automatica*, vol. 38, pp. 585–596, 2002.

[6] R. Ortega and E. García-Canseco, "Interconnection and Damping Assignment Passivity-Based Control: A Survey," *European Journal of Control*, vol. 10, no. 5, pp. 432–450, Jan. 2004.

[7] F. Dörfler, J. K. Johnsen, and F. Allgöwer, "An introduction to interconnection and damping assignment passivity-based control in process engineering," *Journal of Process Control*, vol. 19, no. 9, pp. 1413–1426, Oct. 2009.

[8] H. Rodriguez, H. Siguerdidjane, and Ort, "Experimental Comparison of Linear and Nonlinear Controllers for a Magnetic Suspension," in *Proceedings of the 2000 IEEE International Conference on Control Applications. Anchorage, Alaska (USA)*, 2000.

BIBLIOGRAPHY

[1] Anthony M Bloch, Dong Eui Chang, Naomi Ehrich Leonard, and Jerrold E. Marsden. 'Controlled Lagrangians and the stabilization of mechanical systems. II. Potential shaping.' In: *Proceedings of the IEEE Transactions on Automatic Control* 46.10 (2001), pp. 1556–1571 (cit. on pp. 17, 18).

[2] Anthony M Bloch, Naomi Ehrich Leonard, and Jerrold E. Marsden. 'Stabilization of Mechanical Systems Using Controlled Lagrangians.' In: *Proceedings of the 36th Conference on Decision & Control*. December. San Diego, CA, 1997, pp. 2356–2361 (cit. on pp. 13, 17, 18).

[3] Anthony M Bloch, Naomi Ehrich Leonard, and Jerrold E Marsden. 'Controlled Lagrangians and the Stabilization of Mechanical Systems I: The First Matching Theorem.' In: *IEEE Transactions on Automatic Control* 45.12 (2000), pp. 2253–2270 (cit. on pp. 17, 18).

[4] F Castaños and R Ortega. 'Energy-balancing passivity-based control is equivalent to dissipation and output invariance.' In: *Systems & Control Letters* 58.8 (2009), pp. 553–560. DOI: 10.1016/j.sysconle.2009.03.007 (cit. on pp. 6, 18).

[5] Abhijit Das, Frank Lewis, and Kamesh Subbarao. 'Backstepping approach for controlling a quadrotor using lagrange form dynamics.' In: *Journal of intelligent and robotic systems* (2009), pp. 127–151. DOI: 10.1007/s10846-009-9331-0 (cit. on pp. 4, 13, 14, 19, 50).

[6] Florian Dörfler, Jorgen K. Johnsen, and Frank Allgöwer. 'An introduction to interconnection and damping assignment passivity-based control in process engineering.' In: *Journal of Process Control* 19.9 (Oct. 2009), pp. 1413–1426. DOI: 10.1016/j.jprocont.2009.07.015 (cit. on pp. v, vii, 6, 13, 15, 16, 32, 35, 46, 47, 62).

[7] Jin Erdong and Sun Zhaowei. 'Passivity-based control for a flexible spacecraft in the presence of disturbances.' In: *International Journal of Non-Linear Mechanics* 45.4 (May 2010), pp. 348–356. DOI: 10.1016/j.ijnonlinmec.2009.12.008 (cit. on p. 13).

[8] Kenji Fujimoto, Kazunori Sakurama, and Toshiharu Sugie. 'Trajectory tracking control of port-controlled Hamiltonian systems via generalized canonical transformations.' In: *Automatica* 39.12 (Dec. 2003), pp. 2059–2069. DOI: 10.1016/j.automatica.2003.07.005 (cit. on pp. 16, 36).

[9] Lvs Hager. 'Adaptive neural control of a single-rotor small-scale helicopter.' PhD thesis. 2013 (cit. on pp. 3, 9, 10, 21, 23, 65).

[10] B Hald, Ulrik, Mikkel V Hesselbæk, Jacob T Holmgaard, Christian S Jensen, Stefan L Jakobsen, and Martin Siegumfeld. *Autonomous Helicopter Modelling and Control*. Tech. rep. Aalborg University, 2005, p. 110 (cit. on pp. 9–12, 21–23, 27).

[11] T John Koo, Yi Ma, and S Shankar Sastry. *Nonlinear control of a helicopter based unmanned aerial vehicle model*. Tech. rep., pp. 1–25 (cit. on pp. 9, 10, 21, 23).

[12] WS Koon and JE Marsden. 'The Hamiltonian and Lagrangian approaches to the dynamics of nonholonomic systems.' In: *Reports on Mathematical Physics* 40.I (1997) (cit. on p. 15).

[13] P J Kruger, K R Uren, and G Van Schoor. 'Demystifying interconnection and damping assign- ment passivity-based control.' In: *South African Universities Power Engineering Conference*. 2015, pp. 407–412 (cit. on pp. 18, 19, 32, 61, 66).

[14] Naomi Ehrich Leonard and Jerrold E. Marsden. 'Stability and drift of underwater vehicle dynamics: Mechanical systems with rigid motion symmetry.' In: *Physica D: Nonlinear Phenomena* 105.1-3 (June 1997), pp. 130–162. DOI: 10.1016/S0167-2789(97)83390-8 (cit. on p. 13).

[15] Jianyong Li, Yanhong Liu, Chunwen Li, and Bing Chu. 'Passivity-Based Nonlinear Excitation Control of Power Systems with Structure Matrix Reassignment.' In: *Information* 4.3 (Aug. 2013), pp. 342–350. DOI: 10.3390/info4030342 (cit. on p. 13).

[16] T. McRuer, Duane and Ezra S. Krendel. *Mathematical Models of Human Pilot Behavior*. Tech. rep. London, 1974, pp. 12, 31 (cit. on p. 53).

[17] Duane T. McRuer, Ezra S. Krendel, Dunstan Graham, and William Reisener. *Human Pilot Dynamics in Compensatory Systems*. Tech. rep. 1965 (cit. on p. 53).

[18] Abeje Y Mersha, Raffaella Carloni, and Stefano Stramigioli. 'Port-based Modeling and Control of Underactuated Aerial Vehicles.' In: *2011 IEEE International Conference on Robotics and Automation*. Shanghai, China, 2011, pp. 14–19 (cit. on p. 15).

[19] RM Murray. 'Nonlinear control of mechanical systems: A Lagrangian perspective.' In: *Annual Reviews in Control* 21 (1997), pp. 31–42 (cit. on pp. 13, 14, 17).

[20] Jacques Arno NaudÃ©. 'Control Design Using Energy-Shaping Methods.' PhD thesis. University of the Witwatersrand, 2012 (cit. on pp. 13, 15–18, 35).

[21] Romeo Ortega and EloÃsa GarcÃa -Canseco. 'Interconnection and Damping Assignment Passivity-Based Control: A Survey.' In: *European Journal of Control* 10.5 (Jan. 2004), pp. 432–450. DOI: 10.3166/ejc.10.432-450 (cit. on pp. 6, 17, 18, 31, 32, 35, 36, 41).

[22] Romeo Ortega, Antonio LorÃa, Per Johan Nicklasson, and Hebertt Sira-RamÃrez. *Passivity-based Control of Euler-Lagrange Systems*. Communications and Control Engineering. London: Springer London, 1998. DOI: 10.1007/978-1-4471-3603-3 (cit. on pp. 3, 4, 6, 13–18, 47).

[23] Romeo Ortega, Arjan Van Der Schaft, Bernhard Maschke, and Gerardo Escobar. 'Interconnection and damping assignment passivity-based control of port-controlled Hamiltonian systems.' In: *Automatica* 38 (2002), pp. 585–596 (cit. on pp. 3, 4, 6, 15–17, 31, 32, 34, 35).

[24] Romeo Ortega and AJ Van der Schaft. 'Putting energy back in control.' In: *Control Systems* 21.2 (2001), pp. 18–33 (cit. on pp. 3, 4, 6, 13–15, 17–19, 31–34, 61, 62, 64, 66, 77).

[25] M Abdolhosseini Y M Zhang C A Rabbath. 'An Efficient Model Predictive Control Scheme for an Unmanned Quadrotor Helicopter.' In: (2013), pp. 27–38. DOI: 10.1007/s10846-012-9724-3 (cit. on pp. 14, 49, 50).

[26] J Roskam. *Airplane Flight Dynamics and Automatic Flight Controls*. Airplane Flight Dynamics and Automatic Flight Controls p. 1. Roskam Aviation and Engineering Corporation, 1995, pp. 763–769 (cit. on pp. v, vii, 53).

[27] Tushar K Roy, Matt Garratt, H R Pota, and H Teimoori. 'Hover Flight Control of a Small Helicopter Using Robust Backstepping and PID.' In: *10th World Congress on Intelligent Control and Automation*. 2012, pp. 1688–1693 (cit. on pp. 14, 49, 50).

[28] D Ã Schafroth, C Bermes, S Bouabdallah, and R Siegwart. 'Control Engineering Practice Modeling , system identification and robust control of a coaxial micro helicopter.' In: *Control Engineering Practice* 18 (2010), pp. 700–711. DOI: 10.1016/j.conengprac.2010.02.004 (cit. on p. 50).

[29] Cristian Secchi, H B Heinrich, Antonio Franchi, and Burak Yüksel. 'Reshaping the Physical Properties of a Quadrotor through IDA-PBC and its Application to Aerial Physical Interaction.' In: *2014 IEEE Int. Conf. on Robotics and Automation*. 2014, pp. 1–8 (cit. on pp. iv, vi, 4, 13, 17, 19, 38, 46, 49, 50, 63).

[30] C Souza, G V Raffo, and E B Castelan. 'Passivity Based Control of a Quadrotor UAV.' In: *19th IFAC World Congress*. 2014, pp. 3196–3201 (cit. on pp. iv, vi, 4, 6, 13, 14, 18, 19, 23, 36, 38, 41, 42, 46, 50, 64).

[31] B L Stevens and F L Lewis. *Aircraft Control and Simulation*. Wiley, 2003, pp. 34–40 (cit. on p. 57).

[32] M C Terblanche. 'System identification and optimal control of a small-scale unmanned helicopter.' In: *NWU Masters Study* November (2013) (cit. on pp. 3, 9, 10, 12, 23).

[33] J C Avila Vilchis, B Brogliato, A Dzul, and R Lozano. 'Nonlinear modelling and control of helicopters.' In: *Automatica* 39 (2003), pp. 1583–1596. DOI: 10.1016/S0005-1098(03)00168-7 (cit. on p. 50).

[34] Z Wang and P Goldsmith. 'Modified energy-balancing-based control for the tracking problem.' In: *IET Control Theory and Applications* 2.4 (2008), pp. 310–322. DOI: 10.1049/iet-cta (cit. on pp. 31, 36, 37, 41).

[35] Zheng Wang. 'Control of Port-Controlled Hamiltonian Systems.' PhD thesis. University of Calgary, 2008, pp. 1–141 (cit. on pp. 14, 36, 40, 41).

[36] B.Erik Ydstie. 'Passivity based control via the second law.' In: *Computers & Chemical Engineering* 26.7-8 (Aug. 2002), pp. 1037–1048. DOI: 10.1016/S0098-1354(02)00041-8 (cit. on p. 13).

[37] B.Erik Ydstie and Antonio A. Alonso. 'Process systems and passivity via the Clausius-Planck inequality.' In: *Systems & Control Letters* 30.5 (June 1997), pp. 253–264. DOI: 10.1016/S0167-6911(97)00023-6 (cit. on p. 13).

COLOPHON

This document was typeset using the typographical look-and-feel `classicthesis` developed by André Miede with adaptions made by Petrus J. Kruger. The style was inspired by Robert Bringhurst's seminal book on typography *"The Elements of Typographic Style"*, but required certain adaptions to accomodate the figures, equations and other preferences of the author of this work.

`classicthesis` is available for both LaTeX and LyX:

https://bitbucket.org/amiede/classicthesis/

Final Version as of December 3, 2015 (`classicthesis` version 4.2).